ABSTRACT

DAVIS, MICHAEL FOSTER. Structural Studies of Inhibitor and Substrate Binding in the Hemoglobin Dehaloperoxidase. (Under the direction of Stefan Franzen).

Dehaloperoxidase (DHP) is a dual function heme protein found in the marine polychaete *Amphitrite ornata*. *A. ornata* is filter feeding worm that inhabits estuary inlets alongside other annelids such as *Notomastus lobatus* and *Thelepus crispus*, which secrete various haloaromatics theoretically as a means of territorial protection. *N. lobatus*, in particular, expels mono-, di-, and trihalogentated phenols. Even though DHP is one of two hemoglobins found in *A. ornata*, the protein possesses significant peroxidase activity and is capable of oxidatively dehalogenating certain halophenols found in its environment. The ability of DHP to bind monohalogenated phenols in an internal distal cavity separates the protein from any other known globin. A variety of spectroscopic and enzymatic techniques have been utilized to probe halophenol binding in DHP. In order to perform these techniques, codon optimization of the DHP gene was first performed. ^{1}H NMR experiments on low-spin metcyano DHP revealed separate modes of binding between mono-, di-, and trihalogentated phenols. Specifically it was found that binding of mono- and dihalogenated phenols occurs in the internal binding pocket, while trihalogenated phenols bind at a second, external site. This led to enzymatic studies that revealed inhibition of DHP peroxidase activity upon monohalogenated phenol binding in the internal pocket. NMR experiments on the protein backbone of ^{13}C and ^{15}N labeled DHP show trihalogenated substrates induce chemical shift deviations in the distal histidine H55 NεH and amide protons near tryptophan 120. This indicates binding of trihalophenols may occur on the external side of H55 resulting in allosteric changes at the dimer interface, or that binding may occur directly at W120.

Structural Studies of Inhibitor and Substrate Binding in the Hemoglobin Dehaloperoxidase

by

Michael Foster Davis

A dissertation submitted to the Graduate Faculty of
North Carolina State University
in partial fulfillment of the
requirements for the degree of
Doctor of Philosophy

Chemistry

Raleigh, North Carolina

2009

APPROVED BY:

_____	_____
Dr. Stefan Franzen Committee Chair	Dr. Edmond Bowden
_____	_____
Dr. Tatyana Smirnova	Dr. Steven Lommel

DEDICATION

This work is dedicated to my parents, Marie and Arthur Davis Jr., and to my sister, Heather Robinson. Your constant love and support has carried me through my time as a graduate student. To my grandparents, Mary Alice and Arthur Davis Sr.; Evelyn and Ernest Jones, thank you for being my inspiration. Also to Ethan, Bryce, and Ridge Robinson, I hope this inspires you to one day follow your own dreams. I would also like to dedicate this to Katie Price for her endearing faith, love, and support. Thank you all for everything. I am truly blessed.

BIOGRAPHY

Michael Foster Davis, the second child of Marie and Arthur Davis, was born on December 18th, 1978. He and his older sister, Heather, were raised in Rock Hill, SC, where they both attended and graduated from Northwestern High School. Upon graduation Mike enrolled at the University of South Carolina (USC). While attending USC, he taught undergraduate Organic Chemistry labs under the supervision of Dr. George Handy. He also participated in undergraduate research on the construction of polymer composite optical surfaces and vacuum coating of materials under Dr. Wally Scrivens. Mike graduated from USC in four years with a double major in Biology and Chemistry, and subsequently began his graduate work in chemistry at North Carolina State University (NCSU). At NCSU, his graduate research was focused on the heme protein dehaloperoxidase under Dr. Stefan Franzen. His primary investigative tool was 1D, 2D, and 3D NMR spectroscopy, although X-band EPR, cryogenic FT-IR, UV-Vis spectroscopy, picosecond transient absorption spectroscopy, and site-directed mutagenesis were all utilized during his research. During his graduate work he also established collaborations with other researchers at Mt. Holyoke College, Ecole Polytechnique (France) and INSERM (France). These collaborations have contributed greatly to his growth as a scientist.

ACKNOWLEDGMENTS

Sincerest thanks go to all who have given guidance and encouragement throughout my research. Thank you to Dr. Hanna Gracz and Dr. Sean Decatur for helping me understand and appreciate NMR spectroscopy. Dr. Franck A. P. Vendeix and Dr. Benjamin Bobay were also invaluable mentors for the NMR experiments. Thank you to Dr. Tim Sit and Dr. Steve Lommel for allowing use of their lab to perform the molecular biology work. Special thanks to Dr. Sit for all his guidance and advising through my graduate work. Thank you to my graduate committee: Dr. Edmond Bowden, Dr. Tatyana Smirnova, and Dr. Steve Lommel for their advice and encouragement. Most sincere thanks to Dr. Stefan Franzen for allowing me the opportunity to perform research in his lab. His insight and objective criticism have been instrumental in my growth as a scientist. Sincerest thanks to all members of the Franzen group, past and present, and anyone else who has worked on the DHP project. Thank you especially to Katie for all your encouragement and support, I would be truly lost without your guidance. Last and most importantly thank you to my family for their never ending love and support. I could never have made it to where I am without it.

TABLE OF CONTENTS

LIST OF TABLES

LIST OF SCHEMES

LIST OF FIGURES

Chapter 5

Chapter 6

Appendix 1

Appendix 2

Appendix 3

LIST OF ABBREVIATIONS

2,4,6-TBP	2,4,6-tribromophenol
2,4,6-TCP	2,4,6-trichlorophenol
2,4,6-TFP	2,4,6-trifluorophenol
2,4-DCP	2,4-dichlorophenol
2,6-DBQ	2,6-dibromo-1,4-benzoquinone
2,6-DCQ	2,6-dichloro-1,4-benzoquinone
4-BP	4-bromophenol
^{1}H NMR	proton nuclear magnetic resonance
Ap	ampicillin
Cam	chloramphenicol
CcP	cytochrome c peroxidase
COSY	correlation spectroscopy
DHP	dehaloperoxidase
DHPCN	cyanide-ligated dehaloperoxidase
DHPCO	CO-ligated dehaloperoxidase
EPR	electron paramagnetic resonance
FT-IR	Fourier transform infrared spectroscopy
HRP	horseradish peroxidase
HSQC	heteronuclear single quantum coherence
HYSCORE	hyperfine sublevel correlation spectroscopy
IPTG	isopropyl-beta-D-thiogalactopyranoside
Mb	myoglobin
MCPBA	meta-chloroperbenzoic acid
NOESY	nuclear Overhauser effect spectroscopy
WEFT	water eliminated Fourier transform

CHAPTER 1

Dehaloperoxidase Structure and Function: A Mini-Review

Introduction

Dehaloperoxidase (DHP) from the marine polychaete *Amphitrite ornata* is a dual function protein which exhibits both globin and peroxidase characteristics (*1-2*). Structural, kinetic, and spectroscopic analysis of the protein have detailed the binding and oxidative dehalogenation of various halophenols upon addition of co-substrate H_2O_2 (*2-5*). While the peroxidase activity of DHP towards trihalogenated phenols is well established, the impact that other naturally occurring halophenols, such as mono- and dihalogenated phenols, have on this process has received little attention. Earlier reports illustrated and emphasized the unique internal distal binding pocket of the protein (*3, 6*). X-ray data clearly indicate the ability of monohalogenated phenols to bind in this pocket (*3*). Why monohalogenated phenols bind at this site, given the lack of observable product conversion of these molecules, is a fundamental question consistently glossed over in earlier reports. Moreover, the molecules that exhibit highest product conversion rates (2,4,6-trihalophenols) have never been shown to bind in the distal binding pocket *under ambient conditions*.

Current research shows that binding of monohalogenated phenols in the distal binding pocket leads to inhibition of DHP peroxidase activity (see Chapter 5). In addition, halophenols with high product conversion rates (2,4,6-trihalophenols) are now experimentally shown to bind at a separate external location *under ambient conditions* (see Chapters 3, 4, and 6). Herein we review key structural, kinetic, and spectroscopic data which led to the current discoveries regarding the inhibition of peroxidase activity in the dual function protein DHP.

DHP Structure

The heme protein DHP is one of two hemoglobins found in the terebellid polychaete *Amphitrite ornata* (*1*). The dimeric hemoglobin consists of two identical 15.5 kDa subunits, each containing a heme prosthetic group. To date only four structures of wild type DHP are available in the PDB (1EW6, 1EWA, 2QFK, and 3DR9). Six unreleased structures, for which coordinate files have been deposited, include those of DHP with bound monohalogenated 4-bromophenol and 4-chlorophenol, and a structure of cyanide-ligated DHP. X-ray structures currently available show the general globin fold of DHP, with 8 alpha helices and the protein backbone ligated to the heme prosthetic group via a proximal histidine (*2-4*). DHP is structurally homologous to myoglobin (Mb) and appears as a dimer in all current X-ray structures. In the structure the dimer interface appears to involve interactions of three key residues: D72, V74, and R122. There is also a single surface cysteine (C73) located near the interface. Formation of a disulfide bond between the surface cysteine of each subunit is unlikely given the ~11 Å of separation between the two sulfur atoms (*3*).

Dual conformations of the distal histidine were observed in the first DHP X-ray structure. The structure indicated that H55 was found in both a "closed" and "open" conformation (*3*). The "closed" conformation, typically seen in Mb at basic pH, shows H55 inside the distal pocket but not close enough for hydrogen bonding of the H55 Nε to an axial ligand. In the "open" conformation, observed under acidic conditions in Mb, H55 is swung out of the distal pocket. More recent X-ray studies indicate the presence of a single "closed" H55 conformation in metaquo or ferrous oxy DHP (*4*). The recent X-ray structures, collected at pH 6 and 100K, indicated that the H55 residue is located ~0.75 Å closer to the heme iron

than in previous studies (*4*). This places the distal histidine at a distance, with respect to the heme iron, similar to that observed in Mb. Consequently, hydrogen bonding is observed in these more recent structures between the distal histidine H55 Nε and coordinated axial ligands, such as H_2O or O_2 (*4*). While only one conformation of H55 was observed in the metaquo or ferrous oxy state of the protein, X-ray structures of the deoxy form indicated different results. The deoxy X-ray structures showed the histidine in two distinctly different "open" orientations when there is no coordinated axial ligand (*5*).

Perhaps the most frequently emphasized structural feature of DHP is the novel distal binding pocket. X-ray structures show the ability of DHP to bind a monohalogenated phenol in this hydrophobic distal cavity (*3*). The internal binding of 4-iodophenol (4-IP) in this cavity distinguishes DHP from any other known globin (*6*). All observable structural changes induced by binding of the monohalogenated phenol occur at the heme or in the distal binding pocket. The location of monohalogenated binding in the crystal structure and binding pocket resides of the active site of DHP can be seen in Figure 1. Upon 4-IP binding, the distal histidine is observed solely in the "open" conformation. The location of 4-IP in the pocket necessitates this change in conformation, as "closed" H55 and 4-IP appear to vie for the same space in the distal pocket. As seen in Figure 1, the three closest residues to bound 4-IP are V59, F35, and F21 with nearest C-C distances of 2.98, 2.98, and 3.41 Å, respectively. Notable conformations changes are seen in the distal pocket residues H55, F35, and F21. In addition, small changes in orientation are observed in the 2-vinyl, 4-vinyl, 6-propionate, and 7-propionate heme substituents. Binding of 4-IP does not, however, induce structural changes outside of the distal pocket.

DHP Activity

Activity in peroxidases normally occurs through a reactive intermediate known as compound I (*7*). One of the most well known and commonly studied peroxidases is horseradish peroxidase (HRP). Activation of the enzyme occurs through formation of an active intermediate known as compound I. Formation of this intermediate occurs via the Poulos-Kraut mechanistic activation of peroxidases, as seen in Figure 2 (*8*). In this mechanism, H_2O_2 binds to the ferric heme iron and is stabilized by hydrogen bonding to the Nε of the distal histidine. Proton transfer between the α-oxygen of H_2O_2 to the β-oxygen, subsequent heterolytic cleavage of the O-O bond, and release of H_2O leads to formation of the high valence Fe(IV)=O species which contains a π-cation radical. This reactive intermediate is unknown as compound I. Loss of the π-cation radical results in a second reactive intermediate known as compound II, which is the referred to as a Fe(IV)=O or Fe(IV)-OH species. Regeneration of the Fe(III) resting state from compound I is achieved by oxidation of a substrate molecule via two sequential one-electron oxidation steps.

Initial enzymatic analysis probing the peroxidase activity of DHP was reported along with initial spectroscopic and crystallization of the protein in 1996 (*2, 9*). The activity of DHP was found to be similar to that of HRP (*10*). DHP was shown to oxidatively dehalogenate trihalophenols in a hydrogen peroxide dependent manner. Specifically, the peroxidase activity of DHP towards 2,4,6-bromophenol (2,4,6-TCP) and 2,4,6-tribromophenol (2,4,6-TBP) was demonstrated and initial product characterization was performed. Product characterization of the 2,4,6-TBP and 2,4,6-TCP assays using mass

spectrometry resulted with molecular ions characteristic of 2,6-dibromo-1,4-benzoquinone (2,6-DBQ) and 2,6-dichloro-1,4-benzoquinone (2,6-DCQ), respectively (*9*). These initial enzymatic assays set precedent for further enzymatic reports which included using co-substrates other than H_2O_2. Using an alternate oxygen donating co-substrate, meta-chloroperbenzoic acid (MCPBA), resulted in an approximate 3 fold increase in 2,4,6-TCP turnover (*11*). The increased dehalogenation activity of DHP using MCPBA may indicate the natural co-substrate is an oxidant other than H_2O_2 (*11*).

Further investigations into DHP activity revealed a correlation between 2,4,6-TBP turnover and solvent pH. DHP activity and kinetic analysis of product formation was performed using UV-Vis and stopped-flow experiments in pH ranging from 4.0 to 8.0. Highest turnover rates for the "native" substrate, 2,4,6-TBP, were observed at pH 7.5. The second highest turnover for the substrate occurred at pH 7.0 (*12*). Since 2,4,6-TBP exists in the phenolate form at pH > 6.8, the data indicate binding and oxidation of substrate in the phenolate form is favorable for protein activity. This is not the case with other peroxidases, such as HRP, which does not oxidize substrates in the phenolate form (*13*). The high activity of DHP between pH 7.0-7.5 may be due to the physiological conditions in which the protein is found. DHP is the coelomic hemoglobin of *A. ornata* where pH is ~ 7.4. Even though 2,4,6-TBP turnover is highest at pH > 7.0, faster kinetics are seen at pH < 7.0. An increase in product formation kinetics comes at the expense of protein stability. An increase in heme degradation is observed lower pH values. This observation may explain why the greater rate constants at lower pH do not lead to higher levels of product formation (*12*).

As DHP activity was investigated in detail, questions about the internal binding site began to arise. Monohalogenated phenols are clearly bound in the distal cavity as shown in the X-ray data. However, binding in this location effectively removes the only residue capable of supporting proton transfer needed for compound I formation upon H_2O_2 binding. To complicate this matter, studies found that order of addition of substrate, 2,4,6-TBP, and co-substrate, H_2O_2, greatly affected protein activity (*14*). Mixing substrate and protein prior to H_2O_2 addition resulted in typical substrate oxidation. However, if DHP and H_2O_2 were incubated for more than about 30 seconds prior to substrate addition, protein activity was inhibited. The results indicated that DHP activity is highest when substrate is added first. This implied that the active form of H55 was solely in the "open" conformation and out of the distal pocket. Removal of H55 means removal of the sole residue capable of the acid base catalysis needed for compound I to form (14). These results raised important questions about the relationship between substrate binding local and protein activity. Based on the results, one of two conclusions can be reached. First, the substrate molecule, now bound in the distal pocket, would have to act as a trigger for the protein to switch from globin to peroxidase activity. Given the displacement of H55 out of the pocket, the mechanism of compound I would also have to be completely different than that dictated by the Poulos-Kraut mechanism. Second, substrate could be binding at a location other than the distal binding pocket. This scenario would allow H55 to remain in the "closed" conformation, thereby facilitating proton transfer needed during compound I formation. Depending on the amount of time of DHP / H_2O_2 incubation, the addition of H_2O_2 prior to substrate could

inhibit protein activity due to heme degradation or cause it to become "stuck" in an inactive compound II state as indicated by current and previous investigations (*11, 12, 14*).

DHP Mutagenesis

Site-directed mutagenesis of the distal and proximal histidines, and residues comprising the distal binding was performed to better ascertain the roles of active site amino acids in DHP peroxidase activity. The relative activity of the following DHP mutants has been compared at pH 7.0 using UV-Vis spectrophotometric assays: Y38F, H55R, H55V, H55V/V59H, V59W, and H89G. The residue tyrosine 38 is important in regards to the distal binding pocket, because it is close enough to form a hydrogen bond to the hydroxyl group of bound monohalogenated phenol (*3*). This is believed to stabilize monohalogenated phenol binding in the distal pocket. Mutation of this residue to phenylalanine will eliminate the hydrogen bond and provide insight into how monohalogenated phenols bind in the distal pocket. V59 is the closest residue to bound monohalogenated phenol in the X-ray structure, with the nearest C-C distance being 2.98 Å (*3*). Mutation of this residue to a tryptophan (V59W, as discussed in Chapter 4) will introduce a very bulky side chain into the distal binding pocket. The hypothesis is that this mutation will "block" binding of monohalogenated phenol in the distal cavity.

The distal (H55) and proximal (H89) histidines are extremely important residues in both globins and peroxidases. The H89 provides the only covalent linkage between the heme and protein backbone. In addition, the Nδ of H89 hydrogen bonds to the backbone carbonyl of Leu 86, which is characteristic of hemoglobins. Peroxidases typically exhibit stronger

hydrogen bonding of the proximal histidine Nδ to an aspartate side chain. This makes the proximal histidine a better electron donor and therefore creates a stronger "push" to the heme iron than observed in globins (*15*). The distal histidine, H55, acts to stabilize the binding of H_2O_2 to the heme iron. The residue is also responsible for transferring a proton from the α-oxygen to the β-oxygen of H_2O_2 and assists in "pulling" apart the O-O bond which leads to formation of compound I (*8*).

Of the six mutations, only Y38F, H55R, and V59W showed significant activity toward 2,4,6-TBP and 2,4,6-TCP (*16, 17*). The Y38F mutant, which eliminates any hydrogen bonding between internal halophenol and the protein, actually shows an ~ 5 fold increase in 2,4,6-TBP product turnover rate compared to DHP. Conversely, the H55R mutation results in an ~10 fold decrease in product turnover (*16*). The V59W mutant exhibits kinetics and product turnover rates similar to DHP. The wild type DHP only exhibited 1.2x greater product formation than V59W mutant (*17*). The H55V, H55V/V59H, and H89G mutants all resulted in negligible protein activity. The activity, albeit lowered, of H55R and the lack of activity in H55V indicates the necessity for a residue capable of acid-base catalysis at amino acid 55. The results of the V59W mutation indicate that having a bulky side chain in the internal cavity does little to affect protein activity. The internal location of V59 and the necessity for a "closed" H55 conformation needed for compound I formation inherently dictate a crowded internal distal cavity. Alternatively, binding of substrate on the external heme edge, as is typical with HRP, would account for the observed activity in V59W. The enzymatic properties of the Y38F mutant also corroborate an exterior binding hypothesis. To date, the Y38F mutant is the most active form of DHP. Initially it

was thought this mutant would lead to a decrease in activity. Since Y38 has the potential to form a hydrogen bond with H55, it was thought that it could be part of a hydrogen bond network needed for peroxidase function. However, the results indicate that removal of the putative internal hydrogen bond network between monohalogenated phenol and the protein *enhances* activity. Collectively, the mutagenesis data indicate a separate mode of binding of trihalophenols and suggest that such binding may occur at site other than the monohalogenated phenol binding pocket.

FT-IR Experiments on DHPCO

For the past 40 years myoglobin (Mb) has served as a model system for studying the structure-function relationship of proteins. Myoglobin, the protein responsible for oxygen storage and transportation in muscle, reversibly binds diatomic ligands such as oxygen (O_2), nitric oxide (NO), and carbon monoxide (CO). DHP shares these characteristically globin features with Mb and, given the strong structural homology between DHP and Mb, any structural analysis used for Mb should translate well to DHP experiments. For example, monitoring the rebinding of diatomic ligands after laser photolysis provides excellent insight into the dynamic structure-function relationship of residues near heme iron, which in DHP also happens to be the monohalogenated phenol binding site (*18*).

If ligand rebinding were to involve a single process, then the kinetics should be single exponential. However, one of the early experiments in biophysical studies of Mb was the demonstration that CO rebinding was actually non-exponential in time below 200K (*19*). This observation suggested that Mb was not static, but could assume a variety of

conformational states each with its own rebinding rate (*19, 20*). Therefore when a ligand, such as CO, is introduced to the protein the ligand acts as a probe of the internal protein cavity around the heme iron. If Mb only had one general conformation then the CO stretching vibration ($\nu_{C\text{-}O}$) of this ligand in the protein would inherently have only one frequency. However, different conformational substates of the protein cause the $\nu_{C\text{-}O}$ to resonate at different frequencies. Upon laser photolysis at cryogenic temperatures, the ligand remains trapped inside the protein for some period of time before escaping into the solvent. After photodissociation, the ligand becomes trapped slightly above the heme group in a so called primary docking site "B" (*21, 22*) and does not recombine by a thermal mechanism, but rather by tunneling. This recombination is sufficiently slow that it can be observed in an X-ray structure. X-ray experiments indicate that after photodissociation, at liquid-helium temperatures, the photodissociated CO moves to this primary docking site (B) just above pyrrole C and the iron shifts slightly out of the heme plane (*22*).

In wild type Mb, three heme bound CO stretching bands resonate at ~1965, ~1945, and ~1933 cm^{-1} respectively. These three substates differ primarily in the position of the distal histidine residue. If the distal histidine swings out of the pocket ("open" conformation) the result is a more apolar environment in the distal pocket. This gives rise to the A_0 band at ~1965 cm^{-1}. If the distal histidine is in the "closed" conformation within the pocket the partial positive charge of the Nε-H interacts with bound CO and hence gives rise to the A_1 and A_3 bands at ~1945 and ~1933 cm^{-1} (*18*). Upon photolysis the CO molecule can populate the primary docking site in opposite orientations with respect to the heme iron. These two orientations, B_2 and B_1, give rise to two IR bands, respectively, at ~2119 and ~2131 cm^{-1}. A

third, smaller, photodissociated band, B_0, at ~2150 cm^{-1} is characteristic of the photodissociated CO at the docking site with the protein in the A_3 conformation (*18*).

There are currently two cryogenic FT-IR studies on ferrous CO ligated DHP (DHPCO). The initial report found strong similarities between the CO stretching frequencies of MbCO and DHPCO. The typical heme-bound CO stretching vibrations of DHPCO were found to be ~1950 cm^{-1} with H55 in the "closed" conformation (corresponding to A_1 = 1945 cm^{-1} in MbCO) and ~1965 cm^{-1} for H55 in the "open" conformation (corresponding to A_0 = 1965 cm^{-1} in MbCO) (*23*). This illustrates the relative similarities between the two globins in regards to distal histidine conformational dynamics. Additional experiments also showed the pKa of H55 protonation, and likewise rotation of the side chain the "open" conformation, occurs around pH 4.5 (*24*).

The FT-IR experiments marked the first time a trihalogenated phenol had been used for binding studies. Given the mM concentrations of protein required for the experiments, the small, highly soluble trihalogenated 2,4,6-trifluorophenol substrate (2,4,6-TFP) was used. The substrate was added to the protein at pH 5.5, 7.0, and 10.0. A new CO stretching band was observed at 4K upon the addition of 2,4,6-TFP. The band, A_s, occurs at ~1972 cm^{-1} and indicates that ~80% of all DHP molecules internally bind 2,4,6-TFP at 4K, pH 5.5 (*23*). This band is not readily observed at pH 7, or pH 10, indicating a preference for internal binding under acidic conditions. The A_s = 1972 cm^{-1} band represents a nonbonding, electrostatic interaction between the aromatic substrate ring and the heme-bound CO ligand. However, the 1972 cm^{-1} band completely disappears as the sample is warmed up, indicating a loss of the internal electrostatic interaction. In other words, as the protein is warmed the 2,4,6-TFP

substrate is removed from the distal binding pocket. The removal of 2,4,6-TFP from the internal pocket occurs at temperatures above 160K. No observable bands corresponding to bound 2,4,6-TFP are observed at ambient temperatures. The results indicated for the first time that trihalogenated phenols (active substrates) could bind in the "substrate" binding site in the distal cavity. However, such binding was only observed at pH 5.5 and temperatures < 160K. Given the activity of DHP toward 2,4,6-TFP it is peculiar that no binding events are observed under ambient conditions (*25, 26*).

X-band EPR on metaquo DHP and Detection of Protein Radicals

Recent investigations using X-band EPR and hyperfine sublevel correlation spectroscopy (HYSCORE) have provided insight into the heme iron ligation state and the nature of 2,4,6-TFP binding (*27*). Additional experiments probing internal substrate binding is necessary in light of recent FT-IR data indicating the internalization of substrate 2,4,6-TFP (*23, 24*). Current X-ray structures of metaquo DHP indicate a coordinated axial water ligand (*28*). Analysis of resonance Raman data indicates a mixture of 5-coordinate and 6-coordinate heme in ferric DHP (*28*). Upon addition of monohalogenated phenol, both resonance Raman and X-ray data show a predominately 5-coordinate heme. This indicates expulsion of the coordinated water molecule. EPR HYSCORE experiments provide an opportunity to probe interactions between the iron and coordinated water. More importantly HYSCORE will help determine the fate of bound water upon addition of trihalogenated 2,4,6-TFP.

HYSCORE is a 2D spectroscopic technique used to correlate electron spins to nearby nuclear spins (*29*). HYSCORE couplings between the four nitrogen nuclei of the porphyrin

ring and the nearby iron-coordinated water protons were observed during the experiment. The strongly coupled water protons at ~6 MHz were assigned based on previous studies of metmyoglobin where the ligated water protons exhibited a 6.0 ± 0.1 MHz hyperfine coupling (*27*). Addition of a 10x excess of 2,4,6-TFP at 4.5K causes the coupled water signal to disappear, indicating displacement of the ligand and a transition from six- to five-coordinate iron. Examination of the X-band EPR spectra of ferric DHP with and without 2,4,6-TFP clearly show the $g_{\perp} = 6$ and $g_{jj} = 2$ features characteristic of high spin (S = 5/2) heme iron (*27*). The collective data indicate a change in coordination state (6-coordinate heme to 5-coordinate heme) with no alteration in spin state upon addition of 2,4,6-TFP at 4.5K. The HYSCORE data corroborate FT-IR studies on DHPCO and indicate that substrate 2,4,6-TFP is internalized at low temperatures.

EPR experiments were also used to detect protein radical formation in DHP upon addition of H_2O_2. Protein radicals are generated by rapid electron transfer of the compound I π-cation radical to the protein, which can include long range electron transfer of the radical to distant sites within the protein (*30, 31*). Protein radicals have been shown to act as catalytic intermediates, a site for subunit cross-linkage, or as a species used to divert an oxidizing equivalent away from the active site (*31*). Recent investigations using EPR on rapid-freeze quenched protein have detected the presence of a protein radical shortly after the addition of H_2O_2 (*32*). This intermediate is similar in nature to the compound ES of cytochrome c peroxidase, which arises from a ferryl heme and tryptophan radical (*33*). The exact location of the radical has yet to be determined, but analysis of the signal *g* factor and hyperfine structure suggest the radical likely arises from a tyrosine side chain. The role of the protein

radical in DHP activity is also undetermined but it may act as a second oxidizing equivalent or as the site of substrate oxidation itself (*34*).

NMR Investigations of metcyano DHP

Heme proteins such as DHP contain the prosthetic group iron protoporphyrin IX, which can exist in three spin states in the ferric form: high spin (S=5/2), intermediate spin (S=3/2), and low spin (S=1/2). The introduction of a strong ligand such as CN^- creates a strong repulsion in the five *d* electrons of Fe(III). This strong repulsion is favored if the five *d* electrons position themselves in an orbital with the lowest possible energy. In this strong ligand field there is only one unpaired electron, and the iron is in a low-spin state (S=1/2). Figure 3 illustrates the electronic configuration of low-spin Fe(III). In relation to NMR, the magnetic moment of an unpaired electron is approximately 660 times greater than that of a proton (*35*). If CN^- ligand is bound to the heme iron the effect is a low spin Fe(III) paramagnetic center with S = 1/2. This has dramatic affects on the NMR spectrum. The magnetic moment of the unpaired electron causes paramagnetic relaxation of protons on the heme and nearby residues (*36*). The protons near the unpaired electron experience paramagnetic relaxation which results in large hyperfine-shifting of the resonances. The hyperfine shifted resonances appear outside of the diamagnetic protein envelope, which do not exhibit a paramagnetic contribution. In metMbCN, protons that lie at a distance greater than 7.5 Å from the heme iron exhibit negligible paramagnetic relaxation (*37*). The hyperfine shifts of the heme environment protons enable their NMR signals to be easily spotted in the ^1H NMR spectrum.

Given the close proximity of the distal binding site to the heme iron, initial ^{1}H NMR experiments utilized the paramagnetic properties of the heme iron to specifically focus efforts on active site resonances (*25*). The low-spin metcyano adduct of DHP was chosen because the hyperfine-shifted resonances are much sharper and less dispersed in the low-spin form than in the high-spin, metaquo form. Using primarily Water Eliminated Fourier Transform-Nuclear Overhauser Enhancement Spectroscopy (WEFT-NOESY) and natural abundance ^{13}C-^{1}H Heteronuclear Single Quantum Coherence (^{13}C-^{1}H HSQC), the majority of hyperfine-shifted resonances were assigned. Using the chemical shifts and spacing of the heme methyls, the projection angle, Φ, of the proximal histidine on the heme plane was found to be different than the angle observed in the X-ray structure (*3, 4*). According to X-ray structures this angle is ~113°, in solution, however, the angle was found to be ~90° based on the NMR data.

Assignment of the active site resonances allowed for substrate binding studies geared toward detection of distal biding site interactions. Upon titration of monohalogenated 4-BP, dihalogenated 2,4-dichlorophenol (2,4-DCP), and trihalogenated 2,4,6-TFP varying perturbations were found. 4-BP and 2,4-DCP both induced line broadening in the 3-CH_3 and Phe97 CζH resonances, which are separated by ~4.5 Å in the X-ray structure (*3, 4*). In addition, chemical shift deviations were observed in the 7α propionate protons. The line broadening and chemical shift deviations were observed over the pH range 5.5 – 9.0. Although the greatest degree of change was observed at pH 5.5, the changes were still observable at the alkaline pH 9.9. Addition of 2,4,6-TFP did not result in observable changes in any hyperfine-shifted resonances. By using ^{19}F NMR, T_1, and T_2 relaxation experiments

on 2,4,6-TFP alone and in the presence of DHPCN, evidence was found indicating possible binding of 2,4,6-TFP at a separate site (*25*). Because the substrates were found to be in fast exchange and no substrate-protein NOEs were detectable, additional $^{13}C/^{15}N$ labeled NMR experiments were conducted to help locate any possible secondary binding locations.

After high levels of DHP expression in $^{13}C/^{15}N$ enriched minimal media were obtained the protein backbone $^{13}C\alpha$, $^{13}C\beta$, carbonyl ^{13}C, amide ^{1}H and amide ^{15}N resonances were assigned in metcyano DHP using ^{15}N-^{1}H HSQC, HNCO, HCACOCANH, HNCOCA, HNCA, and HNCACB NMR experiments. 125 of the 137 residues in DHP were readily assigned as a result of the NMR data. Assignment of the backbone ^{13}C, ^{15}N, and ^{1}H nuclei allowed for detection of binding perturbations throughout the protein upon titration of various halophenols. Isotopically labeled protein also allowed for rapid ^{15}N-^{1}H HSQC data collection upon stoichiometric addition of halogenated phenols. Upon addition of the monohalogenated phenol 4-BP, the largest deviations in amide ^{1}H chemical shift were observed in the three closest residues to bound 4-IP in the X-ray structure: F35, V59, and F21 (*38*). Titration of excess substrate 2,4,6-TCP induced the largest chemical shift deviations in the exchangeable H55 NεH and local residues surrounding W120 , which is ~15 Å away from H55. No significant changes were observed in distal binding pocket resonances F35, V59, and F21 upon addition of 2,4,6-TCP. Addition of the smaller 2,4,6-TFP substrate caused the largest changes in chemical shift deviation at the exchangeable H55 NεH, distal binding pocket resides F35, V59, and F21, and the local area around W120. This indicates 2,4,6-TFP may be small enough to bind at both the 4-BP and 2,4,6-TCP site. The 2,4,6-TCP substrate either binds on the external side of H55 and creates allosteric changes at the dimer

interface near W120, or the substrate binds directly near the W120 residue. Binding at either site could account for oxidation of the substrate. Oxidation could occur along the heme edge, as seen in HRP (*39*), or at a tryptophan radical, as observed in lignin peroxidase (*34, 40, 41*). Site-directed mutagenesis of the W120 residue will help elucidate whether or not the residue plays a significant role in substrate binding and oxidation.

References

(1) Weber, R. E., Magnum, C. P., Steinman, H., Bonaventura, C., Sullivan, B., and Bonaventura, J. (1977) Hemoglobins of two terebellid polychaetes: Enoplobranchus sanguineus and Amphitrite ornata. *Comparative Biochemistry and physiology 56A*, 179-187.

(2) Zhang, E., , Chen, Y. P., Roach, M. P., Lincoln, D. E., Lovell, C. R., Woodin, S. A., Dawson, J.H., and Lebioda, L. (1996) Crystallization and initial spectroscopic characterization of the heme-containing dehaloperoxidase from the marine polychaete *Amphitrite ornata Acta Cryst. D 52,* 1191-1193.

(3) LaCount, M. W., Zhang, E., Chen, Y.P., Han, K., Whitton, M. M., Lincoln, D. E., Woodin, S. A., and Lebioda, L. (2000) The crystal structure and amino acid sequence of dehaloperoxidase from *Amphitrite ornata* indicate a common ancestry with globins. *J. Biol. Chem. 275*, 18712-18716.

(4) de Serrano, V., Chen, Z., Davis, M. F., and Franzen, S. (2007) X-ray crystal structural analysis of the binding site in the ferric and oxyferrous forms of the recombinant heme dehaloperoxidase cloned from Amphitrite ornata. *Acta Crysta. D 63,* 1094-1101.

(5) Chen, Z., de Serrano, V., Betts, L., and Franzen, S. (2009) Distal histidine conformational flexibility in dehaloperoxidase from *Amphitrite ornata*. *Acta Crysta. D 65,* 34-40.

(6) Lebioda, L., LaCount, M. W., Zhang, E., Chen, Y. P., Han, K., Whitton, M. M., Lincoln, D. E., and Woodin, S. A. (1999) Protein structure: An enzymatic globin from a marine worm. *Nature. 401,* 445.

(7) Hewson, W. D., and Dunford, H. B. (1976) Oxidation of *p*-cresol by horseradish peroxidase compound I. *J. Biol. Chem. 251,* 6036-6042.

(8) Poulos, T. L., and Kraut, J. (1980) The stereochemistry of peroxidase catalysis. *J. Biol. Chem. 255,* 8199-8205.

(9) Chen, Y. P., Woodin, S. A., Lincoln, D. E., and Lovell, C. R. (1996) An unusual dehalogenating peroxidase from the marine terebellid polychaete Amphitrite ornata. *J. Biol. Chem. 271*, 4609-4612.

(10) Ferrari, R. P., Laurenti, E., and Trotta, F. (1999) Oxidative 4-dechlorination of 2,4,6-trichlorophenol catalyzed by horseradish peroxidase, *J. Biol. Inorg. Chem. 4*, 232-237.

(11) Osborne, R. L., Taylor, L. O., Han, K. P., Ely, B., and Dawson, J. H. (2004) Amphitrite ornata dehaloperoxidase: enhanced activity for the catalytically active globin using MCPBA. *Biochem. Biophys. Res. Comm. 324*, 1194-1198.

(12) Franzen, S., Gilvey, L.B., and Belyea, J. (2007) The pH dependence of the activity of dehaloperoxidase from *Amphitrite ornata*. *Biochim. Biophys. Acta: Prot. Struct. Mol. Enz. 1774*, 121-130.

(13) Patel, P. K., Mondal, M. S., Modi, S., and Behere, D. V. (1997) Kinetic studies on the oxidation of phenols by the horseradish peroxidase compound II. *Biochim. Biophys. Acta-Prot. Struct. Mol. Enz. 1339*, 79-87.

(14) Belyea, J., Gilvey, L. B., Davis, M. F., Godek, M., Sit, T. L., Lommel, S. A., and Franzen, S. (2005) Enzyme function of the globin dehaloperoxidase from Amphitrite ornata is activated by substrate binding. *Biochemistry 44*, 15637-15644.

(15) Dawson, J. H. (1988) Probing structure-function relations in heme-containing oxygenases and peroxidases. *Science*, 433-439.

(16) Franzen, S., Belyea, J., Gilvey, L. B., Davis, M. F., Chaudhary, C. E., Sit, T. L., and Lommel, S. A. (2006) Proximal cavity, distal histidine, and substrate hydrogen-bonding mutations modulate the activity of *Amphitrite ornata* dehaloperoxidase. *Biochemistry*, 9084-9094.

(17) Davis, M. F., Gracz, H., Vendeix, F. A. P., Somasundaram, A., Kook, B. Y., Negrerie, M., and Franzen, S. The V59W mutation blocks the distal pocket of the hemoglobin dehaloperoxidase from *Amphitrite ornata*. (*In preparation*)

(18) Nienhaus, K., Deng, D., Olsen, J. S., Warren, J. J., and Nienhaus, G. U. (2003) Structural dynamics of myoglobin: Ligand migration and binding in valine 68 mutants. *J. Biol. Chem. 278*, 42532-42544.

(19) Frauenfelder, H., Sligar, S. G., and Wolynes, P. G. (1991) The energy landscapes and motions of proteins. *Science 254*, 1598-1603.

(20) Austin, R. H., Benson, K. W., Eisenstein, L., Frauenfelder, H., and Gunsalus, I. C., (1975) Dynamics of ligand binding to myoglobin. *Biochemistry 14*, 5355-5373.

(21) Kriegl, J. M., Nienhaus, K., Deng, P., Fuchs, J., and Nienhaus, G. U. (2003) Ligand dynamics in a protein internal cavity. *Proc. Natl. Acad. Sci. U. S. A. 100*, 7069-7074.

(22) Ostermann, A., Washipky, R., Parak, F. G., and Nienhaus, G. U. (2000) Ligand binding and conformation motions in myoglobin. *Nature 404*, 205-208.

(23) Nienhaus, K., Deng, P. C., Belyea, J., Franzen, S., and Nienhaus, G. U. (2006) Spectroscopic study of substrate binding to the carbonmonoxy form of dehaloperoxidase from Amphitrite ornata. *J. Phys. Chem. B 110*, 13264-13276.

(24) Nienhaus, K., Nickel, E., Davis, M. F., Franzen, S., and Nienhaus, F. U. (2008) Determinants of substrate internalization in the distal pocket of dehaloperoxidase hemoglobin of *Amphitrite ornata*. *Biochemistry 47*, 12985-12994.

(25) Davis, M. F., Gracz, H., Vendeix, F. A. P., de Serrano, V., Somasundaram, A., Decatur, S. M., and Franzen, S. (2009) Different modes of binding of mono-, di, and tri-halogenated phenols to the hemoglobin dehaloperoxidase from *Amphitrite ornata*. *Biochemistry 48*, 2164-2174.

(26) Chaudhary, C. (2003) Point Mutagenesis and Spectroscopic Probing of Dehaloperoxidase: Characterizing the Mechanism and Activity of the Heme Active Site of the Native Protein. *MS Thesis*, NC State Univ.

(27) Smirnova, T. I., Weber, R. T., Davis, M. F., and Franzen, S. (2008) Substrate binding triggers a switch in the iron coordination in dehaloperoxidase from Amphitrite ornata: HYSCORE experiments. *J. Am. Chem. Soc. 130*, 2128-2129.

(28) Thompson, M. K., Davis, M. F., de Serrano, V., Nicoletti, F. P., Howes, B. D., Smulevich, G., and Franzen, S. Two-site competitive inhibition in dehaloperoxidase from *Amphitrite ornata*. (In preparation)

(29) Hofer, P., Grupp, A., Nebenfuhr, H., and Mehring, M. (1986) Hyperfine sublevel correlation (HYSCORE) spectroscopy: A 2D ESR investigation of the squaric acid radical. *Chem. Phys. Lett. 132*, 279-282.

(30) Lardinois, O. M., and Ortiz de Montellano, P. R. (2001) H_2O_2-mediated cross-linking between lactoperoxidase and myoglobin: Elucidation of protein-protein radical transfer reactions. *J. Biol. Chem. 276*, 23186-23191.

(31) Lardinois, O. M., and Ortiz de Montellano, P. R. (2003) Intra- and intermolecular transfers of protein radicals in the reactions of sperm whale myoglobin with hydrogen peroxide. *J. Biol. Chem. 278*, 36214-36226.

(32) Feducia, J., Dumarieh, R., Gilvey, L., B., G., Smirnova, T., Franzen, S., and Ghiladi, R. A. (2009) Characterization of dehaloperoxidase compound ES and its reactivity with trihalophenols. *Biochemistry 48*, 995-1005.

(33) Sivaraja, M., Goodin, D. B., Smith, M., and Hoffman, B. M. (1989) Identification by ENDOR of Trp^{191} as the free-radical site in cytochrome c peroxidase. *Science 245*, 738-740.

(34) Ruiz-Dueñas, F. J., Pogni, R., Morales, M., Giansanti, S., Mate, M. J., Romero, A., Martínez, M. J., Basosi, R., and Martínez, A. T. (2009) Protein radicals in fungal versatie peroxidase: Catalytic tryptophano radical in both compound I and compound II and studies of W164Y, W164H, and W164S variants. *J. Biol. Chem. 284*, 7986-7994.

(35) Dunford, B. H. (1999) in *Heme Peroxidases,* pp 135-190, Wiley-VCH, New York.

(36) La Mar, G. N., and de Ropp, J. S. (1993) in *Biological Magnetic Resonance,* pp 1-73, Plenum Press, New York.

(37) Emerson, S. D., and La Mar, G. N. (1990) Solution structural characterization of cyanometmyoglobin: resonance assignment of heme cavity residues by two-dimensional NMR. *Biochemistry 29*, 1545-1556.

(38) Davis, M. F., Bobay, B. G., and Franzen, S. (2009) Separation of inhibitor and substrate binding locations in the globin dehaloperoxidase. (In preparation)

(39) Ator, M. A., and Ortiz de Montellano, P. R. (1987) Protein control of prosthetic heme reactivity: Reaction of substrates with the heme edge of horseradish peroxidase. *J. Biol. Chem. 262*, 1542-1551.

(40) Hammel, K. E., and Tardone, P. J., (1988) The oxidative 4-dechlorination of polychlorinated phenols is catalyzed by extracellular fungal lignin peroxidase. *Biochemistry 27*, 6563-6568.

(41) Doyle, W. A., Blodig, W., Veitch, N. C., Piontek, K., and Smith, A. T. (1998) Two substrate interaction sites in lignin peroxidase revealed by site-directed mutagensis. *Biochemistry 37*, 15097-15105.

Figures

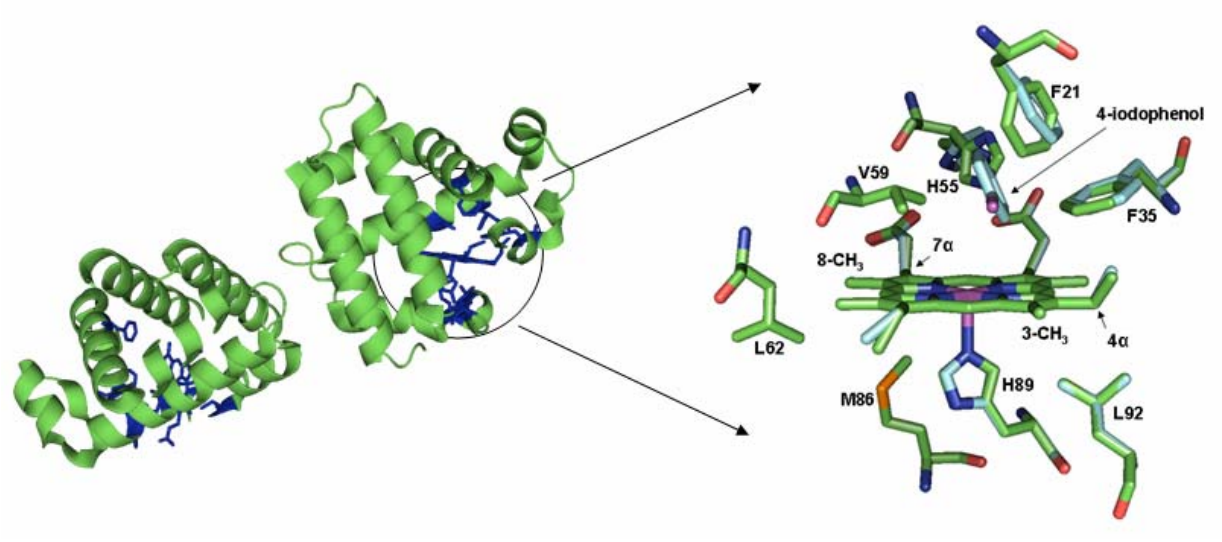

Figure 1. The DHP dimer is seen on the left and the heme active site including the distal binding pocket are enlarged on the right. The green sticks shows the X-ray structure without 4-IP and the light blue sticks show changes which occur in the presence of 4-IP (*3*).

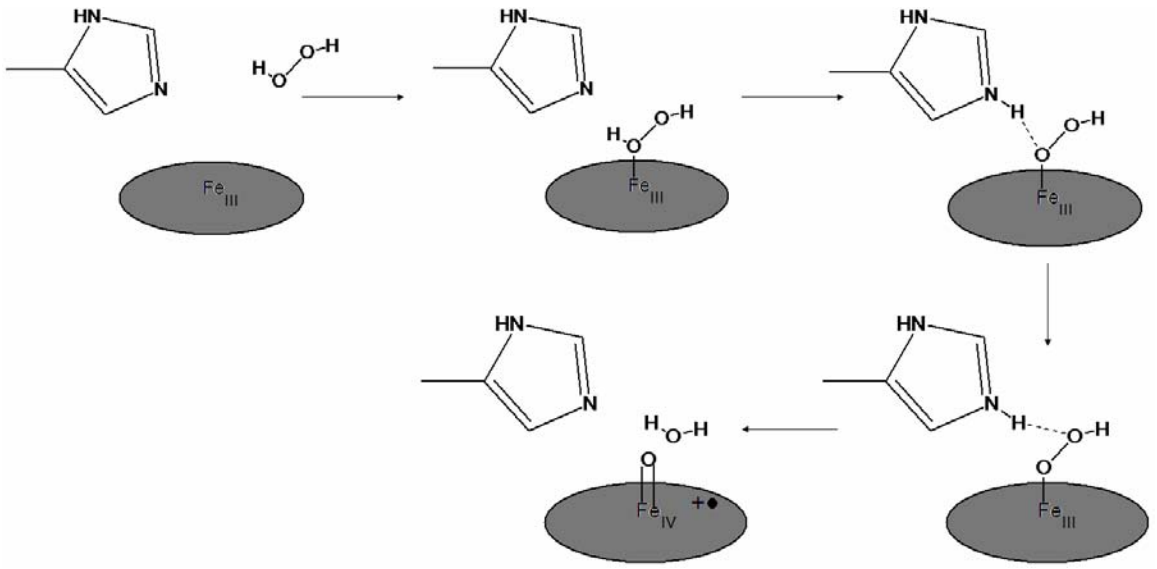

Figure 2. The Poulos-Kraut mechanism illustrating the formation of the reactive intermediate compound I.

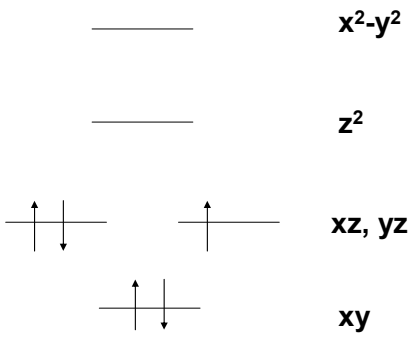

Figure 3. Electronic configuration of low-spin Fe (III).

CHAPTER 2

Codon Optimization of the DHP Gene

Introduction

As an alternative to extracting and isolating DHP from its natural host, the marine worm *Amphitrite ornata,* we have used the bacterium *Escherichia coli* as a host organism for the expression of the DHP protein. High levels of DHP expression in *E. coli* is vital given the large quantities of protein needed for many spectroscopic experiments (e.g. X-ray crystallography, NMR and EPR spectroscopy). NMR experiments particularly, if isotopic labeling is involved, require an optimal expression system. In *E. coli*, as well in most other organisms, there is a preference for usage of certain codons. There is a correlation between the frequency of certain codons and the level of its respective tRNA in the cell (*1*). This correlation dictates that expression of eukaryotic sequences containing codons rarely used in *E. coli* may cause translational problems leading to reduced quantity or fidelity of protein synthesized (*1, 2*). The arginine codons AGG and AGA are the two least frequently used codons in *E. coli* (*3*). Numerous studies have shown that usage of the arginine codon AGG in *E. coli* had adverse effects on protein expression (*2, 4, 5*). Additionally, studies have shown that having consecutive AGG codons in the reading frame leads to a high level of frameshifting (*6*). In addition, it has been shown that a processivity error in translation of a sequence with just two consecutive AGG codons can lead to a 50% decrease in protein yield (*4-6*).

Figure 1 shows that the protein coding region for DHP uses AGG to encode for arginine with a frequency of 57%. In *E. coli*, however, AGG typically occurs at a frequency of only 3%. This codon bias is thought to decrease the expression efficiency of DHP in an *E.*

coli host strain. The host strains of *E. coli* currently used are the BL21 (DE3) and Rosetta™ (DE3) cell lines. The Rosetta™ (DE3) cell line is a BL21 host derivative that was specifically designed to enhance the expression of eukaryotic proteins by supplying additional amounts of low frequency *E. coli* tRNAs, specifically the 6 rarely used tRNAs AGG, AGA, AUA, CUA, CCC, and GGA. Even though the Rosetta™ (DE3) cell line provides additional tRNAs for rare codons such as AGG, the fidelity and productivity of DHP expression is hypothesized to increase still via mutation of these AGG codons to the more amenable CGC arginine codons.

Initial experiments involved cloning the DHP gene ino the pUC 19 vector (*7*). Cloning the gene into the pET 16b expression vector with the Rosetta™ (DE3) cell line as the expression host was perfomed in order to enhance expression levels. The pET system is a high level protein expression system, which utilizes the highly specific T7 RNA polymerase promoter. A chromosomal copy of the gene for T7 RNA polymerase is under the control of the inducible lac promoter. Upon induction of a non-hydrolysable lactose analog, isopropyl-beta-D-thiogalactopyranoside (IPTG), T7 RNA polymerase is synthesized leading to expression of DHP via the T7 promoter (*8*). Upon full induction, the T7 RNA polymerase is so active that it focuses nearly all of the cells resources toward expression of the target gene. The pET 16b vector is shown in Figure 2 (*9*). The protein coding region for DHP is located between the restriction endonuclease sites *Nco* I and *Bam*H I.

The DHP gene contains four AGG codons. As discussed earlier there is a strong bias in *E. coli* against the usage of AGG for arginine. Although the Rosetta™ (DE3) cell line provides additional tRNAs for the AGG codons, the high frequency of usage and location of

the AGG codons within DHP leads us to believe that silent mutations of these codons to CGC could enhance DHP expression. Figure 3 shows the coding sequence of DHP. AGG codons are located at positions 14, 32, 33, and 122. Translation of a sequence with two or more consecutive AGG codons, such as R32 and R33 in DHP, could lead to errors, such as frameshifting, thereby leading to a decrease in both protein fidelity and productivity in *E. coli* (*4*).

Mutation of the four AGG codons to a more frequently used condon, such as CGC should have a substantial impact on DHP expression levels. Introduction of the four mutations was conducted using the QuikChange™ Multi Site-Directed Mutagenesis Kit (Stratagene). The kit offers a method for site-directed mutagenesis of up to five sites simultaneously and consists of three main steps (*10*). The first step involves the annealing of mutagenic primers to a denatured DNA template via thermal cycling followed by extension of the mutagenic strand via a *PfuTurbo*™ DNA polymerase. The resultant double stranded DNA molecule contains a parental strand and a strand with the introduced mutations. The second step involves the use of the restriction endonuclease *Dpn*I, which specifically cleaves methylated DNA, for digestion of the parental strand leaving only the mutated strand. The third and final step is transformation of the multi-mutated DNA into XL10-Gold™ ultracompetent cells, which allow for transformation of single stranded DNAs.

Materials and Methods

The pET 16b-DHP plasmid DNA used for the mutations was transformed into *E. coli* DH5α cells. The cells were then plated on ampicillin (Ap) plates and incubated overnight at

37° C. Single colonies were isolated from the plates and inoculated into 2mL LB Ap broth for overnight growth at 37 °C with shaking at 300 RPM. DNA from the growths was purified using QIAprep™ plasmid mini prep spin kits and then sent to MWG-Biotech, Inc. for sequencing. All DNA used for the mutagenic experiments were sequenced prior to use. The mutations were performed using the QuikChange™ Multi Site-Directed Mutagenesis Kit from Stratagene. After a round of mutation the DNA was transformed into the provided XL10-Gold™ ultracompetent cells. DNA was purified from transformants as discussed previously. The DHP2R and DHP4R mutants were transformed into competent Rosetta™ (DE3) cells and plated onto Ap/Chloroamphenicol (Cam) plates and grown overnight at 37° C. Single colonies were isolated and used to inoculate 2mL 2xYT broth containing both Ap/Cam which was subsequently grown at 37° C overnight with shaking at 300 RPM. This growth was used to inoculate a scaled up growth from which the cell pellets were harvested. The resulting soluble DHP protein was purified as describe elsewhere (*11*).

Results

Three mutagenic primers were used for the mutations. The R32R and R33R silent mutations (AGG to GCG) were incorporated onto the same primer. This primer also contained a silent Y28Y (TAC to TAT) mutation which incorporated a recognition site for the restriction endonuclease *Bsp*E I. This would allow for screening of the transformants by restriction analysis to see if the second and most important primer annealed. No silent mutations could be made to introduce restriction sites near the R14R and R122R mutation sites without alteration to a less frequently used codon. From the first round of mutations 12

colonies were isolated and the DNA of each was purified and cut with *Bsp*E I. The result is shown in Figure 4. The *Bsp*E I analysis indicated that the second primer annealed in 4 out of the 12 colonies isolated. After sending these 4 samples for sequencing only 2 of the 4 actually contained the desired R32R/R33R mutations. Sequencing also revealed that neither R14 nor R122 were successfully mutated. A second round of mutagenesis was then performed using the newly synthesized R32R/R33R DHP mutant (DHP2R) as the template. Out of this round 12 colonies were isolated and their DNA was extracted, purified, and sent for sequencing. Again neither of the two remaining mutations was present. A third round of mutagenesis was performed again using DHP2R as the template, but the *Dpn* I incubation period was increased by 50%. 16 colonies were then isolated and the DNA was purified as earlier. Sequencing results for these 16 colonies showed that the remaining two AGG mutations (R14R/R122R) had been successfully made for 2 of the 16 colonies. Expression levels of the DHP2R (R32R/R33R) and DHP4R (R14R/R32R/R33R/R122R DHP) mutant DHP genes were then compared.

Discussion

Percent usage of respective Arg codons for the DHP2R mutant appears to be the most comparable to that of *E. coli* (Figure 5). Even though DHP4R has the majority of its Arg codons encoded by the more frequently used CGC codon its usage frequency of CGC is now much higher than that in *E. coli.* The Rosetta™ cell line supplies additional tRNAs for AGG, AGA, AUA, CUA, CCC, and GGA codons. It does not supply additional tRNAs for CGC codons. One could hypothesize that while the DHP4R mutant should express higher

than w.t., it may not express as well as DHP2R due to the large excess of CGC codon usage. The advantage of the DHP2R or DHP4R mutant is possible expression of the protein from *E. coli* host strains other than Rosetta™ without adverse effects on protein levels.

The DHP2R mutant was grown as an initial comparison to see if the AGG to CGC mutations effected DHP protein expression. The DHP2R mutant contained the mutations for the two consecutive AGG codons at positions 32 and 33. The result was a cell pellet that was much redder in color than typical cell pellets from wild type DHP growths. A comparison between the two is shown in Figure 6. The red color in the cell pellet is an indicator of higher levels of the red DHP holoprotein. It is apparent from visualizing the cell pellets that the 2R mutant expresses better than w.t. DHP in Rosetta™ cells. It appears that mutating the two consecutive AGG codons to CGC has had a dramatic effect on the amount of DHP expressed. A comparison of the arginine codon usage in DHP, DHP2R, and DHP4R vs. the usage in *E. coli* can be seen in Figure 5. Preliminary data suggested that DHP protein yields from the DHP2R mutant showed expression levels near ~15 mg/L. This may be ~5x that of normal yields from w.t. DHP. Analysis of the complete DHP4R mutant indicate expression levels that average ~20 mg/L, indicating at least a 6x or 7x increase in protein expression levels. Additional studies have resulted in yields as high as ~50 mg/L with optimization of growth conditions, as seen elsewhere (*11*). In nutrient deficient minimal media, expression of the DHP4R gene has resulted in protein yields as high as 24 mg/L, indicating the effectiveness of the codon optimization (*12*). Up to the present, however, we have not used induction of the pET system in the BL21 (DE3) cell line. The fact that we still get protein expression with the lack of induction shows that the T7 promoter is not extremely stringent.

There is still low level expression of T7 RNA polymersase from the *lac* promoter in DE3 lysogens, this therefore leads to basal expression of the target DHP protein (*9*).

References

(1) Del Tito, B. J., Ward, J. M., Hodgson, J., Gershater, J. L., Edwards, H., Wysocki, L. A., Watson, F. A., Sathe, G., and Kane, J. F. (1995) Effects of a minor isoleucyl tRNA on heterologous protein translation in *Esherichia coli*. *J. Bacteriol. 177*, 7086-7091.

(2) Kane, J. F. (1995) Effects of rare condon clusters on high-level expression of heterologous proteins in *Escherichia coli*. *Curr. Opin. Biotech. 6*, 494-500.

(3) Zhang, S., Zubay, G., Goldman, E. (1991) Low-usage condons in *Escherichia coli*, yeast, fruit fly and primates *Gene 105*, 61-72.

(4) Spanjaard, R. A., van Duin, J. (1988) Translation of the sequence AGG-AGG yields 50% ribosomal frameshift. *Proc. Natl. Acad. Sci. U. S. A. 85*, 7967-7971.

(5) Kurland, C., Gallant, J. (1996) Errors of heterologous protein expression. *Curr. Opin. Biotech. 7*, 489-493.

(6) Rosenberg, A. H., Goldman, E., Dunn, J. J., Studier, F. W., Zubay, G. (1993) Effects of consecutive AGG codons on translation in *Escherichia coli*, demonstrated with a versatile codon test system. *J. Bacteriol. 175*, 716-722.

(7) Osborne, R. L., Taylor, L. O., Han, K. P., Ely, B., and Dawson, J. H. (2004) Amphitrite ornata dehaloperoxidase: enhanced activity for the catalytically active globin using MCPBA. *Biochem. Biophys. Res. Comm. 324*, 1194-1198.

(8) pET-16b vector map, Cat. No. 69662-3, (Novagen, Inc.)

(9) pEt system manual 10th ed. (2002) (Novagen, Inc.)

(10) QuikChange^{TM} Multi Site-Directed Mutagenesis Kit, *Instruction Manual* (Stratagene) Cat. No. 200515, Rev. No. 124003a

(11) Davis, M. F., Gracz, H., Vendeix, F. A. P., de Serrano, V., Somasundaram, A., Decatur, S. M., and Franzen, S. (2009) Different modes of binding of mono-, di, and tri-halogenated phenols to the hemoglobin dehaloperoxidase from *Amphitrite ornata*. *Biochemistry 48*, 2164-2174.

(12) Davis, M. F., Bobay, B. G., and Franzen, S. (2009) Separation of inhibitor and substrate binding locations in the globin dehaloperoxidase. (In preparation)

Figures

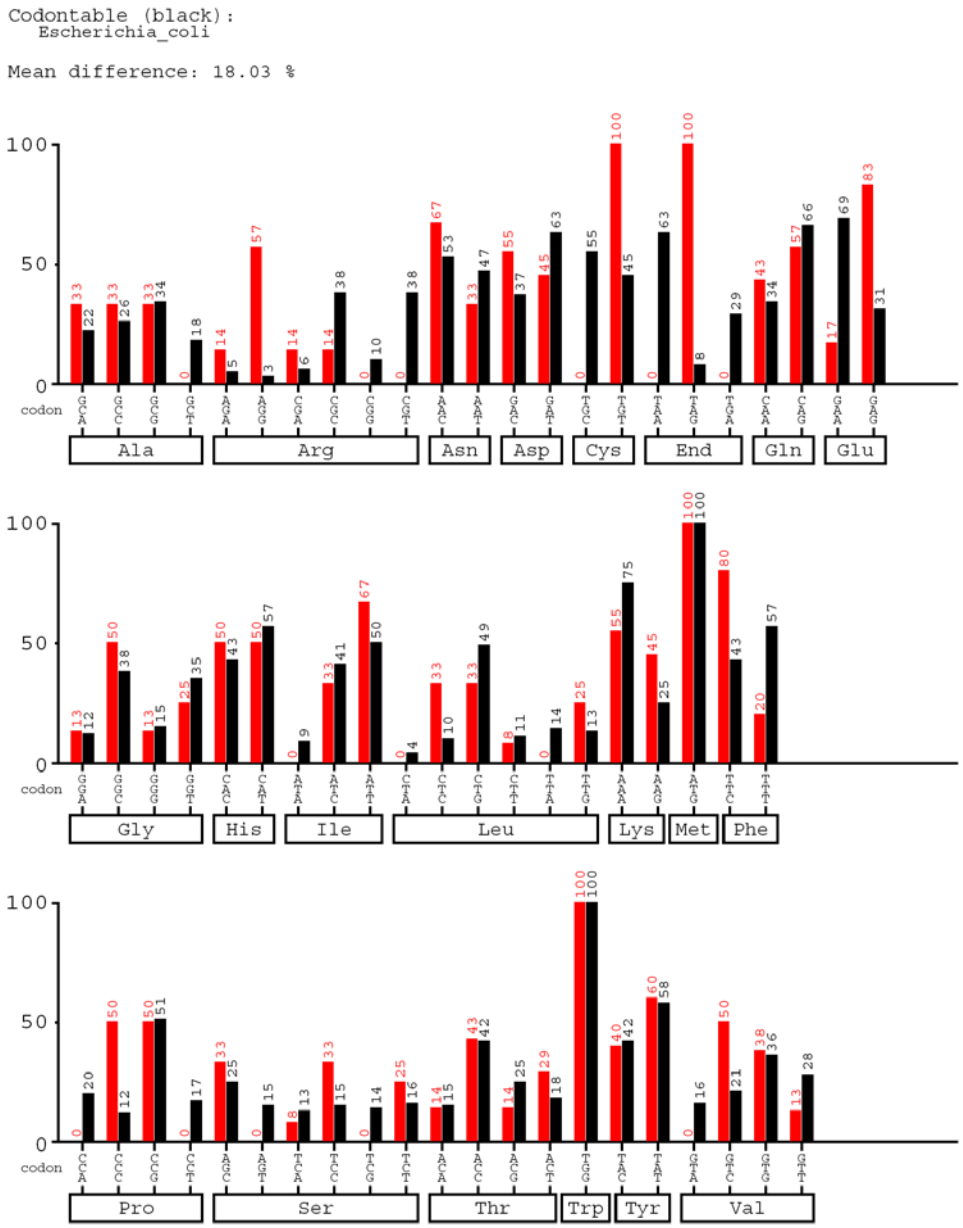

Figure 1. Codon usage in *A. ornata* DHP vs. codon usage in *E. coli*. The red bars represent codon usage in DHP and the black bars represent usage in *E. coli*.

pET-16b sequence landmarks	
T7 promoter	466-482
T7 transcription start	465
His• Tag coding sequence	360-389
Multiple cloning sites	
(*Nde* I -*Bam*H I)	319-335
T7 terminator	213-259
lacI coding sequence	869-1948
pBR322 origin	3885
bla coding sequence	4646-5503

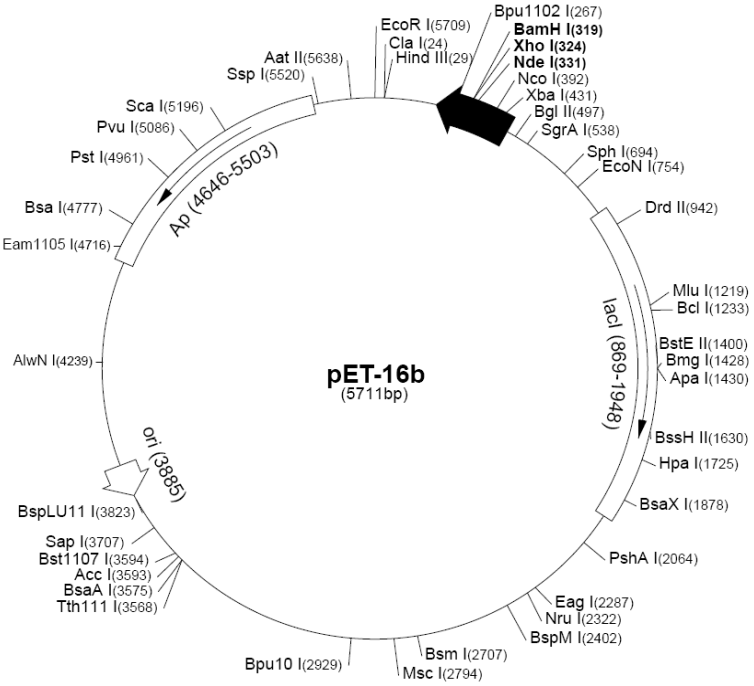

Figure 2. Map of the pET 16b plasmid cloning vector. The protein coding region for DHP is located between *Nco*I and *Bam*HI.

```
ATGGGGTTTAAACAAGATATTGCCACCATCCGCGGTGATCTCAGGACCTAT
M  G  F  K  Q  D  I  A  T  I  R  G  D  L  R  T  Y

GCACAGGACATTTTCCTCGCATTTTTGAATAAGTACCCGGACGAGAGGAGG
A  Q  D  I  F  L  A  F  L  N  K  Y  P  D  E  R  R

TACTTCAAAAACTATGTCGGCAAATCTGACCAAGAGCTCAAGTCAATGGCC
Y  F  K  N  Y  V  G  K  S  D  Q  E  L  K  S  M  A

AAGTTCGGTGATCACACTGAGAAAGTGTTCAACCTGATGATGGAAGTTGCG
K  F  G  D  H  T  E  K  V  F  N  L  M  M  E  V  A

GACCGAGCCACCGATTGTGTCCCCCTTGCGTCCGACGCCAACACACTCGTC
D  R  A  T  D  C  V  P  L  A  S  D  A  N  T  L  V

CAGATGAAACAGCATTCCAGCCTGACGACTGGAAACTTCGAGAAACTGTTC
Q  M  K  Q  H  S  S  L  T  T  G  N  F  E  K  L  F

GTGGCATTGGTGGAGTATATGAGAGCGTCTGGCCAGTCCTTCGACTCTCAA
V  A  L  V  E  Y  M  R  A  S  G  Q  S  F  D  S  Q

AGCTGGGATAGGTTCGGCAAGAATTTGGTCTCCGCGCTGAGCAGCGCAGGC
S  W  D  R  F  G  K  N  L  V  S  A  L  S  S  A  G

ATGAAGTAG
M  K  *
```

Figure 3. The 5' to 3' DNA sequence of the DHP. All AGG codons are labeled with red text.

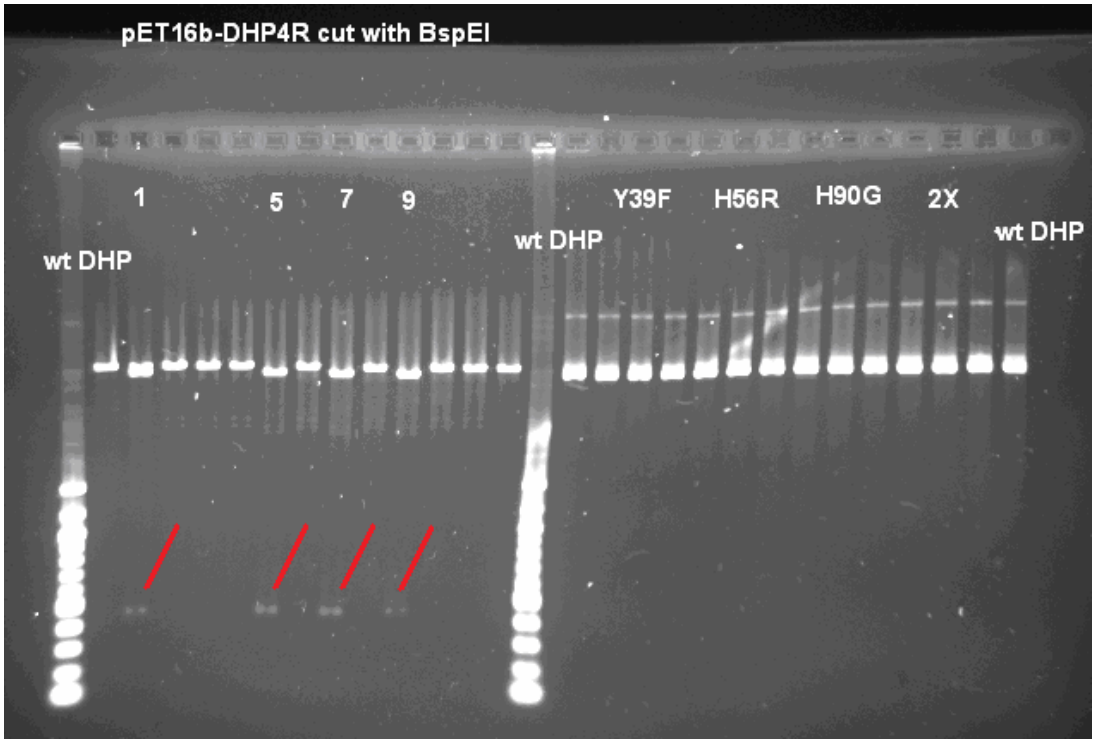

Figure 4. Gel showing the results of the first round of mutagenesis cut with BspE I. Lanes 1, 5, 7, and 9 showed successful cuts at the restriction site introduced near R32 and R33. The right side of the gel shows all mutations of DHP previously made.

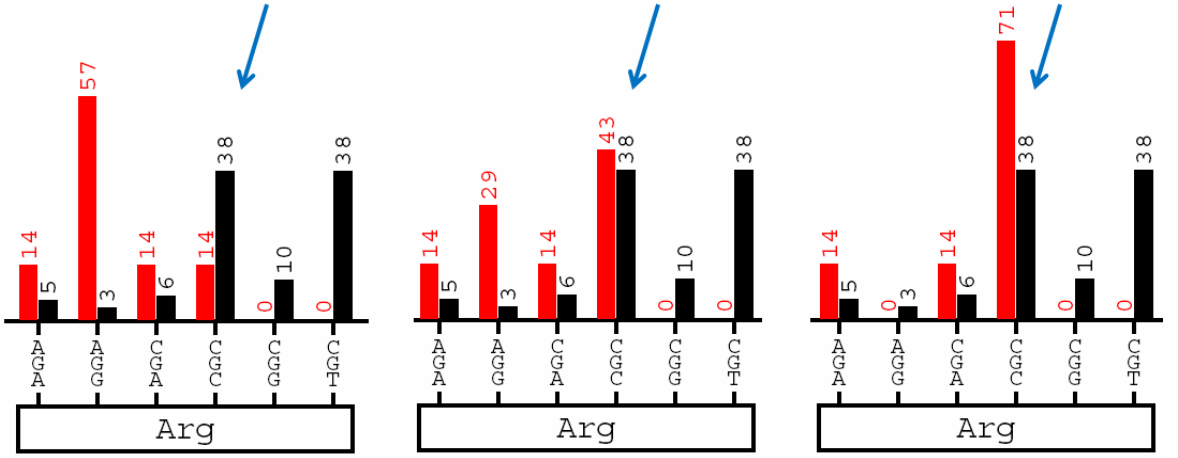

Figure 5. Comparison of Arg codon usage by DHP (left), DHP2R (middle), and DHP4R (right) vs. codon usage in *E. coli.* DHP codons usage is colored red. *E. coli* codon usage is colored black. Note the change in % usage AGG and CGC codons as the various Arg mutations are introduced. The DHP2R appears to be the most similar in codon usage to *E. coli.*

Figure 6. Comparison of cell pellets from w.t. DHP growth (left) and DHP2R mutant growth (right). The red color of the DHP2R growth is an indicator of the presence of increased DHP.

CHAPTER 3

Different Binding Modes of Mono-, Di- and Trihalogenated Phenols to the Hemoglobin Dehaloperoxidase from *Amphitrite ornata*

Abstract

The hemoglobin dehaloperoxidase (DHP), found in the coelom of the terebellid polychaete *Amphitrite ornata*, is a dual function protein that has the characteristics of both hemoglobins and peroxidases. In addition to oxygen transport function, DHP readily oxidizes halogenated phenols in the presence of hydrogen peroxide. The peroxidase activity of DHP is high relative to wild type myoglobin or hemoglobin, but the most definitive difference in DHP is a well-defined substrate-binding site in the distal pocket, which was reported for 4-iodophenol in the X-ray crystal structure of DHP. The binding of 2,4,6-trihalogenated phenols is relevant since 2,4,6-tribromophenol is considered to be the native substrate and 2,4,6-trichlorophenol also gives high turnover rates in enzymatic studies. The most soluble trihalogenated phenol, 2,4,6-trifluorophenol, acts as a highly soluble structural analog to the native substrate 2,4,6-tribromophenol. To better understand substrate binding, we compared the most soluble substrate analogs, 4-bromophenol, 2,4-dichlorophenol and 2,4,6-trifluorophenol using ^{1}H and ^{19}F NMR to probe substrate-binding interactions in the active site of the low-spin metcyano adduct of DHP. Both mono- and dihalogenated phenols induced changes in resonances of the heme prosthetic group and an internal heme edge side chain, while ^{1}H NMR, ^{19}F NMR, and relaxation data on a 2,4,6-trihalogented substrate indicate a mode of binding with little discernable interaction in the vicinity of the heme.

Introduction

The terebellid polychaete *Amphitrite ornata* inhabits estuarine mudflats with other marine annelids, such as *Notomastus lobatus*, *Saccoglossus kowalevskii,* and *Thelepus crispus*, which secrete brominated aromatic compounds as a means of territorial protection (*1-3*). While such repellents would be deterrents for some organisms, *A. ornata* has developed a novel defense mechanism in the hemoglobin dehaloperoxidase (DHP). DHP is found in the coelom of *A. ornata* and is one of two hemoglobins in the organism (*4*). Structurally, the DHP monomer is homologous to myoglobin containing the globin fold with 8 helices and a heme prosthetic group ligated to the protein backbone via a proximal histidine (*5, 6*). The novelty of DHP lies in its ability to oxidatively dehalogenate haloaromatics found in its environment while simultaneously maintaining an oxygen storage function consistent with its hemoglobin structure (*7-9*). DHP has the highest turnover rate for 2,4,6-trihalogentated phenols, which have been shown to be extremely toxic to marine life (*10, 11*).

The first X-ray crystal structure of substrate-bound DHP revealed that 4-iodophenol binds in the distal pocket, but is not coordinated to the heme iron (Figure 1) (*5, 6*). This internal binding site distinguishes DHP, not only from other globins, but also from other heme peroxidases that typically bind substrates on the heme periphery (*12*). According to this X-ray structure (1EWA) the average occupancy of the substrate analog 4-iodophenol in the internal binding site is only ~23% (*6*). Examination of the substrate-bound DHP crystal structure shows primary structural changes occurring solely at the heme and surrounding residues when substrate is bound. We have also confirmed by X-ray crystallography that

para-halogenated (4-bromo- and 4-iodophenol) phenols can occupy this internal binding site (de Serrano and Franzen, unpublished data). However, 2,4-di- and 2,4,6-trichlorophenols do not readily enter the distal pocket in the crystal form. This is ironic considering the high turnover rate of 2,4,6-trihalophenols, which are the most active substrates for DHP. 2,4,6-trifluorophenol (2,4,6-TFP) has been shown to enter the distal pocket of the metaquo and carbonmonoxy forms of DHP at low temperature. We have recently shown that 2,4,6-TFP can displace the coordinated water molecule of the metaquo form at low temperature (*13*). However, it is apparently expelled from the distal pocket in the carbonmonoxy form at room temperature *(14)*. The interaction of diatomic ligands and hydrogen peroxide, in the internal binding site is highly relevant to the function of DHP. The competition for binding in the distal pocket may involve the site occupied by 4-iodophenol in the 1EWA crystal structure.

We have used the carbonmonoxy form of DHP (DHPCO) as a model for the interaction of halogenated phenols and a heme-coordinated diatomic ligand in the distal pocket. 2,4,6-TFP has been observed to enter the distal pocket of the DHPCO at low temperature at pH 5.5, but not at room temperature (*14*). We have recently shown that 2,4,6-TFP also binds to the DHPCO form at room temperature at pH 4.7 (Nienhaus et al., Biochemistry in Press). The functional relevance of this binding is still not clear. Since trihalogenated substrates, such as 2,4,6-tribromophenol (2,4,6-TBP), exhibit the highest turnover rates, it is key from a functional aspect to determine whether oxidation of the substrate can occur in the internal site. The fact that the native substrate, 2,4,6-TBP, and other trihalophenols do not bind in that site under physiological conditions at room temperature and pH 7.4 presents a conundrum for DHP function. These data suggest that the

internal binding site is not the active site. Therefore, the binding site for the native substrate, 2,4,6-TBP, has not yet been determined. The well-defined internal binding site for monohalogenated phenols, such as 4-bromophenol, may interfere with the binding of oxygen or hydrogen peroxide and could regulate either the hemoglobin or peroxidase function of DHP.

The X-ray crystal structure of DHP shows that the entire 4-iodophenol molecule binds within 6 Å of the iron center (*6*). The close proximity of the internal molecular binding site to the heme permits the application of paramagnetic NMR experiments to elucidate specific structural changes near the heme iron when molecules bind in the internal binding pocket (*15*). NMR has been used extensively for active site characterization of high (S = 5/2) and low (S = 1/2) spin forms of many peroxidases and globins (*16-23*) and provides a sensitive method for probing structural details of the heme prosthetic group. Addition of a strong-field ligand, e.g., cyanide, to the ferric Fe(III) oxidation state of DHP creates a low spin (S = 1/2), paramagnetic species. This metcyano form is the focus of the current NMR study, as active site resonances are much sharper and less dispersed in the low-spin form than the high-spin, metaquo counterpart.

Herein, we report the first assignment and active site characterization of DHP using NMR spectroscopy and present evidence that there is both an internal and external binding site for halogenated phenols. Assignment of the resonances was accomplished primarily through natural abundance ^{13}C-^{1}H HSQC (*24*) and WEFT-NOESY (*25*) experiments. Differential perturbation of certain active site resonances were observed upon titration of three different halogenated phenols chosen for their high water solubility: 4-bromophenol (4-

BP), 2,4,-dichlorophenol (2,4-DCP), and 2,4,6-trifluorophenol (2,4,6-TFP). The effects of substrate binding were also compared over a wide range of pH.

Materials and Methods

Protein Preparation. The pET 16b plasmid containing the 6XHisDHP4R DNA insert (*7*) was transformed into competent BL21 (DE3) *Escherichia coli* cells and then plated out on LB agar plates with 100 μg/mL ampicillin (Ap) and allowed to grow at 37 °C for ~14 hrs. Single colonies were isolated and starter growths were used to inoculate 6 L *E. coli* growths. The cells were incubated at 37 °C with shaking for 13 hrs. Expression of 6XHisDHP4R protein was not induced via addition of ITPG. Basal expression of the protein in the non-stringent BL21 (DE3) cell line yielded significantly high levels of holoprotein. The cells were collected via centrifugation, then allowed to freeze overnight at -20 °C. The cells were re-suspended in lysis buffer (2 mLs/per gram cell pellet) (50 mM NaH_2PO_4, 300 mM NaCl, 10 mM imidazole, pH 6) and lysozyme was added to a final concentration of 1 mg/mL. The cell slurry was allowed to stir at 4 °C for 1 hr. The slurry was then sonicated for 30 min. and 200 μL of DNase I (16 mg/mL) and RNase A (10 mg/mL) were added. The cell slurry was again stirred at 4 °C for ~1 hr before freezing overnight at -20 °C. After re-thawing, the cells were centrifuged at 18000 rpm for 45 minutes and supernatant His-tagged DHP protein was collected. The crude His-DHP was applied to a Ni-NTA agarose column (Qiagen), washed with 50 mM NaH_2PO_4, 300 mM NaCl, 20 mM imidazole, pH 6 buffer, and eluted with 50 mM NaH_2PO_4, 300 mM NaCl, 250 mM imidazole, pH 6 buffer. The isolated His-DHP was buffer exchanged in 20 mM KH_2PO_4, pH 6 using a Sephadex G-25 column. The protein was

further purified on a CM 52 ion exchange column and was eluted stepwise between pH 6, 20 mM KH_2PO_4 and pH 6, 150 mM KH_2PO_4. The concentration of the protein was determined using the Soret band at 406 nm with a molar absorptivity of 116400 M^{-1} cm^{-1} (*26*). Final yields of purified w.t. DHP protein was approximately 20 mg/L broth with A_{406}/A_{280} ratios greater than 4. Purified His-DHP was exchanged in 99.9% D_2O, 100 mM potassium phosphate buffer, pH 7. The reported pH values are left uncorrected for the deuterium isotope effect. The protein was concentrated to a final concentration of ~1-2 mM, and KCN was added to approximately 10 fold excess.

^{1}H NMR Experiments. All ^{1}H NMR and ^{19}F NMR spectra were recorded on a either a 500MHz AVANCE Bruker or 300MHz Bruker NMR spectrometer. The 1D NOE experiments were performed using a decoupling pulse to saturate the resonance of interest (*27*). Identical spectra were then collected with the decoupler slightly off-resonance. Difference spectra were generated by subtracting the on-resonance spectrum from the off-resonance spectrum. The magnitude of the NOE did not increase after 200 ms of resonance saturation via the decoupler. Thus, the 1D NOE data were collected in the steady state regime with a saturation time of 200 ms. The T_1 experiments were obtained using a standard inversion-recovery pulse sequence without a presaturation pulse. The τ values for the TFP relaxation experiments were: 0.2, 0.4, 0.8, 1.6, 3.2, 6.4, 10, and 20 s, with a delay time, *t*, of 22 s. T_2 measurements were collected using a standard Carr-Purcell Meiboom-Gill (CPMG) pulse sequence. The WEFT-NOESY data were collected utilized a 300 ms recovery-delay and 100 ms mixing time. The ^{1}H-^{13}C HSQC experiments were recorded using a recycle time of 200 ms with J = 200 Hz. 2D NOESY spectra incorporating a presaturation pulse were

collected using a spectral width of 27000 Hz. Best results were obtained with a mixing time of 100 ms and a delay time of 1.2 seconds. Gradient-selective COSY spectra were also collected over a spectral width of 27000 Hz. A total of 2048 t_2 points and 512 t_1 blocks were collected with a delay time of 1.2 seconds.

UV-Vis Enzymatic Assays. For all experiments the protein was exchanged into 100 mM potassium phosphate buffer, pH 7. The absorption data was collected using a Hewlett Packard 8453 multi-wavelength spectrometer. The spectra were collected every 5 seconds over a 60 second time frame. The conditions used for the assays were: 5 μM DHP, 360 μM H_2O_2, and 120 μM substrate. Substrate turnover was monitored by the disappearance of the halophenol absorption bands (4-BP – 280 nm; 2,4-DCP – 284 nm; 2,4,6-TFP – 272 nm).

Results

The low-spin metcyano form of DHP at pH 7.0, 25 °C, exhibits a wide dispersion of hyperfine-shifted heme and active site resonances, spanning from -12 ppm to 27 ppm as seen in Figure 2 and reported in Table 1. ^{13}C-^{1}H HSQC, WEFT-NOESY, gradient-selective COSY, 1D NOE difference spectra, and presaturation NOESY were used to assign the majority of the active site resonances. The spectra of resonances pertinent to the substrate binding study are presented. Additional resonance assignments are provided in the Supporting Information.

Examination of the X-ray structures show that only the 3-CH_3 and 5-CH_3 heme methyls are within NOE distance of Phe side chains (*5, 6*), and only the former would have NOE connectivity to a vinyl substituent. The heme methyl at 24.5 ppm, assigned as the 3-

CH_3 heme methyl, exhibits dipolar connectivity to a scalar coupled three-proton system at 14, -1.1, and -1.5 ppm, which is assigned as the vinyl 4αH and 4βHs, respectively (Figure 3) and dipolar connectivity to the CεHs and CδHs resonances of the well-resolved Phe97 side chain at 12.6 and 9.4 ppm (Table 1). The scalar coupled three-proton spin system was readily assigned as a heme vinyl group due to characteristic hyperfine-shifting where the β-vinyl resonances are shifted to much lower frequencies than the α-resonance due to a large decrease in the contact shift contribution (*28*). While the 4β protons are not observed in the ^{13}C-^{1}H HSQC spectra (Figure 4), the 4α resonance was readily assigned at 14 (^{1}H) and 52.8 ppm (^{13}C). The Phe97 side chain was assigned by the natural abundance ^{13}C chemical shifts, CζH at 134.5, CεHs at 132.6, CεHs at 132.2 ppm, and scalar coupling between the ring protons (Supporting Information).

The 4αH resonance also exhibits an NOE cross-peak to the 5-CH_3 heme methyl at 4.3 ppm. The 4.3 ppm resonance is assigned as the 5-CH_3 due the degree of hyperfine shifting in the ^{13}C dimension (-14.8 ppm) and NOEs to 4-proton spin system indicative of the 6-propionate chain. This 4-proton spin system at 11.3, 9.4, 1.2 and 0.3 ppm exhibits mutual dipolar coupling with the 5-CH_3 heme methyl. Only the two 6βH resonances of the propionate chain (1.2 and 0.3 ppm (84.4, ^{13}C)) were found in the ^{13}C-^{1}H HSQC map. NOESY crosspeaks of the two 6αHs (11.3, 9.4 ppm) are observed at higher contour levels. Addition NOESY connectivity between the 6-propionate resonances can be found in the Supporting Information. The remaining downfield heme methyl at 26.8 ppm is assigned as 8-CH_3 based on NOE connectivity to two hyperfine-shifted methylene groups at 12.5, 10.2 ppm (-32.7, ^{13}C) and 0.4, -0.2 ppm (118.8, ^{13}C) indicative of the 7-propionate chain.

Inspection of the COSY data (Supporting Information) shows both methylene groups are scalar coupled, thus confirming their assignment as the 7αHs and7βHs, respectively.

The order of heme methyl shifts in metcyano DHP is 8 > 3 > 5 with the 1-CH_3 not yet assigned. The 1-CH_3 in low spin metcyano heme proteins, at ambient temperatures, typically occurs at lower frequencies than the 5-CH_3 heme methyl. The relative order of heme methyl shifts is correlated to the angle, Φ, of the proximal histidine projection onto the N_{II}-Fe-N_{IV} axis of the heme plane (*23, 29-33*). According to the X-ray structure of DHP the axial histidine Φ is ~ 113° as seen in Scheme 1A (*5, 6*). Models and experimental data have shown the 113° angle corresponds to a 3 > 8 > 5 > 1 order of heme methyls (*33-35*), which is not corroborated by the 8 > 3 > 5 > 1 ordering found in the ^{1}H NMR spectrum. Hence, the NMR data suggests the axial histidine in metcyano DHP is rotated by ~ -25° to ~ 90° in solution, as seen in Scheme 1B.

Effects of Addition of Halogenated Phenols to DHPCN. The effects of three different substrates on the active site of DHPCN can be seen in Figure 5. The molecules 4-BP, 2,4-DCP, and 2,4,6-TFP were chosen for their high water solubility and/or structural similarities to substrates that have high product turnover in DHP. The native substrate 2,4,6-TBP (*1*) and, commonly used model substrate, 2,4,6-trichlorophenol (2,4,6-TCP) (*7*), were not used in the NMR binding studies due to their poor solubility. However, 4-BP is structurally comparable to 4-iodophenol, which was shown to bind in the internal distal cavity of DHP in current X-ray structures (*6*), while 2,4,6-TFP provides a comparison to the native substrate, 2,4,6-TBP, and most active laboratory substrate, 2,4,6-TCP. Figure 5 shows there are two different effects induced by substrate binding. The mono- and dihalogenated 4-BP and 2,4-

DCP cause similar effects within the active site of DHPCN. In both cases the 3-CH_3 heme methyl and internal Phe97 exhibit significant line broadening and when substrate is added in excess. The Phe97 side chain and heme 3-CH_3 are separated by ~4.5 Å according to the X-ray structures (*5, 6*) with the Phe side chain located slightly proximal to the 3-CH_3 heme methyl. Introduction of either 4-BP or 2,4-DCP also causes a slight change in chemical shift of the 7α propionate resonances. The 8-CH_3 resonance exhibits a slight -0.2 ppm shift in the presence of 4-BP and +0.1 ppm in the presence of 2,4-DCP. On the other hand, 2,4,6-TFP interaction with DHP does not create frequency perturbations and/or line broadening of active site resonances in DHPCN at the pH values studied. Comparing the effects of the substrate titrations provides initial evidence for different modes of binding for substrates 2,4-DCP and 4-BP compared to 2,4,6-TFP. The differences in the nature of binding interactions are observed even when a significant molar excess of 2,4,6-TFP is used in DHPCN solutions (Supporting Information).

^{19}F NMR and relaxation data on substrate 2,4,6-TFP in DHPCN. Utilization of ^{19}F NMR permits direct observation of the substrate as a probe of binding. In general, any binding interactions between the smaller 2,4,6-TFP substrate and DHP will result in a decrease in T_2 time and, therefore, an increase in linewidth due to a slower molecular tumbling rate. Alternatively, depending on the rate of exchange, separate resonances may be visible for the fluorinated substrate; one for both the bound and free state of the substrate (*36, 37*).

Figure 6 shows the ^{19}F NMR spectra of substrate 2,4,6-TFP and titration of 2,4,6-TFP to the fully formed DHPCN complex. A significant change in chemical shift is observed in

the *para*- (F4) resonance as it is titrated to DHP. The F4 resonance of TFP, at -123.2 ppm, shifts to -124.4 ppm when the substrate is introduced at a 1:1 ratio. Additionally, the *ortho*- (F2/F6) resonance shifts from -131.2 to -132.1 ppm. During the course of the titration the F4 and F2/F6 resonances shift to slightly higher frequencies, and approach the chemical shifts of 2,4,6-TFP without presence of protein. Slight broadening of both resonances is observed at 1:1 and 3:1 ratios of 2,4,6-TFP to DHPCN. The F4 resonance exhibits a 17% increase in linewidth (24 Hz to 28 Hz), while the linewidth of the F2/F6 resonance increases by 33% (18 Hz to 24 Hz) at a 1:1 ratio. Figure 7 A and B illustrates the change spin-lattice relaxation (T_1) and transverse relaxation (T_2) times of the 2,4,6-TFP *meta*-protons when the molecule is added to DHPCN, respectively. The T_1 time decreased from 8.1 to 5.8 s and the T_2 time decreased from 6.4 to 1.5 s when 2,4,6-TFP is added to DHPCN at a 15:1 molar ratio, respectively.

Enzymatic activity assay for substrates 4-BP, 2,4-DCP and 2,4,6-TFP. The hypothesis that there are two modes of binding is supported by significant difference in reactivity of the three phenols studied in enzymatic assays (see Supporting Information). Using a standard DHP assay, we found that 4-BP has little or no activity. On the other hand, 2,4,6-TFP is a good substrate and shows turnover rates comparable to the native substrate, 2,4,6-TBP *(49)*. The rate of 2,4,6-TFP oxidation is approximately 3 times slower than the widely used test substrate, 2,4,6-TCP *(48,49)*. By contrast, 2,4-DCP shows significantly less activity than the 2,4,6-trihalophenols. There is also an increase in the baseline due to scattering when this substrate is used, which may be indicative of polymerization or other side reactions. Thus the internal and external binding observed in the NMR signals are

correlated with differences in substrate reactivity such that 4-BP and 2,4-DCP, which bind in the internal site, are not highly active and 2,4,6-TFP, that interacts with the protein at an external site, is active.

Discussion

The dehaloperoxidase activity of DHP towards a variety of halogenated phenols, including bromo-, chloro- and even fluorophenols was first reported in 1996 *(2)*. It was subsequently revealed that the original turnover numbers are not accurate *(8)*. The X-ray crystal structure revealed the binding of 4-iodophenol in the distal pocket, which was assigned as the active site *(3)*. Yet, the native substrate is considered to be 2,4,6-TBP and there is no report of activity for 4-BP. The present study uses soluble halogenated phenols to systematically test the differences in binding and correlated activity of those molecules. The molecules, 4-BP and 2,4-DCP, appear to bind or at least interact at an interior site in DHPCN and are poor substrates in a typical ferric DHP peroxidase assay using H_2O_2. On the other hand, 2,4,6-TFP interacts with the protein at an exterior site and has activity comparable to the native substrate, 2,4,6-TBP. In retrospect, this result should not be surprising, since most known peroxidases have exterior substrate binding sites *(12)*.

Binding of the monohalogenated (4-BP) and dihalogenated (2,4-DCP) substrates demonstrated comparable effects on the ^{1}H NMR spectrum of the metcyano adduct of DHP. The effects include perturbations along the internal heme edge near the 3-CH_3 heme methyl and Phe97 side chain. The broadening of these resonances appears to be greatest when the solution pH < pKa of the substrate (Supporting Information). However, even at alkaline pH

(pH 9.9) there is still observable broadening associated with the addition of 4-BP and 2,4-DCP. However, the effect of 4-BP and 2,4-DCP binding is localized to an internal region near the heme 3-CH_3 and Phe97 residue. There is no broadening of other active site resonances, such as the 8-CH_3. Broadening of specific resonances of the heme and its substituents has been observed previously in substrate binding studies of horseradish peroxidase (HRP). Titration of the substrate benzohydroxamic acid to HRPCN resulted in significant broadening of the 8-CH_3 heme methyl and a 7α propionate resonance, in a manner similar to the observed broadening of the 3-CH_3 and Phe97 resonances in DHPCN (*39-41*). Substrate binding is known to be external to the distal pocket in HRP. However, the 3-CH_3 and Phe97 are more deeply buried than the 8-CH_3 heme methyl and 7α protons in both DHP and HRP. Consequently, the binding interactions between 4-BP and 2,4-DCP and DHPCN appear to occur at the internal site in the distal pocket. On the other hand, WEFT-NOESY and presaturation NOESY experiments did not reveal NOEs between DHPCN and the substrate analogs, 4-BP and 2,4,-DCP. The lack of NOEs may be due to fast exchange of the substrate between bound and free states. These experiments suggest that the binding of 4-BP, and 2,4-DCP in the distal pocket of DHPCN may involve rapid exchange with solvent.

While the addition of 4-BP and 2,4-DCP induced observable changes in active site resonances, 2,4,6-TFP essentially had no effect on the ^{1}H NMR spectrum. The ^{19}F NMR data, however, show that the F2/F6 and F4 fluorine resonances of 2,4,6-TFP exhibit slight broadening and perturbations in chemical shifts when present at 1:1 molar ratio with DHPCN. Resonance broadening, and/or changes in chemical shift, is commonly used to identify binding of small molecule protein ligands (*42-44*). The linewidth of the F2/F6 and

F4 resonances at 1:1 molar ratio DHPCN to 2,4,6-TFP increases by 33 and 17%, respectively. This broadening translates to a decrease in apparent transverse relaxation time (T_2) from 17.7 ms to 13.3 ms for F2/F6, and 13.3 ms to 11.4 ms for F4 (*45*) as discussed in the Supporting Information. The decrease in T_2 suggests a longer rotational correlation time (τ_c) of the molecule (*46*). Based on the Stokes-Einstein equation τ_c = 34 ns for DHPCN assuming that the radius is r = 20 Å at a viscosity of 1 centipoise, whereas free 2,4,6-TFP would be expected to have τ_c on the picosecond time scale (see Supporting Information).

To elucidate the binding of 2,4,6-TFP to DHPCN, T_1 and T_2 relaxation experiments were used to observe changes in the rotational correlation time, τ_c. The T_1 relaxation time of the 2,4,6-TFP *meta*-protons decreased from 8.1 s to 5.8 s and the T_2 relaxation time of these same resonances decreased from 6.4 to 1.5 seconds when 2,4,6-TFP was present at a 15:1 molar ratio (Figure 7). The high ratio of 2,4,6-TFP:DHPCN was needed to fully resolve the 2,4,6-TFP signal over the background of the protein resonances. Because the same value for T_1 is consistent with two separate rotational correlation times in the limits $\omega_o\tau_c \ll 1$ and $\omega_o\tau_c \gg 1$, T_2 values were analyzed to determine whether the decrease in T_1 is attributable to a significant decrease in τ_c of 2,4,6-TFP in the presence of DHPCN (*47*). The analysis of the decrease in T_1 and T_2 times corresponds to $\tau_c \sim 35$ ps for free 2,4,6-TFP and $\tau_c \sim 50$ ns for 2,4,6-TFP in the presence of DHPCN. This increase in τ_c is in accord with the expected value for complexation of 2,4,6-TFP to DHPCN. Further details of the analysis are supplied in the Supporting Information. Although the analysis is based on a single dipolar interaction between a ^{19}F nucleus at a distance of 2.47 Å from the meta hydrogen nucleus, we recognize that the relaxation may be more complicated in the bound state. The point of the analysis is

to establish the 2,4,6-TFP binds at an external site and behaves differently from the other two phenols studied, 4-BP and 2,4-DCP.

Although, the relaxation data are consistent with an external binding site for 2,4,6-TFP, the location of that site has not been determined based on the data obtained here. FTIR studies at cryogenic temperatures showed that 2,4,6-TFP can bind in the internal substrate binding pocket of the CO form of ferrous DHP, which is isoelectronic with DHPCN *(14)*. However, at physiologically relevant pH there was no binding of 2,4,6-TFP above 260 K in the internal site *(14)*. At room temperature, 2,4,6-TFP binding in the distal pocket is also observed in the CO form using FTIR, but only at pH < 4.7 (Nienhaus et al., Biochemistry in Press). It is difficult to study in DHPCN at pH < 5.0 to investigate the relevance of this observation using NMR due to the protonation of CN^- to form HCN. The ^1H NMR data corroborate the FTIR data in that no observable internal pocket perturbations are observed for the trihalogenated substrate at ambient temperatures in the pH range from 5.5 < pH < 9.9.

The origin of the alteration of axial histidine torsion angle shown in Scheme 1 requires further explanation. The value of the torsion angle $\Phi \sim 113^o$ shown in Scheme 1A was obtained by X-ray crystallography. The X-ray structures further indicates stabilization of the proximal histidine H89 by a strong hydrogen bond of the imidazole Nε-H to the carbonyl oxygen of L83 with a N…O distance of 2.74 Å (*5, 6*). The value of $\Phi \sim 90^o$ in solution (Scheme 1B) is based on the well-established correlation of the ordering of heme methyl hyperfine shifts. The discrepancy in these data may arise from dynamics of H89 and associated amino acid residues. The average thermal factors for amino acid residues 87-92, which includes the proximal histidine H89, was observed to be 50% larger than the average

value in DHP as a whole (*5*). The region near H89 has the largest thermal motion in the molecule despite the fact that it is buried in the interior of the protein and bonded to the heme cofactor. The flexibility of H89 could be the reason for the decrease in the axial histidine torsion angle, Φ from 113° to 90°, which was determined by the spacing and 8 > 3 > 5 > 1 order of heme methyl chemical shifts in the ^{1}H NMR spectrum. Similar deviations in proximal histidine plane orientation between X-ray and solution structures have been observed in mouse neuroglobin (*38*), where higher thermal factors in the region of the proximal histidine indicated greater flexibility.

Conclusion

The present study has shown that substrates interact with the six-coordinate DHPCN form in two different ways. Binding of both 4-BP and 2,4-DCP effects internal amino acid residues and heme group substituents in a pH-dependent manner, with greatest affinity under acidic conditions. The NMR data suggest that the binding has a strong and specific effect on the heme, which may result from an internal binding site in rapid exchange with solvent. The molecules 4-BP and 2,4-DCP have significantly less activity than 2,4,6-trihalogenated phenols, which were previously studied as substrates of DHP *(7,48)*. Binding of 2,4,6-TFP, which is a structural homolog of the native substrate 2,4,6-TBP, did not induce effects on the internal amino acid residues, as indicated by ^{1}H NMR. However, broadening and chemical shift perturbations of the fluorine resonances are consistent with an external binding interaction. In the presence of DHPCN the rotational correlation time of 2,4,6-TFP was found to increase from the *ps* to *ns* time scale consistent with the hypothesis that there is an

external binding site. Although 2,4,6-TBP is not sufficiently soluble to permit a ^{1}H NMR study, the conclusion that 2,4,6-TFP binds at an external site clearly implies that the native substrate, 2,4,6-TBP, also binds at an external site. The similar reactivity of both of these substrates leads us to conclude that the active site for substrate oxidation in DHP is an external site, as observed in other heme peroxidases.

Supporting Information Available

1D NOE, gradient-selective COSY, presaturation NOESY data, variable-temperature ^{1}H NMR spectra, and hyperfine-shifted resonances in response to varying pH are presented. Additional titrations of substrate 2,4,6-TFP at alternative pH are also provided. Equations used for analysis of relaxation data are presented. Spectroscopic data for enzyme assays of 4-BP, 2,4-DCP and 2,4,6-TFP are provided. This material is available free of charge via the Internet at http//pubs.acs.org.

Acknowledgements

This work was done in collaboration with Hanna Gracz (NCSU), Franck A. P. Vendeix (NCSU), Vesna de Serrano (NCSU), Aswin Somasundaram (NCSU), Sean M. Decatur (Oberlin College), and Stefan Franzen (NCSU). This project was supported by Army Research Office grant 52278-LS.

References

(1) Han, K., Woodin, S. A., Lincoln, D. E., Fielman, K. T., and Ely, B. (2001) Amphitrite ornata, a marine worm, contains two dehaloperoxidase genes. *Mar. Biotechnol.* 3, 287-292

(2) Chen, Y. P., Woodin, S. A., Lincoln, D. E., and Lovell, C. R. (1996) An unusual dehalogenating peroxidase from the marine terebellid polychaete Amphitrite ornata. *J. Biol. Chem. 271*, 4609-4612.

(3) Lebioda, L., LaCount, M. W., Zhang, E., Chen, Y. P., Han, K., Whitton, M. M., Lincoln, D. E., and Woodin, S. A. (1999) Protein structure: An enzymatic globin from a marine worm. *Nature. 401,* 445.

(4) Weber, R. E., Magnum, C. P., Steinman, H., Bonaventura, C., Sullivan, B., and Bonaventura, J. (1977) Hemoglobins of two terebellid polychaetes: Enoplobranchus sanguineus and Amphitrite ornata. *Comparative Biochemistry and physiology 56A*, 179-187.

(5) de Serrano, V., Chen, Z., Davis, M. F., and Franzen, S. (2007) X-ray crystal structural analysis of the binding site in the ferric and oxyferrous forms of the recombinant heme dehaloperoxidase cloned from Amphitrite ornata. *Acta Crysta. D 63,* 1094-1101.

(6) Zhang, E., , Chen, Y. P., Roach, M. P., Lincoln, D. E., Lovell, C. R., Woodin, S. A., Dawson, J.H., and Lebioda, L. (1996) Crystallization and initial spectroscopic characterization of the heme-containing dehaloperoxidase from the marine polychaete *Amphitrite ornata Acta Cryst. D 52,* 1191-1193.

(7) Belyea, J., Gilvey, L. B., Davis, M. F., Godek, M., Sit, T. L., Lommel, S. A., and Franzen, S. (2005) Enzyme function of the globin dehaloperoxidase from Amphitrite ornata is activated by substrate binding. *Biochemistry 44*, 15637-15644.

(8) Osborne, R. L., Taylor, L. O., Han, K. P., Ely, B., and Dawson, J. H. (2004) Amphitrite ornata dehaloperoxidase: enhanced activity for the catalytically active globin using MCPBA. *Biochem. Biophys. Res. Comm. 324*, 1194-1198.

(9) Lebioda, L. (2000) The honorary enzyme haemoglobin turns out to be a real enzyme. *Cell. Mol. Life. Sci. 57,* 1817-1819.

(10) Kishino, T., and Kobayashi, K. (1995) Relation between toxicity and accumulation of chlorophenols at various pH, and their absorption mechanism in fish. *Water Res. 29*, 431-442.

(11) Allonier, A., Khalansk, M, Camel, V., and Bermond, A. (1999) Characterization of chlorination by-products in cooling effluents of coastal nuclear power stations. *Mar. Poll. Bull. 38,* 1232-1241.

(12) Ator, M. A., and Ortiz de Montellano, P. R. (1987) Protein control of prosthetic heme reactivity. Reaction of substrates with the heme edge of horseradish peroxidase. *J. Biol. Chem. 262*, 1542-1551.

(13) Smirnova, T. I., Weber, R. T., Davis, M. F., and Franzen, S. (2008) Substrate binding triggers a switch in the iron coordination in dehaloperoxidase from Amphitrite ornata: HYSCORE experiments. *J. Am. Chem. Soc. 130*, 2128-2129.

(14) Nienhaus, K., Deng, P. C., Belyea, J., Franzen, S., and Nienhaus, G. U. (2006) Spectroscopic study of substrate binding to the carbonmonoxy form of dehaloperoxidase from Amphitrite ornata. *J. Phys. Chem. B 110*, 13264-13276.

(15) La Mar, G. N., and de Ropp, J. S. (1993) in *Biological Magnetic Resonance,* pp 1-73, Plenum Press, New York.

(16) Emerson, S. D., and La Mar, G. N. (1990) Solution structural characterization of cyanometmyoglobin: resonance assignment of heme cavity residues by two-dimensional NMR. *Biochemistry 29*, 1545-1556.

(17) Banci, L., Bertini, I., Turano, P., Ferrer, J. C., and Mauk, A. G. (1991) Comparative ^{1}H NMR study of ferric low-spin cytochrome-c peroxidase and horseradish-peroxidase. *Inorg. Chem. 30*, 4510-4516.

(18) Yu, L. P., La Mar, G. N., and Rajarathnam, K. (1990) ^{1}H NMR resonance assignments of the active site residues of paramagnetic proteins by 2D bond correlation spectroscopy: metcyanomyoglobin. *J. Am. Chem. Soc. 112*, 9527-9534.

(19) Yamamoto, Y., Iwafune, K., Nanai, N., Akemi, O., Chujo, R., and Suzuki, T. (1991) NMR study of Galeorhinus japonicus myoglobin. ^{1}H NMR study of molecular structure of the heme cavity. *Eur. J. Biochem. 198*, 299-306.

(20) Bertini, I., Turano, P., and Vila, A. J. (1993) Nuclear magnetic resonance of paramagnetic metalloproteins. *Chem. Rev. 93*, 2833-2932.

(21) Satterlee, J. D., and Erman, J. E. (1991) Proton NMR assignments of heme contacts and catalytically implicated amino acids in cyanide-ligated cytochrome c peroxidase determined from one- and two-dimensional nuclear overhauser effects. *Biochemistry 30*, 4398-4405.

(22) Sukits, S. F., and Satterlee, J. D. (1996) Assignment of ^{1}H and ^{13}C hyperfine-shifted resonances for tuna ferricytochrome c. *Biophys. J. 71,* 2848-2856.

(23) Shokhireva, T. Kh., Shokhirev, N. V., and Walker, F. A. (2003) Assignment of heme resonances and determination of the electronic structures of high- and low-spin nitrophorin 2 by ^{1}H and ^{13}C NMR spectroscopy: An explanation of the order of heme methyl resonances in high-spin ferriheme proteins. *Biochemistry 42,* 679-693.

(24) Maudsley, A.A., Ernst, R.R. (1977) Indirect detection of magnetic resonance by Heteronuclear Two-dimensional Spectroscopy. *Chem. Phys. 50,* 368-372.

(25) Patt, S.L., Sykes, B.D. (1972) Water Eliminated Fourier Transform NMR Spectroscopy. *J. Chem. Phys. 56,* 3182-3184.

(26) Osborne, R. L., Sumithran, S., Coggins, M. K., Chen, Y., Lincoln, D. E., and Dawson, J. H. (2006) Spectroscopic characterization of the ferric states of Amphitrite ornata dehaloperoxidase and Notomastus lobatus chloroperoxidase: His-ligated peroxidases with globin-like proximal and distal properties. *J. Inorg. Biochem. 100,* 1100-1108.

(27) Satterlee, J. D., Erman, J. E., and DeRopp, J. S. (1987) Proton hyperfine resonance assignments in cyanide-ligated cytochrome *c* peroxidase using the nuclear Overhauser effect. *J. Biol. Chem. 262*, 11578-11583.

(28) Alam, S. L., and Satterlee, J. D. (1994) Complete heme proton hyperfine resonance assignments of the Glycera dibrachiata component IV metcyano monomer hemoglobin. *Biochemistry 33*, 4008-4018.

(29) Decatur, S. M., and Boxer, S. G. (1995) ^{1}H NMR characterization of myoglobins where exogenous ligand replace the proximal histidine. *Biochemistry 34*, 2122-2129.

(30) Thanabal, V., de Ropp, J. S., and La Mar, G. N. (1987) ^{1}H NMR study of the electronic and molecular structure of the heme cavity in horseradish peroxidase. Complete heme resonance assignments based on saturation transfer and nuclear overhauser effects. *J. Am. Chem. Soc. 109*, 265-272.

(31) Yamamoto, Y., Nanai, N., Chujo, R., and Suzuki, T. (1990) Heme methyl hyperfine shift pattern as a probe for determining the orientation of the functionally relevent proximal histidyl imidazole with respect to the heme in hemoproteins. *FEBS 264*, 113-116.

(32) Traylor, T. G., and Berzinis, A. P. (1980) Hemoprotein models: NMR of imidazole chelated protohemin cyanide complexes. *J. Am. Chem. Soc. 102*, 2844-2846.

(33) Shokhirev, N. V., and Walker, F. A. (1998) The effect of axial ligand plane orientation on the contact and pseudocontact shifts of low-spin ferriheme proteins. *J. Biol. Inorg. Chem. 3*, 581-594.

(34) *ShiftPatterns - Heme methyl shift patterns. v.2,* http://www.shokhirev.com/nikolai/programs/prgsciedu.html

(35) Banci, L., Bertini, I., Pierattelli, R., Tien, M., and Vila, A. J. (1995) Factoring of the hyperfine shifts in the cyanide adduct of lignin peroxidase from P. chrysosporium. *J. Am. Chem. Soc. 117,* 8659-8667.

(36) Crull, G. B., Kennington, J. W., Garber, A. R., Ellis, P. D., and Dawson, J. H. (1989) ^{19}F Nuclear Magnetic Resonance as a probe of the spatial relationship between the heme iron of cytochrome p-450 and its substrate. *J. Biol. Chem. 264*, 2649-2655.

(37) Decatur, S. M., DePillis, G. D., and Boxer, S. G. (1996) Modulation of protein function by exogenous ligands in protein cavities: CO binding to a myoglobin cavity mutant containing unnatural proximal ligands. *Biochemistry 35,* 3925-3932.

(38) Walker, F. A. (2006) The heme environment of mouse neuroglobin: histidine plane orientations obtained from solution NMR and EPR spectroscopy as compared with x-ray crystallography. *J. Biol. Inorg. Chem. 11*, 391-397.

(39) La Mar, G. N., Hernandez, G., and de Ropp, J. S. (1992) ^{1}H NMR investigation of the influence of interacting sites on the dynamics and thermodynamics of substrate and ligand binding to horseradish peroxidase. *Biochemistry 31,* 9158-9168.

(40) Thanabal, V., de Ropp, J. S., La Mar, G. N. (1987) Identification of the catalytically important amino acid residue resonances in ferric low-spin horseradish peroxidase with nuclear Overhauser effect measurements. *J. Am. Chem. Soc. 109,* 7516-7525.

(41) de Ropp, J. S., Mandal, P. K., and La Mar, G. N. (1999) Solution ^{1}H NMR investigation of the heme cavity and substrate binding site in cyanide-inhibited horseradish peroxidase. *Biochemistry 38,* 1077-1086.

(42) Reibarkh, M., Malia, T. J., and Wagner, G. (2006) NMR distinction of single- and multiple-mode binding of small-molecule protein ligands. *J. Am. Chem. Soc. 128,* 2160-2161.

(43) Matsuo, H., Walters, K. J., Teruya, K., Tanaka, T., Gassner, G. T., Lippard, S., J., Kyogoku, Y., and Wagner, G. (1999) Identification by NMR spectroscopy of residues at contact surfaces in large, slowly exchanging macromolecular complexes. *J. Am. Chem. Soc. 121,* 9903-9904.

(44) Reibarkh, M., Malia, T. J., Hopkins, B. T., and Wagner, G. (2006) Identification of individual protein-ligand NOEs in the limit of intermediate exchange. *J. Biomol. NMR. 36,* 1-11.

(45) Evans, J. N. S. (1995) in *Biomolecular NMR Spectroscopy,* pp 240, Oxford University Press, Oxford.

(46) Tengel, T., Fex, T., Emtenäs, H., Almqvist, F., Sethson, I., and Kiflber., J. (2004) Use of ^{19}F NMR spectroscopy to screen chemical libraries for ligands that bind to proteins. *Org. Biomol. Chem. 2,* 725-731.

(47) Carrington, A., and MacLachlan, A. D. (1967) in *Introduction to Magnetic Resonance,* pp 176-203.

(48) Franzen, S., Gilvey, L.B., and Belyea, J. (2007) The pH dependence of the activity of dehaloperoxidase from *Amphitrite ornata*. *Biochim. Biophys. Acta: Prot. Struct. Mol. Enz. 1774*, 121-130.

(49) Chaudhary, C. (2003) Point Mutagenesis and Spectroscopic Probing of Dehaloperoxidase: Characterizing the Mechanism and Activity of the Heme Active Site of the Native Protein. *MS Thesis*, NC State Univ.

Tables, Schemes, and Figures

Table 1. ^{1}H and ^{13}C NMR assignments as well as T_1 measurements for selected resonances of DHPCN at 25 °C, pH 7.0.

[a] Calculated using $(R_{Fe}^{i} / R_{Fe}^{j}) = (T_1^{i} / T_1^{j})^{1/6}$. [b] Measurements taken from the X-ray structure (*5*, *6*). [c] Not applicable due to contact shift contribution. [d] Not accurate measurements due to overlapping resonances.

	^{1}H δ (ppm)	^{13}C δ (ppm)	^{1}H T_1 (ms)	R_{Fe} (Å)[a]	R_{Fe} (Å)[b]
Heme					
8-CH_3	26.8	-53.1	188	*c*	5.70
3-CH_3	24.5	-59.5	204	*c*	5.72
5-CH_3	4.3	-14.8	*d*	--	5.43
4α	14.0	52.8	149	5.43	5.68
$4\beta_1$	-1.1	Not observed	*d*	--	6.75
$4\beta_2$	-1.5	Not observed	303	6.1	6.75
6α1	13.4	84.4	--	--	5.8
6α2	9.4	84.4	--	--	6.29
6β1	1.2	Not observed	*d*	--	6.23
6β2	0.3	Not observed	*d*	--	7.56
7α1	12.5	-32.7	*d*	--	6.44
7α2	10.2	-32.7	213	5.76	5.83
7β1	0.4	118.8	*d*	--	6.27
7β2	-0.2	118.8	*d*	--	6.14
Phe 97			--		
CζH	15.9	134.5	90	4.79	5.25
CεHs	12.6	132.6	*d*	--	5.45, 6.99
CδHs	9.4	132.2	*d*	--	7.27, 8.48
His 89					
$N\varepsilon_2H$	19.9	N/A	--	--	5.22
Cβ1H	13.4	24.5	*d*	--	6.45
Cβ2H	10.4	24.5	105	5.12	6.29

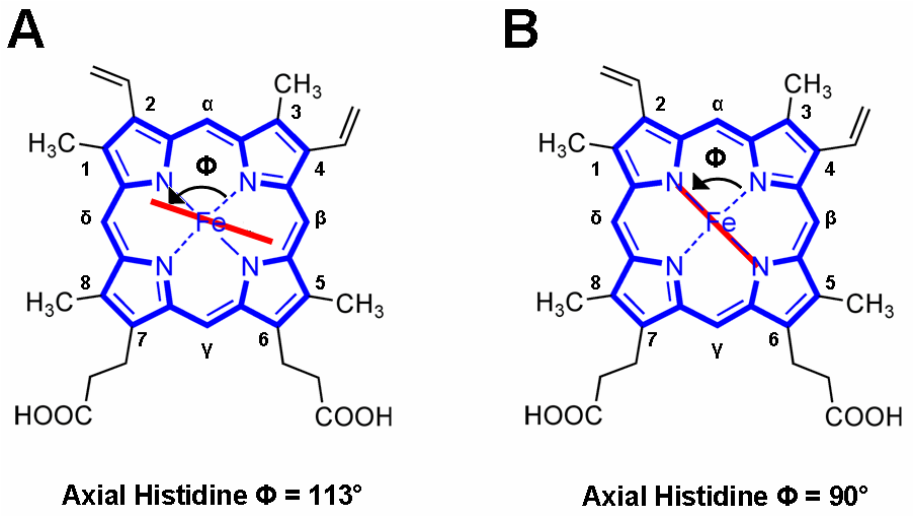

Scheme 1. Axial histidine projection angle as shown in the X-ray structures (A) and by relative order of heme methyl chemical shifts (B).

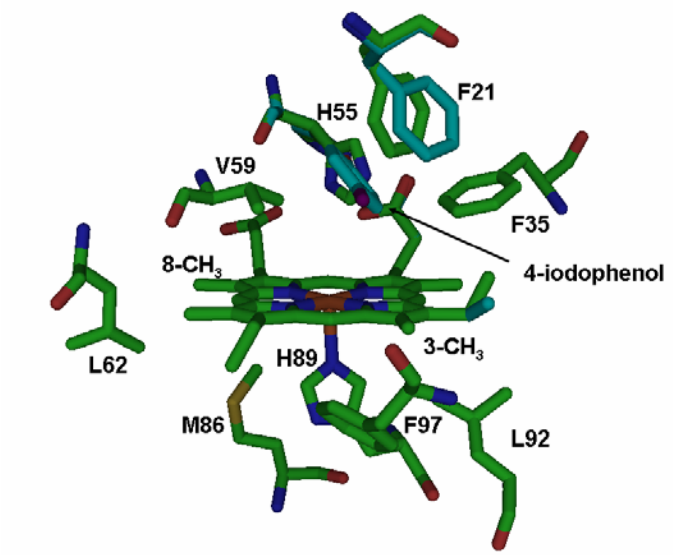

Figure 1. The X-ray crystal structures of the local heme environment and substrate binding residues of DHP are shown with (light blue) and without (green) bound substrate 4-iodophenol. Upon binding of substrate the 4-vinyl heme substituent shows slight changes in orientation. More predominant changes are observed in the orientations of His55 and Phe21.

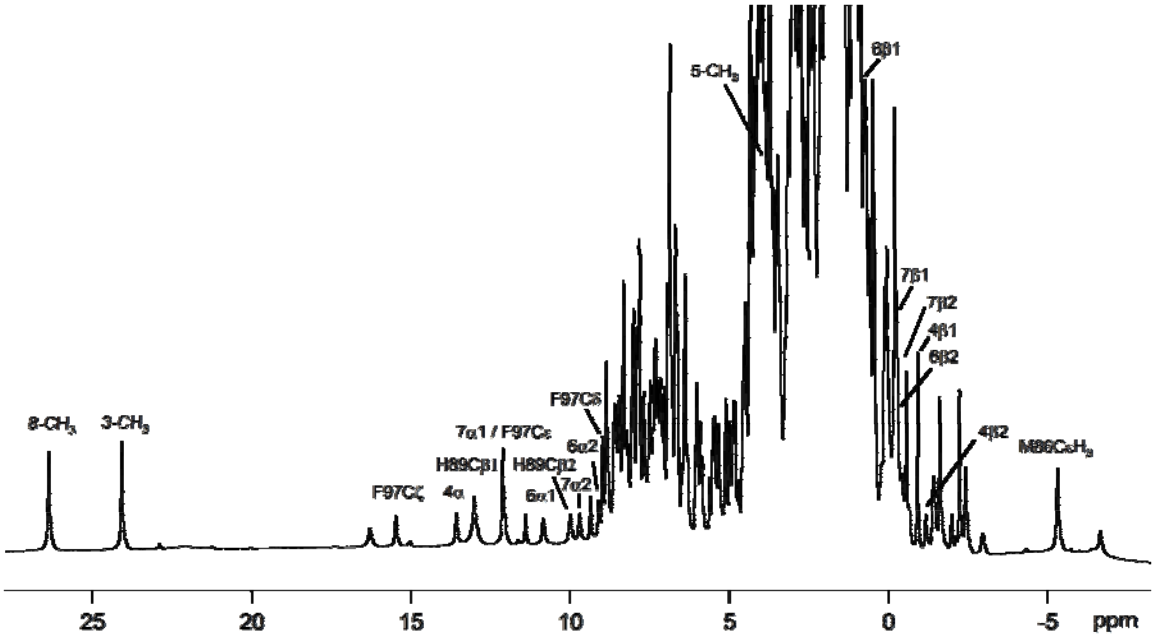

Figure 2. ^{1}H NMR spectrum of DHPCN. Spectrum taken at 298K, 99.9% D_2O, 100mM potassium phosphate, pH 7.0. The assigned hyperfine-shifted resonances are labeled.

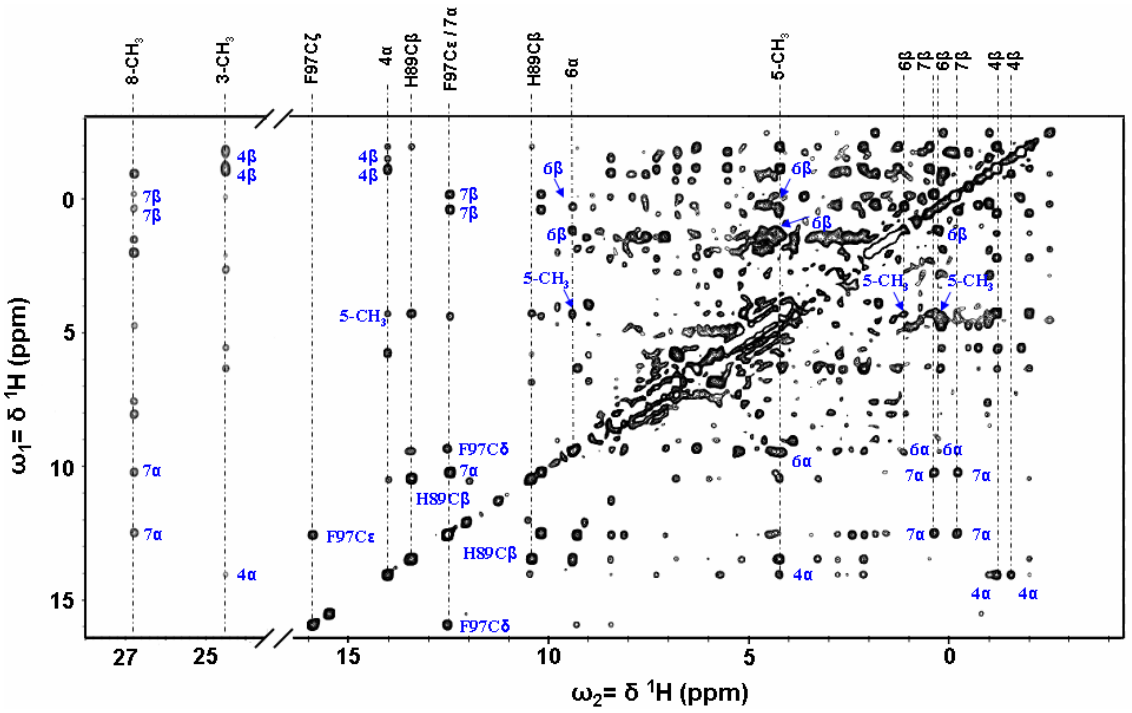

Figure 3. WEFT-NOESY map of metcyano DHP at 298 K, in 99.9% D_2O, 100 mM potassium phosphate, pH 7.0. The mixing time was 100 ms. The labeled crosspeaks represent the observed ^1H dipolar connectivity.

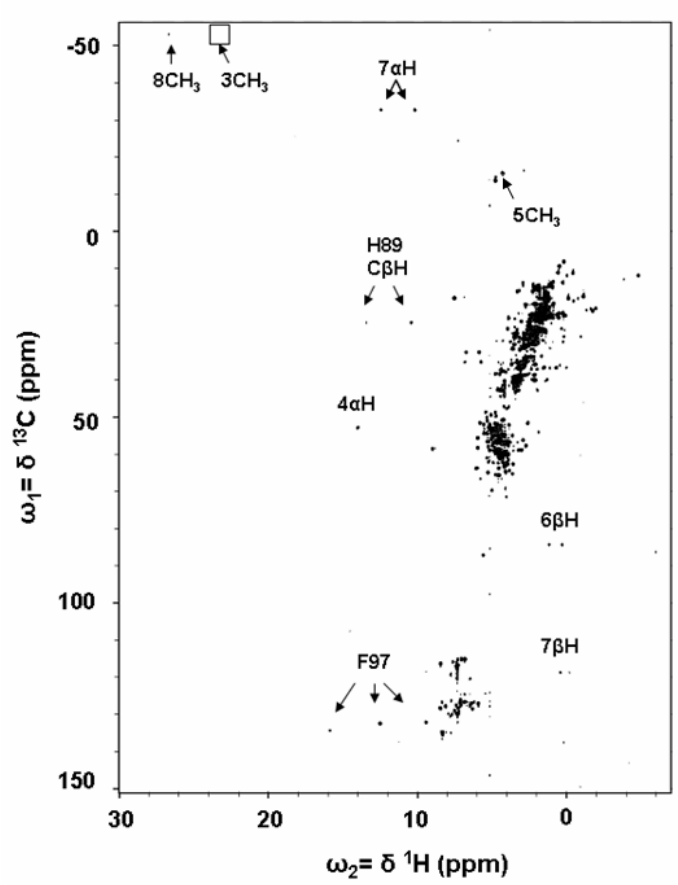

Figure 4. ^{13}C-^{1}H HSQC spectrum of DHPCN taken at 298K, 99.9% D_2O, 100 mM potassium phosphate, pH 7.0. Hyperfine-shifted resonances of the heme and local amino acids are labeled. The box region indicates crosspeak is observed at higher contour levels.

Figure 5. High frequency hyperfine-shifted resonances of DHPCN in 100mM potassium phosphate, pH 7.0, 25 °C. A) Without (top) and with a 15 fold excess of 4-bromophenol (bottom). B) Without (top) and with excess 2,4-dichlorophenol (bottom). C) Without (top) and with excess 2,4,6-trifluorophenol (bottom). Addition of either 4-BP or 2,4-DCP induces line broadening of the internal heme 3-CH_3 and Phe97 ring resonances, while the external 7α1H and 7α2H resonances show changes in their respective chemical shift. Addition of 2,4,6-trifluorophenol does not effect any of the hyperfine-shifted resonances.

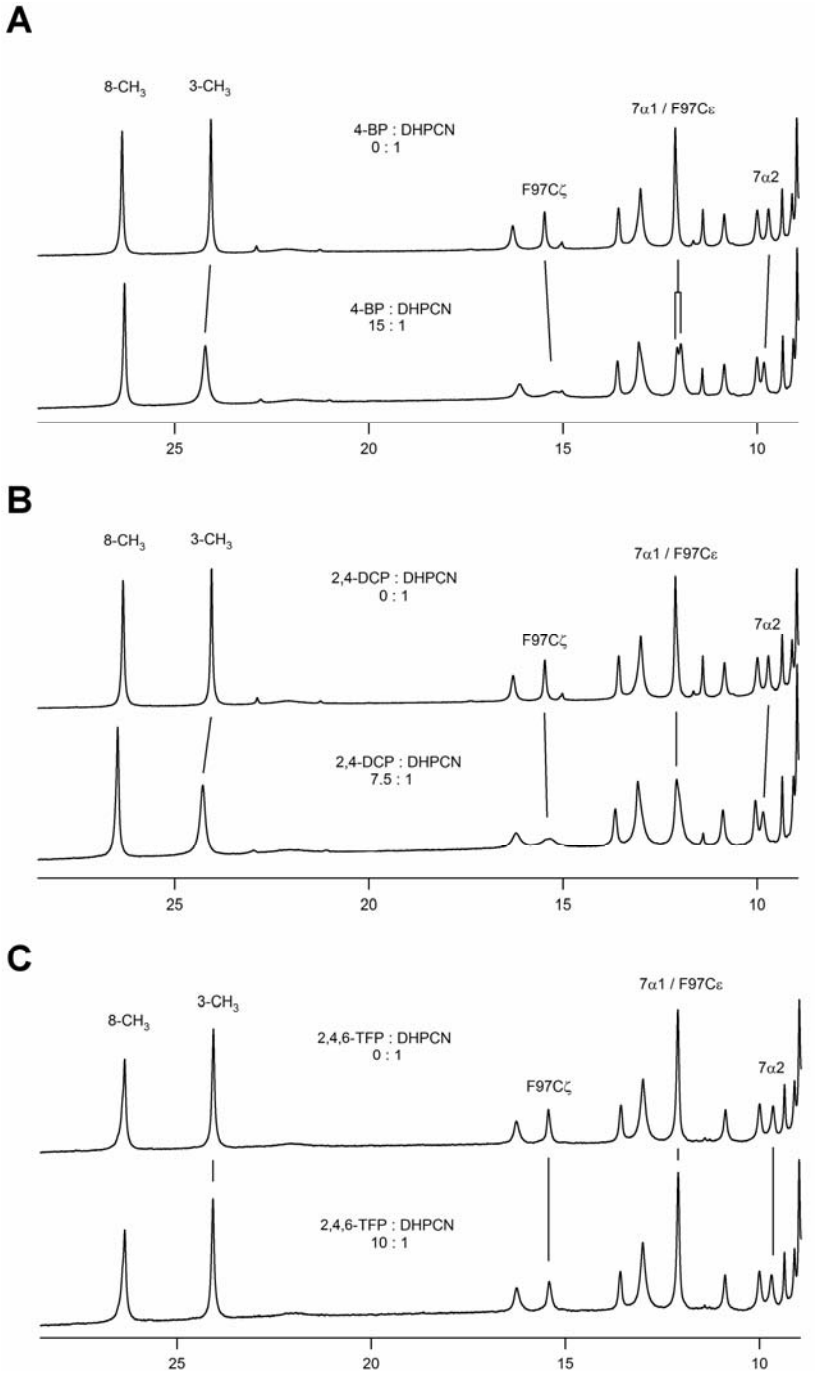
A
8-CH3
3-CH3
4-BP : DHPCN
0 : 1
F97Cζ
7α1 / F97Cε
7α2
4-BP : DHPCN
15 : 1
25
20
15
10
B
8-CH3
3-CH3
2,4-DCP : DHPCN
0 : 1
F97Cζ
7α1 / F97Cε
7α2
2,4-DCP : DHPCN
7.5 : 1
25
20
15
10
C
8-CH3
3-CH3
2,4,6-TFP : DHPCN
0 : 1
F97Cζ
7α1 / F97Cε
7α2
2,4,6-TFP : DHPCN
10 : 1
25
20
15
10

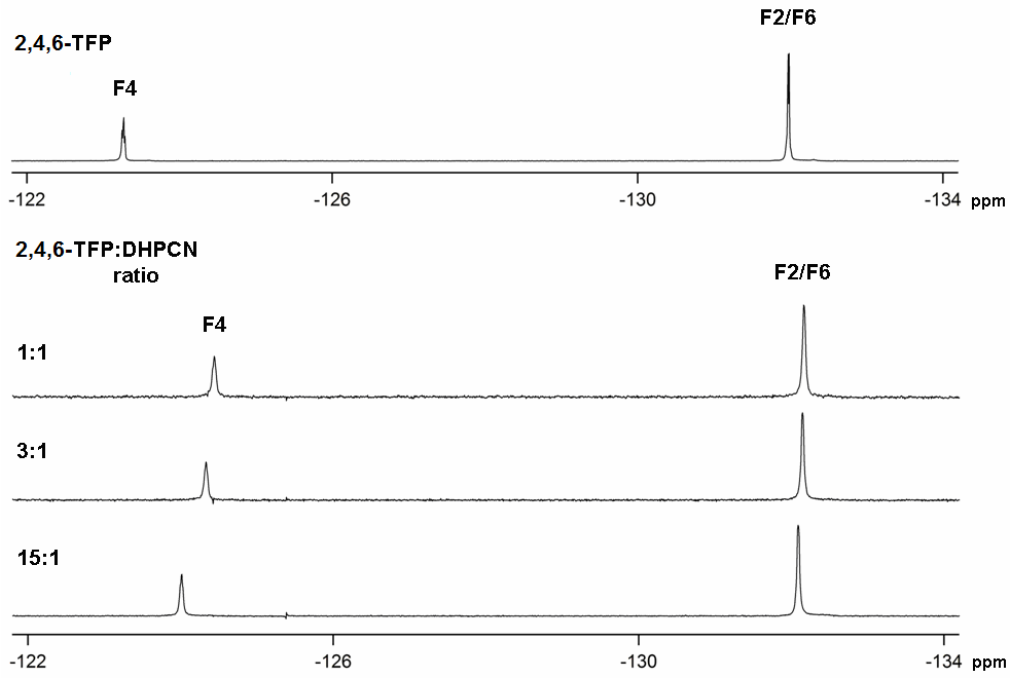

Figure 6. ^{19}F NMR spectra of the 2,4,6-TFP substrate analog in pH 7, 100 mM potassium phosphate, 99.9% D_2O buffer (top) and titration of this substrate to metcyano DHP at 1:1, 3:1, and 15:1 concentration ratios.

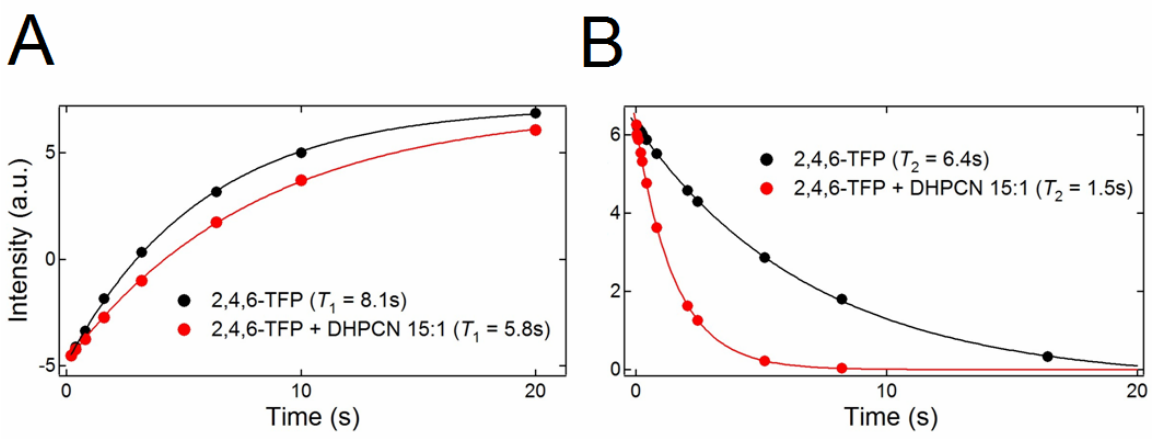

Figure 7. A) T_1 relaxation curves and B) T_2 relaxation curves for the *meta*-protons of 2,4,6-trifluorophenol, alone (black), and in the presence of DHPCN (red) at a 15:1 molar ratio.

CHAPTER 4

A V59W Mutation Blocks the Distal Binding Pocket of the Hemoglobin Dehaloperoxidase from *Amphitrite ornata*

Abstract

The hemoglobin dehaloperoxidase (DHP) is a dual function heme protein capable of functioning as both a globin and peroxidase. Unlike any known globins, DHP binds monohalogenated phenols in an internal distal binding pocket above the heme iron. The peroxidase activity of DHP is similar to the commonly studied horseradish peroxidase in that the 2,4,6-trihalophenols are subjected to two sequential one-electron oxidation steps that result in the formation of a 2,6-dihaloquinone. Recent experiments have demonstrated evidence for a secondary binding site specific for 2,4,6-trihalogenated phenols. In order to understand how binding events in the distal pocket affect the peroxidase activity of the globin, a tryptophan has been introduced into the primary binding site. ^{1}H NMR experiments and NO recombination kinetics were used to probe the mutated binding pocket. The results indicate a V59W mutation denies monohalogenated phenol access to the distal pocket. Blockage the distal binding pocket, however, did not result in a significant decrease in peroxidase activity, thereby corroborating the existence of an external substrate binding site.

Introduction

The marine worm *Amphitrite ornata* is a filter feeding polychaete that inhabits estuarine inlets alongside other polychaetes such as *Notomastus lobatus* and *Thelepus crispus*. *N. lobatus* and *T. crispus* secrete brominated aromatics, theoretically as a means of territorial protection (*1*-*3*). In the case of *N. lobatus*, monohalogenated 4-bromophenol (4-BP) and trihalogenated 2,4,6-tribromophenol (2,4,6-TBP) are produced at nearly 2:1 stoichiometric ratios by the heme protein chloroperoxidase (*4*). *A. ornata* is therefore likely to encounter mixtures of mono- and tri-halogenated phenols in its natural environment. The tri-halogenated phenols 2,4,6-TBP and 2,4,6-trichlorphenol (2,4,6-TCP) have been studied extensively and are considered the best substrates for DHP, given high product turnover for both molecules (*5*-*7*). The smallest 2,4,6-trihalophenol, 2,4,6-TFP, is also a substrate although it does not exhibit turnover rates as high as 2,4,6-TCP or 2,4,6-TBP (*8*). Studying substrate binding interactions of trihalogenated phenols, as well as the well-documented monohalogenated phenol binding, is imperative to understanding the physiologically relevance of the substrates (*3*, *9*).

We have shown by ^{1}H NMR characterization of the DHP active site (*10*) that monohalogenated 4-bromophenol (4-BP), and substrate analog 2,4-dichlorophenol (2,4-DCP) induce binding interactions in the internal distal pocket of DHP at pH < 7.0. These binding interactions were observed in the hyperfine-shifted resonances of the internal 3-CH_3 heme methyl and distal pocket Phe97 ring protons. Over the pH range of 5.5 – 9.9, binding interactions were also seen in the solvent exposed external heme 7α propionate protons. A

second mode of binding was observed with 2,4,6-TFP using ^{19}F NMR, T_1 and T_2 experiments (*10*). This second mode of binding did not involve perturbations of the internal binding site resonances, but the fluorine resonances of TFP exhibited significant decreases in T_2 time and broadening which indicated exchange between free and bound states (*10*). Although substrate-protein NOEs have been undetectable thus far (due to fast exchange of the halophenols), preliminary indication of an external substrate binding site raises the possibility that DHP oxidizes substrates by an edge electron transfer mechanism typical of peroxidases and myoglobin mimics of peroxidases (*10-13*). The role of monohalogenated phenol binding in the internal site is still unclear. A clearer understanding of what governs binding events in the distal pocket, and how this relates to binding under physiological conditions, is required to understand the peroxidase function of the hemoglobin DHP.

To understand the dynamics of internal binding and substrate oxidation we introduced a V59W mutation into the distal binding pocket of DHP. Valine 59 is one of the closest residues to the bound monohalogenated phenol in the crystal structure 1EWA, with the $C\gamma_2H_3$ of Val59 being 2.7 Å away from the *o*-carbon of 4-iodophenol (Figure 1) (*9*). Mutation of V59 to a tryptophan (V59W) was predicted to block the base of the internal binding site, thereby preventing access to the heme via an internal pathway. In this report we compare binding interactions and enzymatic activity of DHP to the DHP V59W mutant. Differences in internal binding interactions between DHP and V59W are presented by analysis of ^1H NMR data, and differences in the NO recombination kinetics are also discussed. In addition, enzymatic assays comparing product turnover of 2,4,6-TCP are presented for both forms of the protein.

Materials and Methods

Protein Preparation. The pET 16b plasmid containing the 6XHisDHP4R or 6XHisDHP4R V59W DNA insert was transformed into BL21 (DE3) *Escherichia coli* cells and then plated out on 2xYT/Ap agar plates. Single colonies were isolated and overnight cultures were scaled up to 6 L growths. Expression of 6XHisDHP protein was not induced via addition of ITPG. After subsequent cell harvesting and lysis, the His-tagged DHP was isolated using a Ni-NTA agarose column (Qiagen) followed by further purification on a CM 52 ion exchange column as discussed elsewhere (*10*). Purified DHP was exchanged in 0.1 M potassium phosphate buffer, pH 7. For the NMR experiments the protein was exchanged 99.9% D_2O, 0.1 M potassium phosphate buffer, pH 7. The protein was concentrated to a final concentration of ~1-2 mM, and KCN was then added to a final concentration of approximately 5 mM. The concentration of the protein was determined using the Soret peak at 406 nm with a molar absorptivity of 116400 M^{-1} cm^{-1} (*14*). Final yields of purified w.t. DHP protein was approximately 35 mg/L broth with A_{406}/A_{280} ratios greater than 4. Final yields of the DHP V59W mutant was much lower, however, at approximately 7 mg/L broth with A_{409}/A_{280} ratios at 3.4.

^{1}H NMR Experiments. The ^{1}H NMR spectra were obtained on a 500MHz AVANCE Bruker spectrometer. The WEFT-NOESY utilized a 300 ms recovery-delay and 100 ms mixing time. For the 2D NOESY spectra a presaturation pulse was incorporated into the pulse sequence and the data were collected with a spectral width of 27000 Hz for DHPCN and DHPCN V59W. The best results were collected using a mixing time of 100 ms and a

delay time of 1.2 seconds. Gradient-selective COSY spectra were also collected over the aforementioned spectral widths and a total of 2048 t_2 points and 512 t_1 blocks were collected with a delay time of 1.2 seconds.

UV-Vis Assays. For all experiments the protein was exchanged into 100 mM potassium phosphate buffer, pH 7. The absorption data was collected using a Hewlett Packard 8453 multi-wavelength spectrometer. The spectra were collected every 2 seconds over a 600 second time frame. The conditions used for the assays were: 6 μM protein (DHP or DHP V59W), 500 μM H_2O_2, and 500 μM TCP. Substrate turnover was monitored by the appearance of the 2,6-dichloro-1,4-benzoquinone (2,6-DCQ) product at 275 nm, while the disappearance of substrate TCP was monitored at 316 nm.

Picosecond Transient Absorption Spectroscopy. Approximately 100 μL of ~30 μM ferric DHP was added to a 1 mm pathlength quartz cell. The cell was sealed with a rubber septa and degassed by purging with and evacuating argon gas. The protein was reduced by addition of sodium dithionite to a final concentration of ~3 mM. NO gas diluted to 10% in N_2 was then introduced to form the NO-ligated ferrous DHP species. The transient absorption data were collected and recorded as a time-wavelength matrix using the pump-probe laser system described previously (*15*). Photodissociation of the NO was performed using an excitation pulse at ~560 nm with pulse duration of ~40 fs at repetition rate of 30 Hz (*16*). The sample cell was oscillated perpendicularly with respect to the beam constantly during the course of the experiment. A 500 ps time window was scanned and up to 40 scans were averaged. The spectra containing cross-phase modulation were thrown out and the

remaining data were processed using singular value decomposition of the time-wavelength matrix.

Results

UV-Vis enzymatic assays. Enzymatic activity of DHP and V59W, over the course of 600 s, is compared in Figure 2A (DHP) and B (V59W). Inspection of the two assays reveals there is no observed compound II intermediate (Abs_{420}) in the V59W mutant following addition of H_2O_2. However, the overall absorbance of substrate 2,4,6-TCP (316 nm) decreases and the absorbance of the two-electron oxidation product 2,6-DCQ increases at 275 nm (*5, 6*) during the course of the assay. The ΔAbs of the 2,6-DCQ product at 275 nm can be seen in Figure 3. The product turnover observed in V59W is ~ 85% that of DHP. The 2,6,-DCQ product formation goes through an observable maximum at 275 nm in both cases. This absorption band of the product (Abs_{275}) begins to decrease in intensity after 81 s for DHP and 147 s for V59W. The V59W mutant also exhibits a slower decrease in the 2,6-DCQ product absorption band than observed in DHP (Figure 3).

^{1}H NMR substrate titrations. WEFT-NOESY and gradient selective COSY spectra, from which assignments for DHPCN V59W (V59WCN) were obtained, are included in the Supporting Information. Detailed assignments of DHPCN can be found elsewhere (*10*). There are many differences in the overall appearance in the high-frequency ^{1}H NMR spectra of DHPCN and V59WCN. When substrate is not present (Figure 4A and B, top), differences are observed in chemical shifts of DHPCN and V59W. The most notable is the switch in the relative order of the downfield heme methyls. The highest frequency heme methyl is 8-CH_3

in DHPCN. This differs in V59WCN, as the 3-CH_3 heme methyl now occurs at the highest frequency. This is likely due to a slight change in projection angle of the distal histidine on the heme plane. This angle, Φ, is ~90° in DHPCN as based on previously reported NMR data (*10*). The current data suggests the Φ of V59WCN is rotated by ~ + 8° giving rise to the switch in observed order of heme methyls. There have been numerous experiments and models demonstrating the correlation of heme methyl shifts and the Φ of the proximal histidine (*17-24*). This suggests that the bulky tryptophan on the distal side induced large enough active site changes to disturb the orientation of the proximal histidine on the opposite side of the heme.

Upon introduction of monohalogenated 4-BP (Figure 4A), many changes are observed in the high frequency ^{1}H NMR spectrum of wild type DHPCN. The internal 3-CH_3 heme methyl exhibits line broadening and shifts downfield by nearly 0.2 ppm. Most notably, the resonances of active site residue Phe97 exhibit the greatest degree of change in the presence of 4-BP. Specifically, both the Phe97 CζH and motionally-averaged Phe97 CεHs resonance exhibit significant line broadening. Finally, the two external 7α heme propionate protons show deviations in chemical shift upon addition of 4-BP. Changes in the ^{1}H NMR spectra of V59WCN are small in comparison to those in wild type DHPCN. The only changes observed are a slight +0.1 ppm shift in the Phe97 CζH resonance and a -0.1 and -0.2 ppm resonance shift in the 3-CH_3 and 8-CH_3, respectively. Also, very slight broadening of 3-CH_3 is observed. The aforementioned shift of Phe97 CζH causes the resonance to merge with a 4α overlap resonance.

NO Photolysis and Rebinding. The photolysis and subsequent rebinding of a NO molecule to the heme provides a good test case for probing active site differences. NO rebinding has a quantum yield of nearly one for geminate rebinding (*25, 26*). Figure 5A and B shows the kinetic components of the transient differential spectra pertaining to NO rebinding in DHP and V59W with and without excess 4-BP. The data were fit to a biexponential model $S(t) = A_1\exp\{-t/\tau_1\} + A_2\exp\{-t/\tau_2\} + B$. The time constants, τ_j, and amplitudes, A_j, for NO recombination are presented in Table 1. In general, the geminate NO rebinding kinetics in myoglobin, the best structural comparison to DHP, can be classified as having a fast component (~ 10 ps) and a slow component (~ 100 ps) (*26*). The V59W mutant clearly has a greater proportion of fast rebinding component as indicated by the A_1 value of 52% compared to 30% in non-mutated DHP. However, the slower rebinding component (τ_2) of the V59W mutant has a much larger time constant of 488 ps compared to 89 ps in DHP. In the presence of 4-BP, both DHP and V59W indicate nearly identical amplitudes and time constants. This represents a significant decrease in the ability of V59W to trap the photolyzed NO in the primary docking site when 4-BP is present (488 ps without 4-BP, 131 ps with 4-BP). DHP, however, exhibits an increase in trapping photolyzed NO in the distal docking site when 4-BP is present (89 ps without 4-BP, 126 ps with 4-BP).

Discussion

The objective of the current study was two fold: first, to determine if blockage of the distal binding pocket was feasible and, second, to observe if blockage has effects on enzymatic activity, substrate binding, and diatomic ligand dynamics in the distal pocket. The

data indicate that a tryptophan in the distal pocket has sufficient steric interaction that it interferes with the well-established binding of para-halogenated phenols in the distal pocket when CN in ligated to the heme iron (*9*). Introduction of the tryptophan also has an influence on the bonding of diatomics, such as NO, to the heme iron. Inspection of the ^{1}H NMR data indicate the differences addition of 4-BP has on the protein active site. This is seen by the lack of broadened resonances, which was characteristically seen in wild type DHP upon 4-BP addition. As expected, mutation of the closest residue to the bound 4-iodophenol in the crystal structure, valine 59 (*9*), to the bulky tryptophan (V59W) essentially eliminated broadening of internal binding site resonances (Figure 4). While no protein-substrate NOEs have been observed to date, we have suggested elsewhere that the monohalogenated phenols may be in rapid exchange with the protein and perhaps do not fully penetrate into the distal pocket binding site of DHPCN in the pH range studied by ^{1}H NMR ($5.5 < pH < 9.9$) (*10*).

The difference in binding of mono- and tri-halogenated phenols to DHP must have a functional consequence. The fact that there is a natural distribution of 4-BP and 2,4,6-TBP suggests that both of the molecules will be present under physiological conditions in which DHP acts as a dehaloperoxidase, rather than as a hemoglobin. The ^{1}H NMR data provide the strongest support for the hypothesis that monohalogenated phenols bind at least dynamically in the distal pocket in DHPCN. This suggests a possible internal binding interaction with $DHPO_2$, Compound II, or other activated forms during peroxidase catalysis. Based on FTIR, X-ray crystallography, ^{19}F NMR, and relaxation data we conclude that 2,4,6-trihalophenols, such as 2,4,6-TBP, 2,4,6-TCP and 2,4,6-TFP, do not binding at the internal binding pocket, to any significant extent, under physiological conditions. Recent ^{1}H NMR data indicated that

one substrate analog, 2,4,6-TFP, binds to DHP at an external site that has little contact with the heme at pH 7.0 and 298 K (*10*). This finding is consistent with FT-IR studies, which show 2,4,6-TFP is not accommodated in the distal pocket of DHPCO at room temperature above pH 4.7 (*27-28*). The reason for this is that the pKa of the distal histidine, H55, is ~ 4.5 and there is space for the trihalogenated substrate in the pocket when the distal histidine is in the "open" or solvent exposed conformation. The "open" conformation, in turn, is favored by protonation of H55, which requires pH < pKa. In V59W we hypothesize the effect of the mutation is limited to blockage of internal binding interactions only and should have a relatively small effect on external binding substrates such as 2,4,6-TBP, the native substrate, or 2,4,6-TCP, which is frequently used in enzyme assays because of its greater solubility. Before considering the role of an external binding site on the function of DHP, we examine whether the mutation V59W interferes with the binding of diatomic ligands. Our test case for this is the DHPNO complex since NO binds in a bent conformation, which is structurally similar to the binding of O_2 and also to the putative binding of H_2O_2 during activation for peroxidase catalysis.

The picosecond transient absorption experiments provide insight into the dynamics of NO ligand rebinding as a result of the V59W mutation. The data indicate that there is a higher proportion of initial fast-phase NO-rebinding in V59WNO (A_1 = 52%) compared to wild type DHPNO (A_1 = 30%). This increased degree of rebinding is expected if the NO is unable to initially escape into the primary docking site, which may be the B-site observed in X-ray crystal structures for CO recombination (*27*). The presence of a bulky tryptophan could slow the escape of NO from the initial docking site and thereby facilitate the initial

fast-phase rebinding of NO. The slower rebinding phase shows the dramatic differences created by the introduction of tryptophan into the internal binding site. The slower rebinding component (τ_2) of V59W (488 ps) is nearly 5.5x longer than that of DHP (89 ps). This shows that once NO escapes the initial distal docking site, it has a much larger energy barrier to overcome in order to rebind in V59W than in DHP. Perhaps most interesting are the changes in the NO rebinding data upon the introduction of substrate. The kinetic data that differentiated V59W from DHP (larger A_1 and longer τ_2) are essentially negated by the addition of excess substrate 4-BP. The amplitudes and time constants are nearly identical for DHP and V59W once the substrate 4-BP is added (Table 1). The time constants for NO rebinding decreased in all three recombination times ($\tau_1 - \tau_3$) for DHP and increased in all three times in V59W. In the case of DHP this suggests that structural rearrangement of transient NO binding sites, comparable to Xe4 in Mb, are becoming more accessible for population of the NO ligand, thereby leading to increases in the time needed for geminate rebinding. Consequently the opposite may be occurring in V59W with the monohalogenated phenol inducing conformations in the protein backbone negating access to interior cavities, hence leading to a decrease in NO rebinding time constants. These data further confirm the hypothesis the substrate 4-BP interacts with the protein interior. Even in the V59W mutant monohalogenated 4-BP may have an effect due to rapid exchange. However, as clearly shown by the ^{1}H NMR data in Figure 4, this effect does not result in penetration to the internal binding site in metcyano V59W. Therefore, the ligation state of the iron may also contribute to the blockage of the internal binding site. Finally, these data suggest that while there is a difference in ligand dynamics, diatomic ligands have full access to the heme iron

and thus it may be expected that the H_2O_2 binding to the V59W mutant will lead to enzymatic activity.

Figures 2 and 3 show that oxidation of 2,4,6-TCP is catalyzed by the V59W mutant with only minor differences in kinetics relative to wild type DHP. Interestingly the compound II intermediate (Abs_{420}) is not observed in the V59W mutant. It is highly unlikely that the distal binding pocket can accommodate a "closed" conformation of H55 (which is needed for compound I formation), the bulky tryptophan, and a large trihalogenated phenol, such as 2,4,6-TCP. The ^1H NMR data alone suggest that bound cyanide is enough to deter internalization of the smaller monohalogenated phenol in the V59W mutant. Therefore, taken together with the forgoing data, the enzyme kinetic data strongly support the hypothesis that oxidation of the trihalogenated substrate occurs at an external site.

Conclusions

The data presented here provide a clear refutation of the hypothesis that the internal binding site is the oxidation site for oxidative dehalogenation of substrates in DHP. Introduction of a tryptophan mutation (V59W) at the primary location of mono-halogenated 4-IP binding only resulted in a ~ 15% decrease in product conversion. The hypothesis that the internal binding site is the sole oxidation site was based on initial X-ray crystallographic data showing the presence of the monohalogenated 4-IP bound in the internal distal cavity (Figure 1). Our hypothesis is that binding of monohalogenated phenols in the internal site must have an allosteric or inhibitory, rather than catalytic, function and that oxidation of trihalogenated substrates must occur at an external binding site.

Acknowledgements

This work was done in collaboration with Hanna Gracz (NCSU), Byng-Kuk Yoo (Ecole Polytechnique), Aswin Somasundaram (NCSU), Michel Negrerie (Ecole Polytechnique), and Stefan Franzen (NCSU). This project was supported by Army Research Office grant 52278-LS.

References

(1) Han, K., Woodin, S. A., Lincoln, D. E., Fielman, K. T., and Ely, B. (2001) *Amphitrite ornata*, a marine worm, contains two dehaloperoxidase genes. *Mar. Biotechnol.* 3, 287-292

(2) Chen, Y. P., Woodin, S. A., Lincoln, D. E., and Lovell, C. R. (1996) An unusual dehalogenating peroxidase from the marine terebellid polychaete Amphitrite ornata. *J. Biol. Chem. 271*, 4609-4612.

(3) Lebioda, L., LaCount, M. W., Zhang, E., Chen, Y. P., Han, K., Whitton, M. M., Lincoln, D. E., and Woodin, S. A. (1999) Protein structure: An enzymatic globin from a marine worm. *Nature. 401,* 445.

(4) Lincoln, D. E., Fielman, K. T., Marinelli, R. L., and Woodin, S. A. (2005) Bromophenol accumulation and sediment contamination by the marine annelids *Notomastus lobatus* and *Thelepus Crispus*. *Biochem. Syst. Ecol. 33*, 559-570.

(5) Belyea, J., Gilvey, L. B., Davis, M. F., Godek, M., Sit, T. L., Lommel, S. A., and Franzen, S. (2005) Enzyme function of the globin dehaloperoxidase from *Amphitrite ornata* is activated by substrate binding. *Biochemistry 44*, 15637-15644.

(6) Osborne, R. L., Taylor, L. O., Han, K. P., Ely, B., and Dawson, J. H. (2004) Amphitrite ornata dehaloperoxidase: enhanced activity for the catalytically active globin using MCPBA. *Biochem. Biophys. Res. Comm. 324*, 1194-1198.

(7) Franzen, S., Gilvey, L.B., and Belyea, J. (2007) The pH dependence of the activity of dehaloperoxidase from *Amphitrite ornata*. *Biochim. Biophys. Acta: Prot. Struct. Mol. Enz. 1774*, 121-130.

(8) Chaudhary, C. (2003) Point Mutagenesis and Spectroscopic Probing of Dehaloperoxidase: Characterizing the Mechanism and Activity of the Heme Active Site of the Native Protein. *MS Thesis*, NC State Univ.

(9) LaCount, M. W., Zhang, E., Chen, Y.P., Han, K., Whitton, M. M., Lincoln, D. E., Woodin, S. A., and Lebioda, L. (2000) The crystal structure and amino acid sequence of dehaloperoxidase from *Amphitrite ornata* indicate a common ancestry with globins. *J. Biol. Chem. 275*, 18712-18716.

(10) Davis, M. F., Gracz, H., Vendeix, F. A. P., de Serrano, V., Somasundaram, A., Decatur, S. M., and Franzen, S. (2009) Different modes of binding of mono-, di, and tri-halogenated phenols to the hemoglobin dehaloperoxidase from *Amphitrite ornata*. *Biochemistry 48*, 2164-2174.

(11) Ator, M. A., and Ortiz de Montellano, P. R. (1987) Protein control of prosthetic heme reactivity. Reaction of substrates with the heme edge of horseradish peroxidase. *J. Biol. Chem. 262*, 1542-1551.

(12) Matsui, T., Ozaki, S., and Watanabe, Y. (1999) Formation and catalytic roles of compound I in the hydrogen peroxide-dependent oxidations by His64 myoglobin mutants. *J. Am. Chem. Soc. 121*, 9952-9957.

(13) Witting, P. K., Mauk, A. G., and Lay, P. A. (2002) Role of tyrosine-103 in myoglobin peroxidase activity: Kinetic and steady-state studies on the reaction of wild-type and variant recombinant human myoglobins with H_2O_2. *Biochemistry 41*, 11495-11503.

(14) Osborne, R. L., Sumithran, S., Coggins, M. K., Chen, Y., Lincoln, D. E., and Dawson, J. H. (2006) Spectroscopic characterization of the ferric states of Amphitrite ornata dehaloperoxidase and Notomastus lobatus chloroperoxidase: His-ligated peroxidases with globin-like proximal and distal properties. *J. Inorg. Biochem. 100,* 1100-1108.

(15) Cianetti, S., Negrerie, M., Vos, M. H., Martin, J. L., and Kruglik, S. G. (2004) Photodissociation of heme distal methionine in ferrous cytochrome c revealed by subpicosecond time-resolved resonance raman spectroscopy. *J. Am. Chem. Soc. 126*, 13932-13933.

(16) Negrerie, M., Kruglik, S. G., Lambrey, J. C., Vos, M. H., Martin, J. L., and Franzen, S. (2006) Role of heme iron coordination and protein structure in the dynamics and geminate rebinding of nitric oxide to the H93G myoglobin mutant. *J. Biol. Chem. 281*, 10389-10398.

(17) Shokhireva, T. Kh., Shokhirev, N. V., and Walker, F. A. (2003) Assignment of heme resonances and determination of the electronic structures of high- and low-spin nitrophorin 2 by ^{1}H and ^{13}C NMR spectroscopy: An explanation of the order of heme methyl resonances in high-spin ferriheme proteins. *Biochemistry 42,* 679-693.

(18) Decatur, S. M., and Boxer, S. G. (1995) ^{1}H NMR characterization of myoglobins where exogenous ligand replace the proximal histidine. *Biochemistry 34*, 2122-2129.

(19) Thanabal, V., de Ropp, J. S., and La Mar, G. N. (1987) ^{1}H NMR study of the electronic and molecular structure of the heme cavity in horseradish peroxidase. Complete heme resonance assignments based on saturation transfer and nuclear overhauser effects. *J. Am. Chem. Soc. 109*, 265-272.

(20) Yamamoto, Y., Nanai, N., Chujo, R., and Suzuki, T. (1990) Heme methyl hyperfine shift pattern as a probe for determining the orientation of the functionally relevent proximal histidyl imidazole with respect to the heme in hemoproteins. *FEBS 264*, 113-116.

(21) Traylor, T. G., and Berzinis, A. P. (1980) Hemoprotein models: NMR of imidazole chelated protohemin cyanide complexes. *J. Am. Chem. Soc. 102*, 2844-2846.

(22) Shokhirev, N. V., and Walker, F. A. (1998) The effect of axial ligand plane orientation on the contact and pseudocontact shifts of low-spin ferriheme proteins. *J. Biol. Inorg. Chem. 3*, 581-594.

(23) *ShiftPatterns - Heme methyl shift patterns. v.2,* http://www.shokhirev.com/nikolai/programs/prgsciedu.html

(24) Banci, L., Bertini, I., Pierattelli, R., Tien, M., and Vila, A. J. (1995) Factoring of the hyperfine shifts in the cyanide adduct of lignin peroxidase from P. chrysosporium. *J. Am. Chem. Soc. 117,* 8659-8667.

(25) Franzen, S., Jasaitis, A., Belyea, J., Brewer, S. H., Casey, R., MacFalane IV, A. W., Stanley, R. J., Vos, M. H., and Martin, J. L. (2006) Hydrophobic distal pocket affects NO-heme geminate recombination dynamics in dehaloperoxidase and H64V myoglobin. *J. Phys. Chem. B. 110*, 14483-14493.

(26) Ionascu, D., Gruia, F., Ye, X., Yu, A., Rosca., F., Beck, C., Demidov, A., Olson, J. S., and Champion, P. M. (2005) *J. Am. Chem. Soc. 127*, 16921-16934.

(27) Nienhaus, K., Deng, P. C., Belyea, J., Franzen, S., and Nienhaus, G. U. (2006) Spectroscopic study of substrate binding to the carbonmonoxy form of dehaloperoxidase from Amphitrite ornata. *J. Phys. Chem. B 110*, 13264-13276.

(28) Nienhaus, K., Nickel, E., Davis, M. F., Franzen, S., and Nienhaus, F. U. (2008) Determinants of substrate internalization in the distal pocket of dehaloperoxidase hemoglobin of *Amphitrite ornata*. *Biochemistry 47*, 12985-12994.

Figures

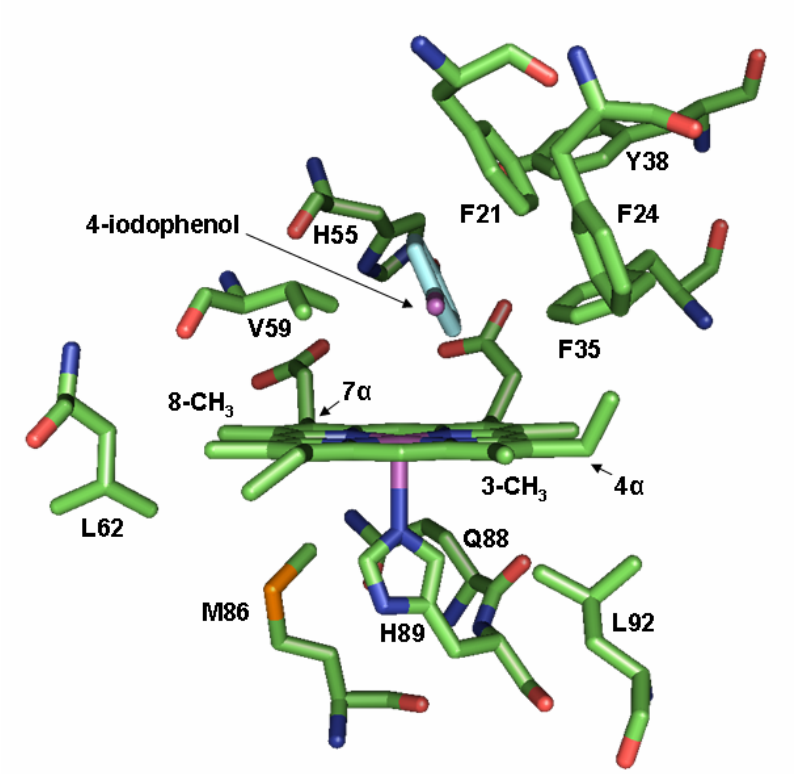

Figure 1. The X-ray crystal structure (1EWA) of the DHP active site is shown with bound monohalogenated 4-iodophenol (light blue) occupying the internal binding site. The two closest residues to bound substrate are Phe35 and Val59. Bound 4-iodophenol is approximately 2.7 Å away from the $C\gamma_2H_3$ methyl group of Val59.

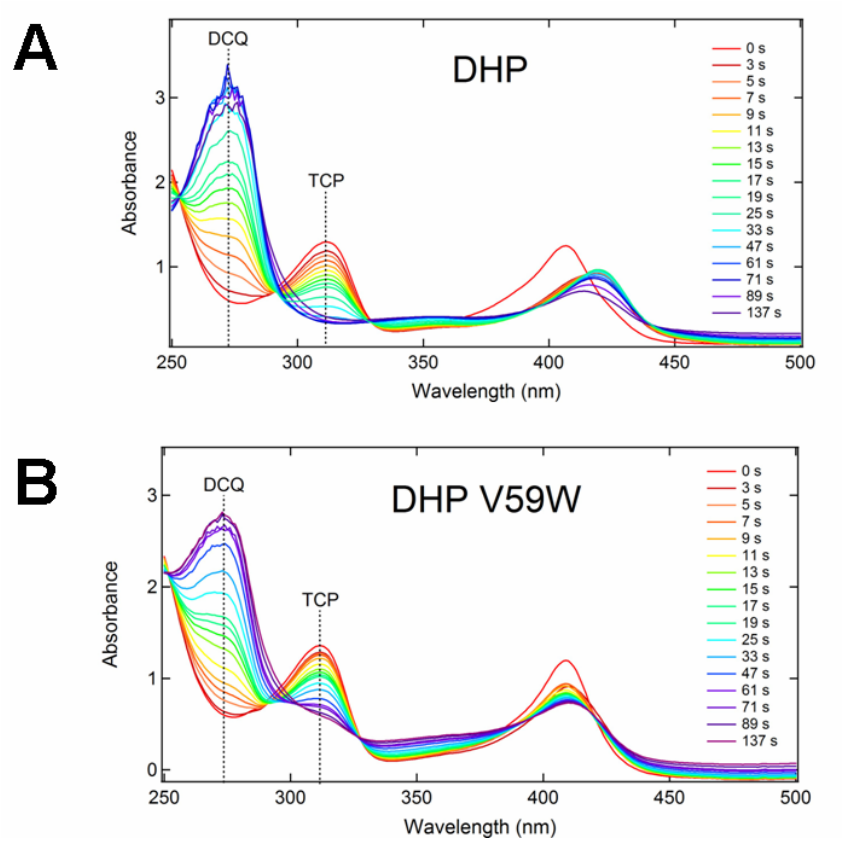

Figure 2. Enzymatic assays of ferric DHP (A) and DHP V59W (B) with 6 μM protein, 500 μM H_2O_2, and 500 μM TCP, pH 7. Substrate 2,4,6-TCP consumption (316 nm) and 2,6-DCQ product formation (275 nm) is observed in both cases.

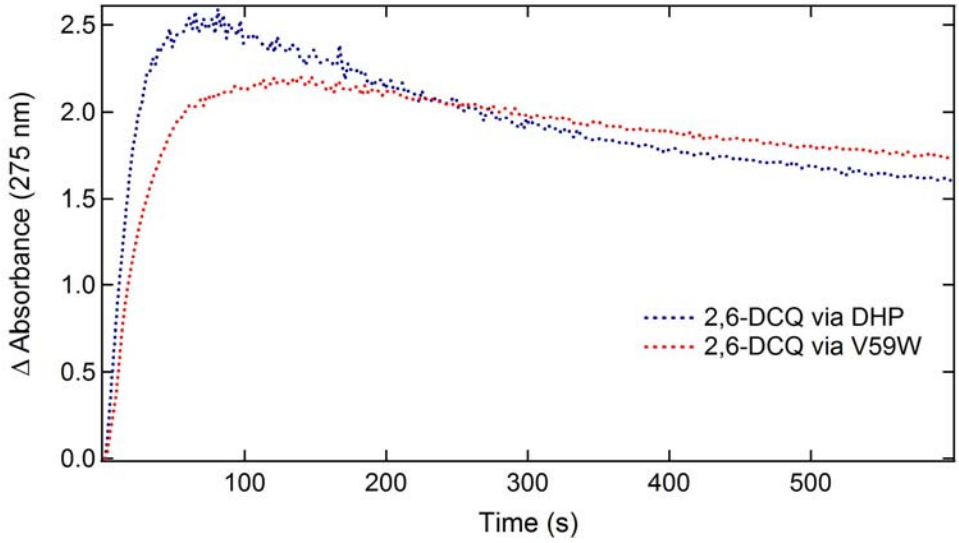

Figure 3. Product formation in both DHP and DHP V59W. DHP exhibits 1.2x larger product conversion than DHP V59W.

Figure 4. High frequency hyperfine-shifted resonances of DHPCN and V59WCN in 100mM potassium phosphate, pH 7.0, 25 °C. A: Without (top) and with a 15x excess of 4-bromophenol (bottom). Addition of 4-BP induces line broadening of the internal heme 3-CH_3 and Phe97 ring resonances, while the external 7α proton resonances show changes in their respective chemical shift. B: ^{1}H NMR spectra of the DHPCN V59W mutant, without (top) and with a 15x excess 4-BP (bottom). A +0.1 ppm shift in the Phe97 CζH resonance and a -0.1 and -0.2 ppm resonance shift in the 3-CH_3 and 8-CH_3 is observed.

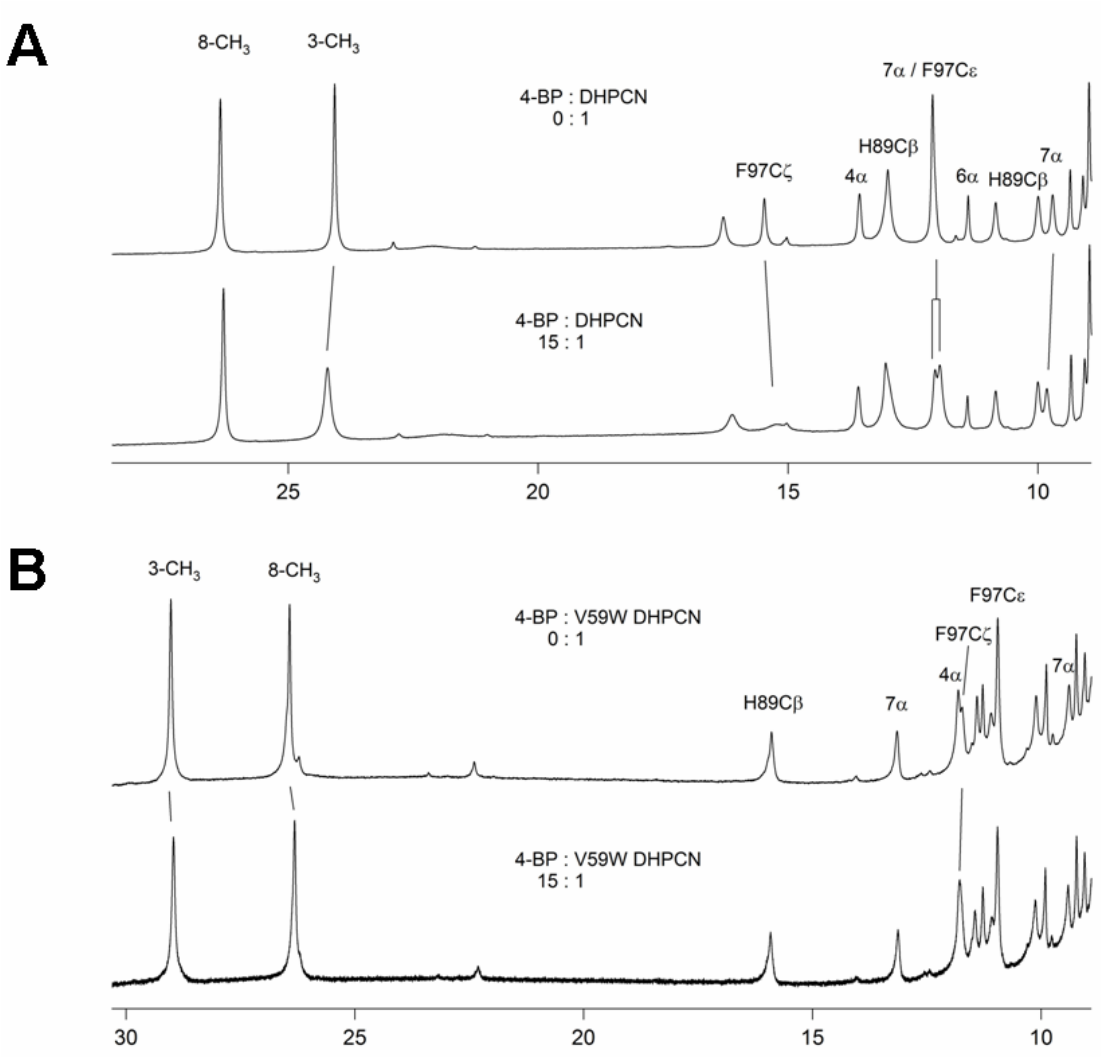
A
8-CH3
3-CH3
4-BP : DHPCN
0 : 1
7α / F97Cε
H89Cβ
F97Cζ
4α
6α
H89Cβ
7α
4-BP : DHPCN
15 : 1
25
20
15
10
B
3-CH3
8-CH3
4-BP : V59W DHPCN
0 : 1
F97Cε
F97Cζ
4α
7α
H89Cβ
7α
4-BP : V59W DHPCN
15 : 1
30
25
20
15
10

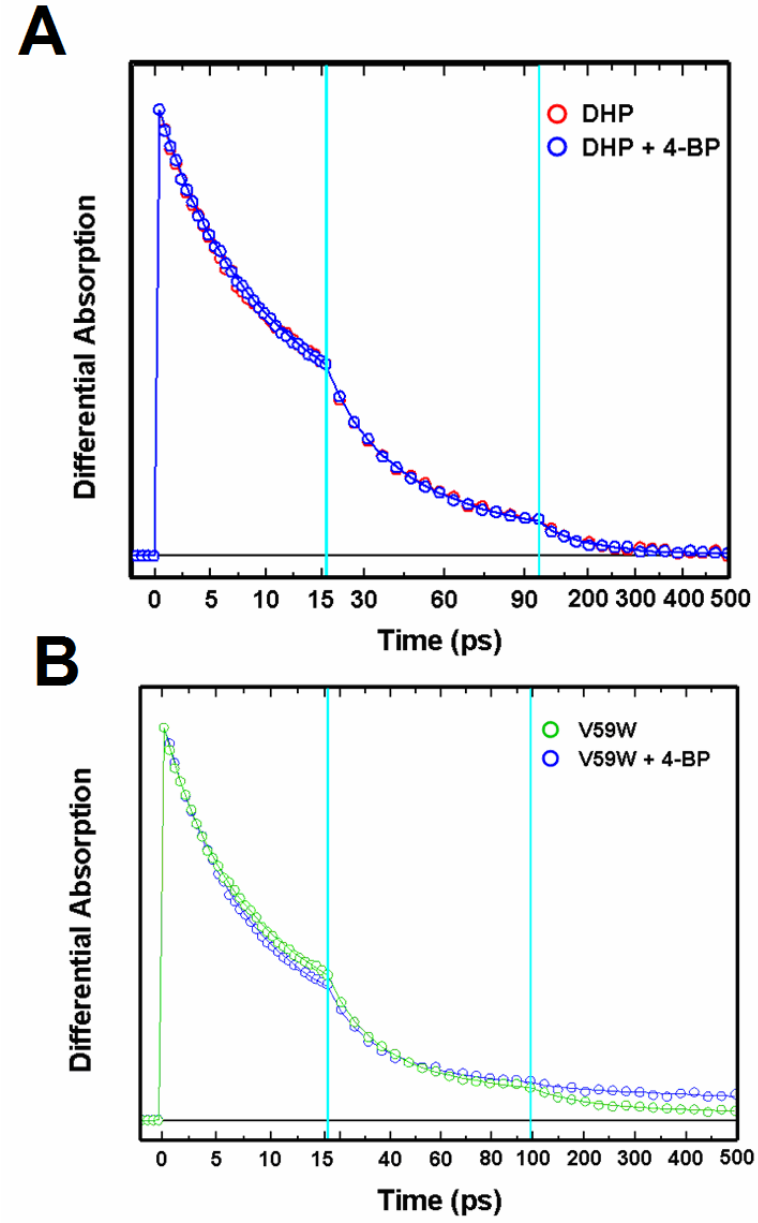

Figure 5. Kinetic components of the transient differential spectra of NO rebinding to (A) DHP with and without excess 4-BP and (B) DHP V59W with and without excess 4-BP.

Table 1. Time constants and amplitude of NO rebinding to DHP and DHP V59W.

Species	τ_1 (*ps*)	A_1	τ_2 (*ps*)	A_2	τ_3 (*ps*)	A_3	C	A_4
DHP	**4.8**	**30%**	**20.6**	**49%**	**88.7**	**20.40%**	**cst**	**0.60%**
DHP + 4-BP	**5.9**	**39%**	**26.1**	**48%**	**125.8**	**13%**	**cst**	**0%**
V59W	**5.6**	**52%**	**23.6**	**38%**	**488.2**	**6.40%**	**cst**	**3.60%**
V59W + 4-BP	**4.8**	**37%**	**19.3**	**48%**	**130.6**	**13%**	**cst**	**2%**

CHAPTER 5

Inhibition of DHP Activity by a Native Monohalogenated Phenol

Introduction

Amphitrite ornata inhabits estuary inlets with other marine polychaetes that secrete a range of haloorganic compounds (*1-3*). The most notable of these is *Notomastus lobatus*. This organism co-inhabits territory with *A. ornata* and uses a haloperoxidase called chloroperoxidase to produce 4-bromophenol (4-BP), 2,4-dibromophenol (2,4-DBP), and 2,4,6-TBP. These three "native" halophenols are found in the sediment around the burrows of *N. lobatus* at 1.8: 0.9: 1 stoichiometric ratios, respectively (*4*). Since *A. ornata* is exposed to these mono-, di-, and trihalogenated phenols, it is physiologically relevant to understand how all these phenols interact with the protein. It has been assumed since the initial crystallography report that binding of all halophenols occurs in the distal binding pocket (*3*). Earlier studies investigating the peroxidase activity of DHP noted that binding of substrate displaces the distal histidine (H55) out of the binding pocket. This presents a conundrum for DHP peroxidase function as H55 is the only residue in the distal pocket capable of the acid-base catalysis needed to form compound I. The distal histidine residue is critical for typical peroxidase activity as it is responsible for proton transfer between the α- and β-oxygen of H_2O_2 and assists in "pulling" apart the O-O bond, thereby leading to compound I formation (*5*).

The peroxidase activity of dehaloperoxidase (DHP) toward trihalogenated phenols such as 2,4,6-tribromo-, 2,4,6-trichloro-, and 2,4,6-trifluorophenols (2,4,6-TBP, 2,4,6-TCP, and 2,4,6-TFP, respectively) has been well documented since discovery of the globin (*1-3, 6-*

9). While peroxidase activity of globins is not uncommon, the ability of DHP protein to bind monohalogenated phenols in an internal distal pocket entirely within 6 Å from the heme iron separates DHP from any other known globin (*3, 10*). The first X-ray crystal structure solved for DHP shows monohalogenated 4-iodophenol bound in the distal pocket directly above the heme plane. To date, it is still unclear if the binding pocket can accommodate larger trihalogenated phenols under ambient conditions. This question is relevant given the ability of DHP to oxidatively dehalogenate larger 2,4,6-trihalogenated substrates such as 2,4,6-TBP and 2,4,6-TCP in the presence of H_2O_2.

Recent EPR HYSCRORE experiments on metaquo DHP and FT-IR studies on DHPCO have also shown the smallest trihalogenated substrate, 2,4,6-TFP bound in the internal distal binding pocket (*11-13*). However, these results were obtained at liquid helium temperature (~ 4 K), and do not provide evidence for such an association under physiological conditions. HYSCORE data indicate that strongly coupled water protons at ~6 MHz (indicative of an axial water ligand) disappear upon addition of a 10x excess 2,4,6-TFP, thereby indicating a displacement of the ligand and a transition from five- to six-coordinate iron (*13*). In addition, X-band EPR experiments show that binding of 2,4,6-TFP does not result in a change of iron spin state. Only a change from 6-coordinate high-spin to 5-coordinate high-spin is observed in the presence of the substrate (*13*). In the FT-IR experiments a CO stretching vibration at ~1972 cm^{-1}, consistent with internally bound 2,4,6-TFP, was observed at 4 K (*11*). The experiments also indicated that ~ 80% of the protein contained internally bound 2,4,6-TFP at this temperature. Upon warming up the protein,

though, the 1972 cm^{-1} band completely disappears around 160 K indicating the loss of 2,4,6-TFP from the internal binding pocket (*12*).

While this data clearly indicates that 2,4,6-TFP is capable of binding in the distal pocket at low temperatures, it does not prove that binding in the distal cavity is requisite for subsequent oxidation of the substrate, particularly under ambient conditions. Enzymatic assays have therefore been carried out to better understand the significance of internal pocket binding as it relates to the peroxidase activity of the protein. Monohalogenated 4-BP has been chosen for the assays, because it is a naturally occurring molecule in sediments occupied by *A. ornata*, and because monohalogenated phenols consistently show an affinity for binding in the distal pocket (*4, 10*). Herein we present enzymatic data indicating the effects of bound monohalogenated 4-BP on the peroxidase activity of DHP toward trihalogenated phenols.

Materials and Methods

UV-Vis Enzymatic Assays. For all experiments His-DHP4R was expressed and purified as discussed elsewhere (*14*). The protein was oxidized via addition of excess $K_3Fe(CN)_6$. Removal of ferricyanide was achieved using a Sephadex G-25 column and the protein was buffer exchanged into 100 mM potassium phosphate, pH 7. All UV-Vis enzymatic assays were collected using a Hewlett Packard 8453 multi-wavelength spectrometer. Spectra were collected every 5 seconds over a 600 second time frame. Turnover of the halophenols were determined by the disappearance of their respective absorption bands at pH 7 (4-BP – 280 nm; 2,4,6-TCP – 313 nm; 2,4,6-TBP – 317 nm and

249 nm) and appearance of product absorption bands (2,6-dichloro-1,4-benzoquinone [2,6-DCQ] – 272 nm, 2,6-dibromo-1,4-benzoquinone [2,6-DBQ] – 290 nm). The conditions used to determine 4-BP turnover were 4.66 μM DHP, 406 μM H_2O_2, and 406 μM 4-BP. The conditions used for 2,4,6-TCP inhibition were: 4 μM DHP, 120 μM H_2O_2, and 120 μM 2,4,6-TCP, pH 7 with and without addition of 240 μM 4-BP. pH 7. Conditions used for 2,4,6-TBP inhibition were identical to those for 2,4,6-TCP except that ~ 5 μM DHP was used. For the Lineweaver-Burk plots the initial velocity of the reaction was recorded from 7 s to 17 s. The conditions used were 4.76 μM DHP, 476 μM H_2O_2, 476, 357, 238, and 119 μM 2,4,6-TCP, with and without 119 μM 4-BP inhibitor, pH 7.0. For the compound II data, spectra were collected 3 s after the addition of 476 μM H_2O_2 to 4.76 μM DHP incubated with varying concentrations of 4-BP.

Results

Upon addition of H_2O_2 to ferric DHP containing 4-BP, there is no observable turnover of 4-BP (Figure 1). The absorption band at 280 nm does not decrease during the course of the assay, indicating no observable oxidation to the quinone product. Figure 2, panel A shows an assay conducted on the substrate 2,4,6-TCP under nearly identical conditions. Upon addition of H_2O_2 to DHP incubated with 2,4,6-TCP, the 2,4,6-TCP absorption band at 313 nm begins to decrease in intensity. On nearly the same time scale, an absorption band indicative of the 2-electron oxidation product 2,6-DCQ begins to grow in at 272 nm. Figure 2, panel B shows an assay under identical conditions *except* for the addition of a 2:1 stoichiometric equivalent of 4-BP (240 μM 4-BP, 120 μM 2,4,6-TCP). This addition

has a dramatic effect on DHP activity and very effectively inhibits 2,4,6-TCP conversion to 2,6-DCQ. The same inhibition effect is seen when 4-BP is mixed with 2,4,6-TBP (Figure 3). There does appear to be a greater degree of baseline drift during the 2,4,6-TBP / 4-BP experiment than observed in the 2,4,6-TCP / 4-BP assay. Hence all absorption bands see a slight increase in absorbance.

Analysis of the initial reaction velocity can be seen in Figure 3. The initial velocity of product formation (ΔA_{272}) was collected for varying concentrations of substrate 2,4,6-TCP with and without 4-BP. The resulting Lineweaver-Burke graph illustrates a competitively inhibited system (Figure 4) with the asymptotes intersecting each other at $1/v_o$. Additional effects of 4-BP inhibition were found by observing how 4-BP effects compound II formation. UV-Vis spectra of DHP with various concentrations of 4-BP were collected 3 s after the addition of H_2O_2. The intermediate compound II has a characteristic 420 nm Soret absorbance in DHP. As seen in Figure 5, by increasing the concentration of 4-BP a reduction in compound II formation is observed.

Discussion

The enzymatic assays in the presence of 4-BP have altered our perception of how DHP binds and oxidizes substrates. As seen in Figure 1 the 4-BP molecule does not exhibit any apparent signs of oxidation by DHP. This observation spurred questions regarding the true role of the 4-BP molecule and the distal binding pocket in general. Other peroxidases found in similar marine worms, such as chloroperoxidase from *N. lobatus*, act as haloperoxidases by halogenating bound phenol (*15*). Once the inactivity of 4-BP was

discovered, the initial thought was that 4-BP could bind internally and be subsequently halogenated in the presence of H_2O_2 and Br^- ions. However, no haloperoxidase activity was observed in the presence of 4-BP or phenol (data not shown). The chloroperoxidase protein also cannot halogenate phenols without a bound flavoprotein. The possibility of DHP acting as a haloperoxidase cannot be ruled out, as there is no sufficient evidence suggesting an associated flavoprotein does not exist. However, it is evident from current data that 4-BP acts as highly effective inhibitor of peroxidase activity *in vitro*.

Figures 2 and 3 show the extent to which a 2 : 1 stoichiometric ratio of 4-BP to 2,4,6-TCP / 2,4,6-TBP inhibits the ability of DHP to oxidize the trihalophenols. This stoichiometric equivalent is physiologically important, because this is the ratio monohalogenated 4-BP and trihalogenated 2,4,6-TBP are produced by competing polychaetes (*15*). However, it is unclear at this point if peroxidase activity of DHP is inhibited *in vivo* when in the presence 4-BP. The mechanism of inhibition, at this point, seems to arise from the prevention of compound I to form. While the reactive compound I intermediate is too fast to observe, the proceeding intermediate, compound II, is easily observed at pH 7. The effect of the 4-BP inhibitor on compound II can easily be seen in Figure 5. At pH 7, DHP compound II is normally observed at 420 nm a few seconds after the addition of H_2O_2. As the concentration of 4-BP is increased, the absorption band for the compound II intermediate shifts to lower wavelengths. This blue shift presumably occurs due to a decrease in the population of compound II (Abs_{420}). As 4-BP is increased, the Soret appears more and more blue-shifted, and subsequently more similar to ferric DHP. This

indicates there is less compound II formed when 4-BP is present. This could indicate a competition between 4-BP and H_2O_2 for access to the distal binding pocket.

As seen in Figure 4, the Lineweaver-Burk plot of the initial velocity of 2,6-DCQ formation with and without 4-BP indicates a competitively inhibited system. This begs the question: Do trihalophenols compete for binding in the distal binding pocket? This does not appear to be the case as larger trihalophenols would occupy even more space in the distal pocket and, given the results with 4-BP, should prevent compound I formation. Recent resonance Raman data have shed light into this problem. In the presence of monohalogenated phenols an increase of 5-coordinate heme is observed in metaquo DHP. This is consistent with the expulsion of a bound water ligand and displacement of the H55 to the "open" conformation as indicated in the X-ray structure (*10, 16*). Addition of 2,4,6-TCP results in the opposite effect. An increase in six-coordinate heme is observed in the presence of 2,4,6-TCP, as if the distal histidine was being "pushed" into the "closed" conformation thereby stabilizing bound water. Additional NMR data also suggest different modes of binding between mono- and trihalogenated phenols and points to the presence of an external binding site for 2,4,6-trihalogenated phenols (*14*). Collectively the UV-Vis, resonance Raman, and NMR data all suggest an external binding site at room temperature for larger trihalogenated phenols. A scenario involving binding of 2,4,6-TCP on the solvent exposed, external side of H55 would be logical given the existing data, however it cannot be proven at this time. This would place the substrate molecule in a binding location similar to the heme edge binding observed in HRP. Additional experiments such as X-ray crystallography or

$^{13}C/^{15}N$ labeled NMR structural analysis on DHP containing active substrates, like 2,4,6-TCP, will help provide details into the exact location of external binding.

References

(1) Han, K., Woodin, S. A., Lincoln, D. E., Fielman, K. T., and Ely, B. (2001) Amphitrite ornata, a marine worm, contains two dehaloperoxidase genes. *Mar. Biotechnol.* 3, 287-292.

(2) Chen, Y. P., Woodin, S. A., Lincoln, D. E., and Lovell, C. R. (1996) An unusual dehalogenating peroxidase from the marine terebellid polychaete Amphitrite ornata. *J. Biol. Chem. 271*, 4609-4612.

(3) Lebioda, L., LaCount, M. W., Zhang, E., Chen, Y. P., Han, K., Whitton, M. M., Lincoln, D. E., and Woodin, S. A. (1999) Protein structure: An enzymatic globin from a marine worm. *Nature. 401,* 445.

(4) Lincoln, D. E., Fielman, K. T., Marinelli, R. L., and Woodin, S. A. (2005) Bromophenol accumulation and sediment contamination by the marine annelids *Notomastus lobatus* and *Thelepus crispus*. *Biochem. Syst. Ecol. 33*, 559-570.

(5) Poulos, T. L., and Kraut, J. (1980) The stereochemistry of peroxidase catalysis. *J. Biol. Chem. 255,* 8199-8205.

(6) Belyea, J., Gilvey, L. B., Davis, M. F., Godek, M., Sit, T. L., Lommel, S. A., and Franzen, S. (2005) Enzyme function of the globin dehaloperoxidase from Amphitrite ornata is activated by substrate binding. *Biochemistry 44*, 15637-15644.

(7) Osborne, R. L., Taylor, L. O., Han, K. P., Ely, B., and Dawson, J. H. (2004) Amphitrite ornata dehaloperoxidase: enhanced activity for the catalytically active globin using MCPBA. *Biochem. Biophys. Res. Comm. 324*, 1194-1198.

(8) Lebioda, L. (2000) The honorary enzyme haemoglobin turns out to be a real enzyme. *Cell. Mol. Life. Sci. 57,* 1817-1819.

(9) Franzen, S., Gilvey, L.B., and Belyea, J. (2007) The pH dependence of the activity of dehaloperoxidase from *Amphitrite ornata*. *Biochim. Biophys. Acta: Prot. Struct. Mol. Enz. 1774*, 121-130.

(10) LaCount, M. W., Zhang, E., Chen, Y.P., Han, K., Whitton, M. M., Lincoln, D. E., Woodin, S. A., and Lebioda, L. (2000) The crystal structure and amino acid sequence of dehaloperoxidase from *Amphitrite ornata* indicate a common ancestry with globins. *J. Biol. Chem. 275*, 18712-18716.

(11) Nienhaus, K., Deng, P. C., Belyea, J., Franzen, S., and Nienhaus, G. U. (2006) Spectroscopic study of substrate binding to the carbonmonoxy form of dehaloperoxidase from Amphitrite ornata. *J. Phys. Chem. B 110*, 13264-13276.

(12) Nienhaus, K., Nickel, E., Davis, M. F., Franzen, S., and Nienhaus, F. U. (2008) Determinants of substrate internalization in the distal pocket of dehaloperoxidase hemoglobin of *Amphitrite ornata*. *Biochemistry 47*, 12985-12994.

(13) Smirnova, T. I., Weber, R. T., Davis, M. F., and Franzen, S. (2008) Substrate binding triggers a switch in the iron coordination in dehaloperoxidase from Amphitrite ornata: HYSCORE experiments. *J. Am. Chem. Soc. 130*, 2128-2129.

(14) Davis, M. F., Gracz, H., Vendeix, F. A. P., de Serrano, V., Somasundaram, A., Decatur, S. M., and Franzen, S. (2009) Different modes of binding of mono-, di, and tri-halogenated phenols to the hemoglobin dehaloperoxidase from *Amphitrite ornata*. *Biochemistry 48*, 2164-2174.

(15) Chen, Y. P, Lincoln, D. E., Woodin, S. A., and Lovell, C. R. (1991) Purification and properties of a unique flavin-containing chloroperoxidase from the capitellid polychaete *Notomastus lobatus*. *J. Biol. Chem. 266*, 23909-23915.

(16) Thompson, M. K., Davis, M. F., de Serrano, V., Nicoletti, F. P., Howes, B. D., Smulevich, G., and Franzen, S. Two-site competitive inhibition in dehaloperoxidase from *Amphitrite ornata*. (In preparation)

Figures

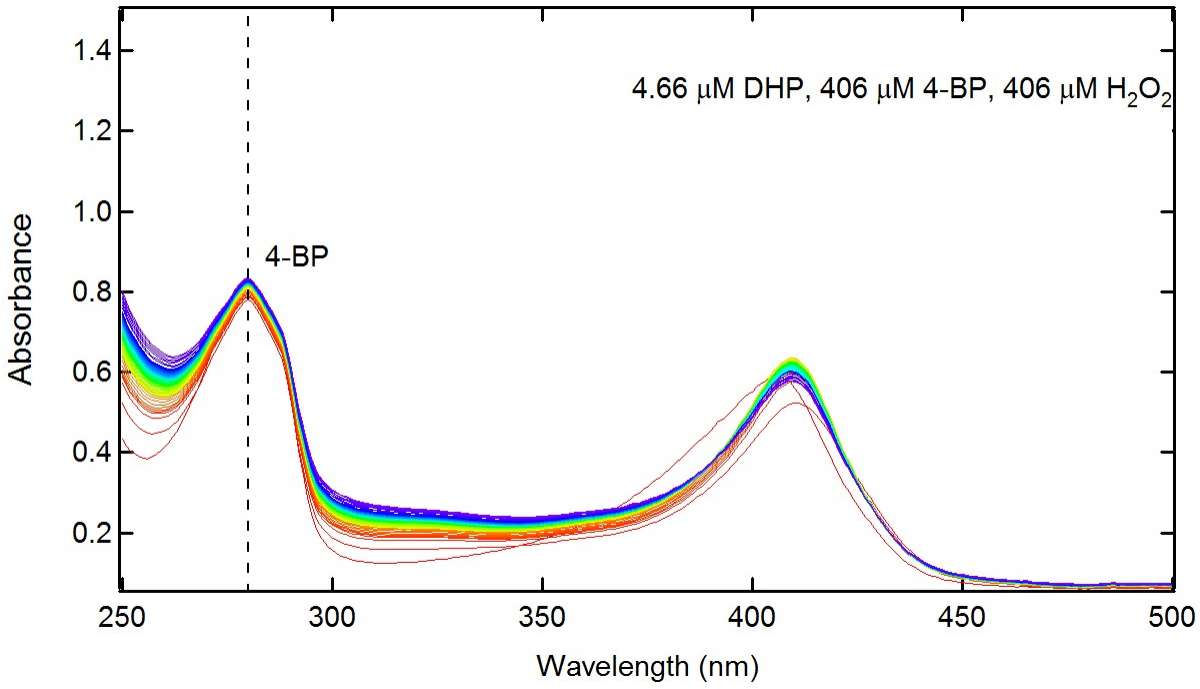

Figure1. UV-Vis assay of DHP activity toward monohalogenated 4-BP. 0 seconds (red) to 600 seconds (purple). Assay conditions were 4.66 μM DHP, 406 μM H_2O_2, and 406 μM 4-BP, pH 7.

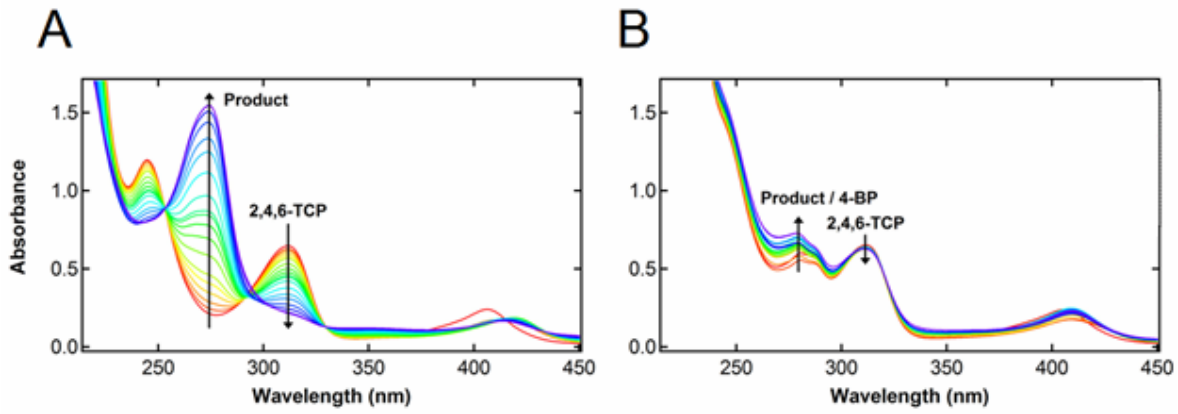

Figure 2. UV-Vis assay illustrating the inhibition of DHP activity toward trihalogenated 2,4,6-TCP upon addition of 4-BP (1:2 ratio) from 0 seconds (red) to 480 seconds (purple). Assay conditions were 2.4 μM DHP, 120 μM H_2O_2, and 120 μM 2,4,6-TCP, pH 7 without (A) and with (B) addition of 240 μM 4-BP.

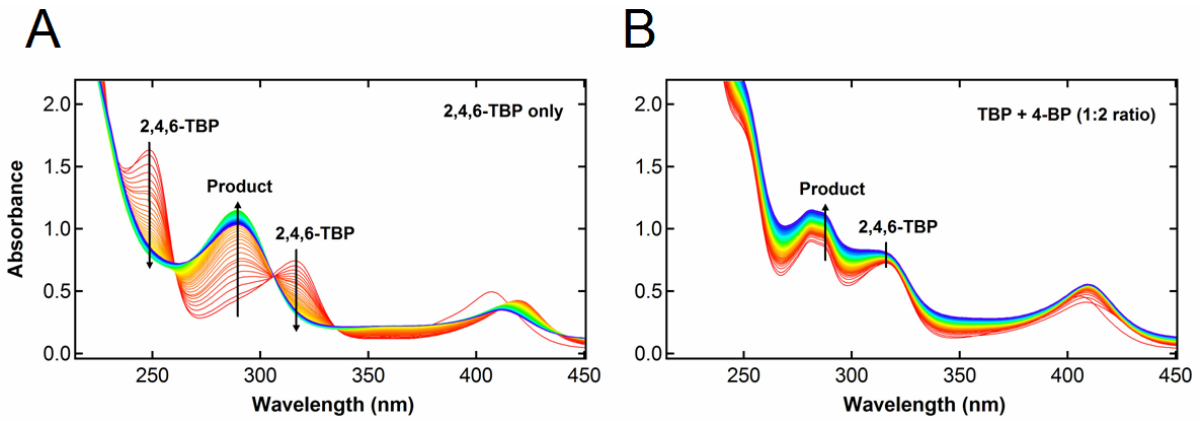

Figure 3. UV-Vis assay showing inhibition of DHP activity toward "native" substrate 2,4,6-TBP in the presence of 4-BP (1:2 ratio) from 0 seconds (red) to 480 seconds (purple). Assay conditions were ~5 μM DHP, 120 μM H_2O_2, and 120 μM 2,4,6-TBP, pH 7 without (A) and with (B) addition of 240 μM 4-BP.

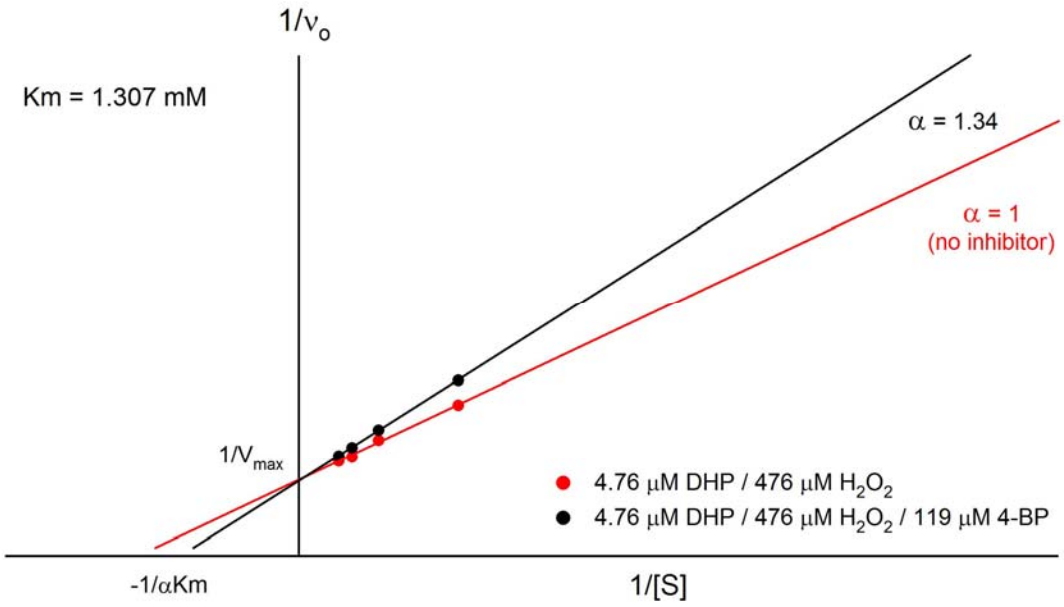

Figure 4. Lineweaver-Burk plot illustrating competitive inhibition of the enzyme by mixing 4-BP and 2,4,6-TCP.

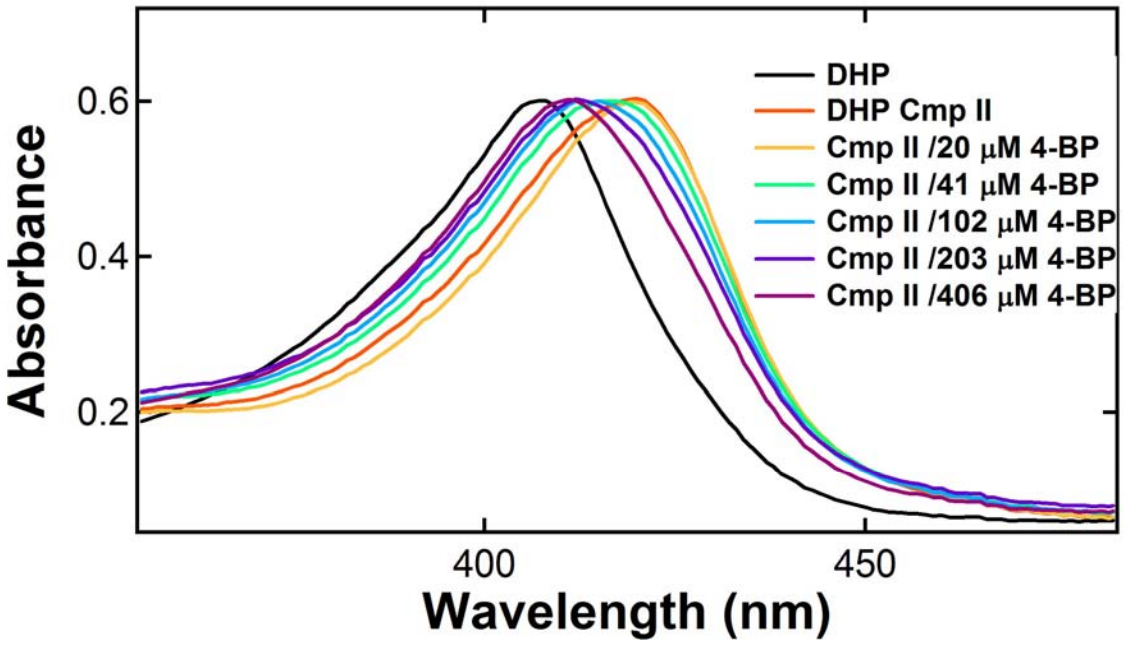

Figure 5. Inhibition of compound II formation in ferric DHP (420 nm) at pH 7 due to increasing concentrations of 4-BP.

CHAPTER 6

Separation of Inhibitor and Substrate Binding Locations in the Globin Dehaloperoxidase

Abstract

The hemoglobin dehaloperoxidase (DHP) is a dual function protein found in the marine polychaete *Amphitrite ornata*. *A. ornata* inhabits estuary mudflats with other polychaetes that secrete a range of toxic halogenated phenols. DHP is capable of binding and oxidatively dehalogenating some of these compounds. The novelty of DHP lies in its ability to bind halophenols in a distinct, internal distal binding pocket. Since its discovery, the distal binding pocket has been reported as the sole binding location for all halophenols. Current data, however, suggest a distinction between inhibitor (monohalogenated phenol) and substrate (trihalogenated phenol) binding locations. Backbone $^{13}C\alpha$, $^{13}C\beta$, carbonyl ^{13}C, amide ^{1}H and amide ^{15}N resonance assignments have been made and various halophenols were titrated into the protein. ^{1}H-^{15}N HSQC experiments were collected at stoichiometric intervals during each titration and binding locations specific for mono- and trihalogenated phenols have been identified. Titration of monohalogenated phenol induced changes around the distal binding pocket, while introduction of trihalogenated phenols created alterations of the distal histidine and the local area surrounding tryptophan 120.

Introduction

The hemoglobin dehaloperoxidase (DHP) is a globin with peroxidase activity found in the terebillid polychaete *Amphitrite ornata*. The protein was initially characterized as one of two globins found in the organism (1) and its general peroxidase activity was characterized in later research (2-5). DHP contains the globin fold and is structurally homologous to Mb (6,7). One novel feature of DHP is its ability to bind halogenated phenols in an internal distal binding pocket (7,8). A bound halophenol in the distal cavity would appear to interfere with the inherent role of globins in oxygen transport and NO scavenging (9, 10). However, *A. ornata* co-inhabits estuary mudflats with other filter feeding marine polychaetes that secrete halophenols presumably for territorial protection (11, 12). One of the co-inhabitants, *Notomastus lobatus*, produces and excretes 4-bromophenol (4-BP), 2,4-dibromophenol (2,4-DBP), and 2,4,6-tribromophenol (2,4,6-TBP) to the surrounding sediment at 1.8 : 0.9 : 1 stoichiometric ratios (13). These small halogenated phenols are extremely toxic, particularly for aquatic organisms. The ability of the globin DHP to bind and oxidatively dehalogenate halophenols may play an important role in the survival of *A. ornata*. In the presence of H_2O_2, DHP readily oxidizes various trihalogenated phenols with reactivity similar to that of horseradish peroxidase (HRP) (4,14-16). However, DHP oxidizes halogenated phenols at an average rate ~13x less than that of HRP (3). The peroxidase activity of DHP towards halophenols is higher than in any hemoglobin measured. The relationship between the internal distal binding pocket and the peroxidase function of DHP has only recently been determined (17).

Since its discovery, the internal binding pocket was thought to be the sole binding site for halophenols in the protein (2, 7, 8, 18). Many studies have illustrated the binding of monohalogenated phenols in the distal pocket, but only a few studies have focused on the general binding of active trihalogenated phenols (19-21). As seen in Figure 1, there is a distinct difference in the activity of DHP towards a monohalogenated versus a trihalogenated phenol. Not only are monohalogenated phenols, such as 4-BP, very poor substrates, recent evidence shows they are inhibitors of peroxidase activity (17). Much of the evidence of inhibition appears linked to the binding location in the distal pocket. The X-ray structure shown in Figure 2 (generated using Pymol) shows bound monohalogenated phenol in a hydrophobic cavity directly above the heme plane (7, 22). Such close binding proximity to the iron inherently reduces the amount of available space for axial ligands. H_2O_2 access to the heme iron is essential for active compound I formation, and subsequent peroxidase activity of the protein (23).

The low water solubility of trihalogenated phenols makes them poor choices for structural studies like X-ray crystallography or NMR experiments. Of the active 2,4,6-trihalophenols only 2,4,6-trifluorophenol (2,4,6-TFP) and 2,4,6-trichlorophenol (2,4,6-TCP) have solubility greater than μM concentrations. 2,4,6-TCP is the closest analog to the native substrate 2,4,6-TBP and is the best laboratory substrate due to its similar size and turnover rates. The most soluble trihalophenol, 2,4,6-TFP, has been used in several structural studies but has typically shown ambiguous results (19, 20). Cryogenic FT-IR and EPR HYSCORE experiments on DHP indicate that 2,4,6-TFP is bound in the distal pocket at low temperatures (< 260K). However, above 260 K the substrate leaves the distal binding pocket and no other

internal perturbations are observed (19). This is apparent lack of substrate binding is counterintuitive given the activity of the substrate at room temperature (15, 21). Previous ^{19}F NMR and relaxation experiments provided initial evidence of a secondary binding site for 2,4,6-TFP at ambient temperatures (21). Eventhough evidence of a secondary binding site exists, the exact location of room temperature 2,4,6-TFP binding has not been reported. Moreover, the use of 2,4,6-TFP as a substrate analog may be a poor choice due to the relative size difference between fluorine and bromine/chlorine substituents.

In this report, assignments of the backbone $^{13}C\alpha$, $^{13}C\beta$, carbonyl ^{13}C, amide ^{1}H and amide ^{15}N resonances have been made using $^{13}C/^{15}N$ labeling and 3D NMR techniques. Paramagnetic low-spin metcyano DHP was used in order to retain continuity with previous NMR investigations. Assignment of 92% of the backbone resonances allowed for observations of structural changes occurring throughout the protein upon introduction of various substrates or inhibitors. Titrations of inhibitor 4-BP and substrates 2,4,6-TCP and 2,4,6-TFP were performed and ^{1}H-^{15}N HSQC experiments were collected at stoichiometric intervals. Deviations in chemical shifts of backbone amide protons were observed for each substrate/inhibitor. The resonances exhibiting the greatest degree of change were then mapped onto current X-ray structures of the protein and the local regions experiencing the largest deviations were analyzed.

Materials and Methods

Protein Expression and Purification. The highly expressing His-DHP4R gene was inserted into the pET-16b vector and transformed into Rosetta^{TM} (DE3) *E. coli* cells. The

Rosetta™ cells were used for their slower growth cycle and additional chloramphenicol (Cam) resistance, not to supply tRNAs for poorly expressed *E. coli* codons. The cells were plated onto LB agar plates containing 100 μg/ml Ap and 34 μg/ml Cam and allowed to grow for ~18 hrs. Single colonies were isolated and 2 ml starter growths in LB broth (100 μg/ml Ap, 34 μg/ml Cam) were allowed to grow at 37 °C overnight. 1 ml of the starter growth was then added to 1L of Spectra 9-CN (Spectra Stable Isotopes, Inc.) medium with >98% ^{13}C and ^{15}N containing aforementioned Ap and Cam concentrations. The 1L double-labeled growth was allowed to grow at 37 °C with shaking until an OD_{600} of 0.3 was reached. IPTG was added to a final concentration of 0.5 mM and the growth temperature was reduced to 25 °C. The cells were then allowed to grow for 20 hrs before being collected via centrifugation. Cell lysis was performed as previously described (21) except that the cleared lysate was incubated with ~100 mg of hemin chloride in 1 ml of 2M NaOH for 8 hrs with stirring at 4 °C. The protein was purified using affinity and ion exchange chromatography described elsewhere (20). Final yields of $^{13}C/^{15}N$ labeled DHP were 24.5 mg/L using this protocol with A_{406}/A_{280} ratios greater than 4.

Sample Preparation and NMR Spectroscopy. All NMR samples were prepared using 90% H_2O / 10% D_2O, 100 mM potassium phosphate buffer, pH 7 and KCN was added between 5-10x excess. The protein was concentrated to 1.6 mM for all 3D NMR experiments. All NMR experiments were collected on a Varian Inova 600 MHz spectrometer at equipped a $^{1}H/^{13}C/^{15}N$ triple resonance probe. For the 4-BP and 2,4,6-TFP titrations, a ^{1}H-^{15}N HSQC experiment was collected at 0:1, 1:1, 2:1, 3:1, 4:1, 5:1, 6:1, 7:1, 10:1, 12:1, and 15:1 halophenol to protein ratio. Only ratios of 0:1, 1:1. 2:1, 3:1, 4:1 were

feasible for the 2,4,6-TCP titration due to its poor water solubility. All NMR experiments were conducted at 298 K, processed via NMRPipe (24), and analyzed using Sparky (25).

UV-Vis Enzymatic Assays. For all experiments DHP was oxidized via addition of excess $K_3Fe(CN)_6$. The excess ferricyanide was removed and DHP was buffer exchanged into 100 mM potassium phosphate, pH 7 using a Sephadex G-25 column. All absorption data were collected on a Hewlett Packard 8453 multi-wavelength spectrometer. Spectra were collected every 5 seconds over a 600 second time frame. The conditions used for the assays were: ~ 2.5 μM DHP, 120 μM H_2O_2, and 120 μM substrate or inhibitor. Turnover of the halophenols were determined by the disappearance of its respective absorption bands at pH 7 (4-BP – 280 nm; 2,4,6-TCP – 313 nm) and appearance of product absorption bands (2,6-dichloro-1,4-benzoquinone (2,6-DCQ) – 272 nm).

Results

Figure 1 illustrates the differences in activity between the monohalogenated 4-BP and trihalogenated 2,4,6-TCP. The activity of substrate 2,4,6-TCP is clearly seen on the left in Figure 1. Upon addition of H_2O_2, complete conversion of 2,4,6-TCP to 2,6-DCQ is observed over the course of the assay (red = 0s; blue = 600s). The oxidation of 2,4,6-TCP can be seen by the decrease in its absorption band at 313 nm or conversely by the appearance of the 2,6-DCQ product band at 273 nm. 4-BP, on the other hand, has been shown to be an efficient inhibitor of DHP activity (17). As can be seen from Figure 1, this inhibition does not involve a pathway indicative of suicide inhibition. Upon addition of H_2O_2 the 4-BP

absorption band at 280 nm is not diminished, and during the 600s assay no detectable product band is observed.

Using ^{15}N-^{1}H HSQC, HNCO, HCACOCANH, HNCOCA, HNCA, and HNCACB experiments on backbone ^{13}Cα, ^{13}Cβ, carbonyl ^{13}C, amide ^{1}H and amide ^{15}N resonances, 125 of the 137 residues in DHP have been assigned. The quality of the ^{15}N-^{1}H HSQC spectrum (Figure 3) indicates good peak dispersion with minimal peak overlap. The inset shows the crowded region between 9.2 and 8.2 ppm (^{1}H). The crosspeaks at 11.8 (^{1}H), 133.0 ppm (^{15}N) and 11.2 (^{1}H), 118.5 ppm (^{15}N) arise from the non-backbone W120 NεH and H55 NεH side chain resonances, respectively. DHP contains 1 TRP (W120) and 2 HIS residues (H89, H55). The two HIS residues are the conserved proximal (H89) and distal (H55) histidines. The exchangeable NεH of H89 occurs at 19.9 ppm (^{1}H) and was assigned in previous work (20). In the ^{1}H NMR spectrum of a H55V mutant, the exchangeable at 11.2 ppm (H55 NεH) disappears while the exchangeable at 11.8 ppm (W120 NεH) remains unchanged, hence confirming the assignments.

The amide protons of F35, V59, V128, F60, F21, L25, K58, and L22 respectively experience the eight largest deviations in chemical shift in the presence of 4-BP. In Figure 4 deviations in V59, F35, and F21 are shown. These three side chains comprise the internal distal binding pocket and conversely show 3 of the top 5 chemical shift deviations upon addition of 4-BP. Current X-ray structures (7) indicate V59, F35, and F21 are the closest to bound 4-iodophenol (4-IP) with C-C distances of 2.98, 2.98, and 3.41 Å, respectively. The panels on the left in Figure 4 show these deviations in the presence of inhibitor 4-BP, while the panels on the right show responses of these same resonances upon addition of substrate

2,4,6-TCP. No changes in chemical shift are seen in these resonances upon addition of 2,4,6-TCP.

The largest chemical shift deviations induced by the substrate 2,4,6-TCP occur in a separate area of the protein compared to 4-BP. The exchangeable H55 NεH and amide protons of D121, G1, R122, V102, F2, K3, and V128 exhibit the greatest change when exposed to 2,4,6-TCP. The deviations in H55 NεH, G1, R122, and K3 are presented in Figure 5. The average change in chemical shift for 2,4,6-TCP is ~28% of that observed with 4-BP. However, solubility of the halophenols only permitted a 4x excess of 2,4,6-TCP versus a 15x excess of 4-BP. 2,4,6-TFP is the only trihalogenated substrate soluble enough to reach a 15x excess at concentrations needed for NMR experiments. The smaller 2,4,6-TFP molecule is an active substrate, but it is not as active as other trihalophenols such as 2,4,6-TCP or 2,4,6-TBP (15, 21). With the addition of 2,4,6-TFP, H55 NεH, G1, F35, D116, F21, F2, K3, and V59 exhibit the greatest changes in chemical shift (Supporting Information). At a 15x excess of 2,4,6-TFP the average deviation in chemical shift is the lowest of the halophenols and the substrate is believed to be the weakest binding trihalogenated phenol. In the monohalogenated phenol series, replacement of the fluorine substituent with a chlorine atom results in an increase in K_D from 1.7 mM to 3.7 mM (17). It is unclear if this decrease in binding affinity translates to the trihalogenated series, but this assumption justifies the significantly lowered observed chemical shift deviation in 2,4,6-TFP.

Discussion

The binding location of active substrates in DHP is a requisite to understand how the protein carries out substrate oxidation. Substrate binding in DHP has been misunderstood since the first reports of internal binding of 4-IP were published (7,8). The internal distal binding pocket (4-IP binding location) is currently believed to be sole binding local for all halophenols in the protein. Recent studies, however, have illustrated that binding of monohalogenated phenols in the distal pocket renders the protein inactive. The inactivation of the protein is believed to occur via two mechanisms. First, the distal histidine is shown in both the "open" and "closed" conformations in X-ray structures (6,7,26). Upon binding of monohalogenated phenols the histidine is solely in the "open" conformation. This effectively removes the only residue capable of the acid-base catalysis needed to form the active compound I species, which is the oxidant in most peroxidases. In DHP, it has been shown that compound ES forms instead of compound I. Compound ES in DHP consists of an oxoferryl heme and a protein radical. Second, the location of monohalogenated phenol prevents H_2O_2 from binding to the heme iron, which is a prerequisite for formation of compound ES. The presence of monohalogenated phenol and H_2O_2 creates a competition for access to the heme. The nature of inhibition can be seen in recent work where the amount of compound ES formed is anti-correlated to the concentration of monohalogenated phenol present (17).

The largest deviations in chemical shift occurring upon addition of 4-BP, 2,4,6-TCP, and 2,4,6-TFP have been mapped onto the X-ray structure of the protein. The location of the top eight chemical shift changes for each halophenol is shown in Figure 6. The four largest deviations are shown in red, while the next four largest are shown in blue. The heme and

W120 side chain are also shown in green. The heme and W120 lie separated by approximately 8.5 Å. These two sites serve as focal points for the analysis of substrate binding, because both are capable of retaining a reactive radical species capable of oxidizing 2,4,6-TCP or 2,4,6-TFP (27, 28). In panel A, the greatest deviations induced by addition of 4-BP are seen. The most prominent changes in chemical shift are all centered at the exact location of 4-IP binding in the X-ray structure. The F35, V59, and F21 residues (Figure 5) are the three closest side chains to bound 4-IP and the amide protons of these residues comprise the greatest, second greatest, and fifth greatest deviation in chemical shift, indicating structural devations in these three distal pocket residues.

As can seen in Figure 5 these same residues are not effected when the substrate 2,4,6-TCP is titrated in. Instead, a separate region of the protein experiences the majority of the effect. While the greatest chemical shift change is found at the exchangeable H55 NεH, the local area surrounding W120 experiences the largest number of chemical shift deviations with D121, G1, R122, V102, F2, and K3 all experiencing all exhibiting large deviations. At first it may appear that the relative size of the halophenol is a factor in its binding location. While this may be true, analysis of the effects induced by the smallest halophenol studied, 2,4,6-TFP, show that both the distal pocket and area of W120 are affected equally. Previous NMR studies showed that internal heme substituents were not affected by addition 2,4,6-TFP. These same heme substituents (notably the 3-CH_3) showed significant changes in the presence of 4-BP. This indicated that the larger 4-BP has a much more pronounced effect in the distal pocket than 2,4,6-TFP (20). The activity of 2,4,6-TFP, and the similarities to 2,4,6-TCP in backbone perturbations near H55 NεH and W120, may indicate the positioning of the

halogens as an important factor in binding location. The NMR data and enzymatic assays suggest that primary binding of the monohalogenated phenols in the distal pocket leads to the inhibition of the protein. In addition, primary structural changes near W120 are only associated with substrates that show activity (i.e. 2,4,6-TCP and 2,4,6-TFP). While 4-BP does induce small chemical shift changes in the area of W120, the primary deviations are localized at the distal binding pocket.

The data indicate that binding of 2,4,6-TCP substrate involves one of the following scenarios. First, binding of the substrate may primarily occur on the external edge of the distal H55. This conclusion is reached on the basis that the largest change in chemical shift observed for both active substrates (2,4,6-TCP and 2,4,6-TFP) occurs at the distal H55 NεH. Whether H55 is in the "open" conformation or in the "closed" conformation and therefore hydrogen bonded to the axial cyanide cannot be determined from current NMR data. Earlier FT-IR experiments on the isoelectric, ferrous DHPCO adduct indicated the orientation of H55 to be in the "closed" conformation at pH 7, 290K (29). These data are consistent with resonance Raman data that show an increase in the 6-coordinate high spin metaquo adduct when 2,4,6-TXP (X = Br, Cl, F) bind to DHP (21). The experiments also showed the pKa for protonation of H55, and subsequent rotation of H55 to the "open" conformation, occurs at pH 4.5. If H55 is in the closed conformation then the observed deviations of H55 NεH are likely the result of a perturbation in the Nε-H· · ·NC hydrogen bond. The lack of internal pocket changes upon 2,4,6-TCP addition rules out binding of the molecule in the distal binding pocket. Binding of the molecule on the solvent exposed, external side of H55 could be the cause for the deviation in the H55 NεH chemical shift. This scenario would place the

substrate near the heme edge in an external fashion which is typical of other heme peroxidases, like HRP. Peroxidases like HRP commonly perform substrate oxidation by electron transfer from the substrate which binds at the heme edge (27). In addition, the resonance Raman data on metaquo DHP indicate an increase in 6-coordinate heme upon addition of 2,4,6-TCP consistent with a "push" of H55 toward the protein interior, lending credence to this binding scenario (8). The remaining large deviations which occur near W120 could be the result of allosteric changes at the dimer interface triggered from the perturbation of H55 NεH. R122, V74, and D72 are the three residues which comprise the interface in the crystal structure. The local area near W120 also lies along the dimer interface. There is a long standing precedent for allosteric changes at dimer interfaces resulting from perturbations of the axial ligand. Eventhough cooperative binding and allosteric changes are typically related to tetrameric Hbs, many well-known studies have illustrated similar changes in more primitive, dimeric Hbs similar to DHP (30-33). Alterations in H55 NεH would affect the hydrogen bond between the H55 side chain and the axial CN ligand. While this scenario seems plausible, the lack of other amide proton deviations around H55 brings doubt to this hypothesis. The amide proton of H55 and those of the nearby Q88 and Y34 residues also do not exhibit alterations in chemical shift.

A second scenario involves direct binding of the substrate in the region near W120. As seen in Figure 6, this specific region experiences the largest number of chemical shift deviations upon introduction of 2,4,6-TCP. This scenario is highly plausible given that the chemical shift deviations in D121, G1, R122, V102, F2, and K3 represent 6 of the 7 largest deviations upon addition of 2,4,6-TCP. All of these residues are located near W120. In

addition, many peroxidases, such as lignin peroxidase, manganese peroxidase, and versatile peroxidase, are known to bind and oxidize high redox potential aromatics near an exposed tryptophan radical (34-37). Lignin peroxidase, in particular, performs an oxidative 4-dechlorination of 2,4,6-TCP just as HRP or DHP (38). Even one of the most commonly studied peroxidases, cytochrome c peroxidase (CcP), is known to generate a tryptophan radical (39). Upon addition of requisite co-substrate H_2O_2, X-band EPR experiments do indicate the presence of a yet unidentified protein radical in DHP (40). In fact, electronic similarities between the DHP intermediate and the TRP191 radical species of CcP compound ES, has led to naming the intermediate "DHP compound ES" (40). The only caveat being the nearly 9 Å distance between the heme edge and W120 in DHP. Therefore, long range electron transfer of the radical must occur to account for this scenario. The NMR data paired with the ability of a W120 radical to act as an oxidizing equivalent means a scenario involving 2,4,6-TCP binding and oxidation near W120 cannot be ruled out. Binding of the substrate at this site must however account for the change in H55 NεH. Because the heme edge and W120 are separated by nearly 9 Å, substrate binding near W120 must produce transferable long range binding effects to the axial CN, and likewise the H-bonded H55 NεH. Conducting enzymatic assays of various W120 mutants will help determine the role W120 plays in substrate binding and overall protein activity.

Conclusion

The current study has shown a distinction in binding perturbations of mono- and trihalogenated phenols. The monohalogenated inhibitor 4-BP created the greatest deviation

in backbone amide ^{1}H chemical shifts at the exact area of the distal binding pocket. This corroborates X-ray data by showing the largest changes in chemical shift at the 3 closest residues to bound 4-IP in the crystal structure. Addition of trihalogenated substrate 2,4,6-TCP resulted with the largest single deviation being the exchangeable H55 NεH. However, the next 6 largest deviations in chemical shift were centered at W120, over 8.5 Å away from the heme group and nearly 15 Å away from H55. No significant changes were observed in binding pocket resonances upon addition of 2,4,6-TCP, clearly illustrating that binding of substrate 2,4,6-TCP is substantially different than binding of inhibitor 4-BP. Introduction of the smaller 2,4,6-TFP produced its largest alterations in chemical shifts at distal binding pocket resonances, H55, and resonances in the local area of W120. 2,4,6-TFP also produced the lowest average deviation in chemical shift. The molecule may be small enough to bind at the inhibitor site, but also causes significant deviations at the 2,4,6-TCP site. This could indicate halogen positioning as a factor in halophenol binding location. Two scenarios were presented that may tie together the activity of 2,4,6-TCP and its observed binding perturbations. First, binding of the substrate on the external side of H55 could create allosteric changes in the local area of W120, near the dimer interface. A second scenario involves direct binding near W120 itself. In both cases, the 2,4,6-TCP substrate would be in favorable position for oxidation either along the heme edge or at a tryptophan radical, respectively. The NMR results have provided crucial insight into binding interactions between the protein and a highly active substrate, 2,4,6-TCP. Site-directed mutagenesis of W120 will help determine the role of the residue in binding and/or oxidation of trihalogenated substrates. Increased knowledge of the true substrate binding site in DHP will

hopefully lead to improvements in protein specificity toward other highly toxic haloaromatics and increase the opportunity to use DHP for additional bioremediation processes.

Acknowledgements

This work was done in collaboration with Benjamin Bobay (NCSU) and Stefan Franzen (NCSU). This project was supported by Army Research Office grant 52278-LS.

References

1. Weber, R. E., Mangum, C., Steinman, H., Bonaventura, C., Sullivan, B., and Bonaventura, J. (1977) *Comp. Biochem. Physiol.* **50A,** 179-187
2. Chen, Y. P., Woodin, S. A., Lincoln, D. E., and Lovell, C. R. (1996) *J. Biol. Chem.* **271,** 4609-4612
3. Belyea, J., Gilvey, L. B., Davis, M. F., Godek, M., Sit, T. L., Lommel, S. A., and Franzen, S. (2005) *Biochemistry* **44,** 15637-15644
4. Osborne, R. L., Taylor, L. O., Han, K. P., Ely, B., and Dawson, J. H. (2004) *Biochem. Biophys. Res. Comm.* **324,** 1194-1198
5. Lebioda, L. (2000) *Cell. Mol. Life. Sci.* **57,** 1817-1819
6. de Serrano, V., Chen, Z., Davis, M. F., and Franzen, S. (2007) *Acta Crysta. D* **63,** 1094-1101
7. Zhang, E., , Chen, Y. P., Roach, M. P., Lincoln, D. E., Lovell, C. R., Woodin, S. A., Dawson, J.H., and Lebioda, L. (1996) *Acta Cryst. D* **52,** 1191-1193
8. Lebioda, L., LaCount, M. W., Zhang, E., Chen, Y. P., Han, K., Whitton, M. M., Lincoln, D. E., and Woodin, S. A. (1999) *Nature.* **401,** 445
9. Shikama, K. (2006) *Prog. Biophys. Mol. Bio.* **91**, 83-162
10. Flögel, U., Merx, M. W., Gödecke, A., Decking, U. K. M., and Schrader, J. (2001) *Proc. Nat. Acad. Sci. U. S. A.* **98,** 735-740
11. Han, K., Woodin, S. A., Lincoln, D. E., Fielman, K. T., and Ely, B. (2001) *Mar. Biotechnol.* **3,** 287-292
12. Chen, Y. P., Lincoln, D. E., Woodin, S. A., and Lovell, C. R. (1991) *J. Biol. Chem.* **266,** 23909-23915
13. Lincoln, D. E., Fielman, K. T., Marinelli, R. L., and Woodin, S. A. (2005) *Biochem. Syst. Ecol.* **33,** 559-570
14. Franzen, S., Gilvey, L.B., and Belyea, J. (2007) *Biochim. Biophys. Acta: Prot. Struct. Mol. Enz.* **1774,** 121-130

15. Chaudhary, C. (2003) *MS Thesis* NC State University
16. Ferrari, R. P., Laurenti, E., and Trotta, F. (1999) *J. Biol. Inorg. Chem.* **4,** 232-237
17. Thompson, M. K., Davis, M. F., de Serrano, V., Nicoletti, F. P., Howes, B. D., Smulevich, G., and Franzen, S. (Submitted, Nature)
18. Franzen, S., Belyea, J., Gilvey, L. B., Davis. M. F., Chaudhary, C. E., Sit, T. L., and Lommel, S. A. (2006) *Biochemistry* **45,** 9085-9094
19. Nienhaus, K., Nickel, E., Davis, M. F., Franzen, S., and Nienhaus, G. U. (2008) *Biochemistry* **47,** 12985-12994
20. Smirnova, T. I., Weber, R. T., Davis, M. F., and Franzen, S. (2008) *J. Am. Chem. Soc.* **130,** 2128-2129
21. Davis, M. F., Gracz, H., Vendeix, F. A. P., de Serrano, V., Somasundaram, A., Decatur, S. M., and Franzen, S. (2009) *Biochemistry* **48,** 2164-2172
22. DeLano, W. L. (2002) *The PyMOL Molecular Graphics System*, DeLano Scientific, Palo Alto, CA
23. Poulos, T., and Kraut, J. (1980) *J. Biol. Chem.* **255,** 8199-8205
24. Delaglio, F., Grzesiek, S., Vuister, G.W., Zhu, G., Pfeifer, J., and Bax, A. (1995) *J. Biomol. NMR* **6,** 277–293
25. Goddard, T. D., and Kneller, D. G. *SPARKY 3*, University of California, San Francisco
26. Chen, Z., de Serrano, V., Betts, L., and Franzen, S. (2009) *Acta Crysta. D* **65,** 34-40
27. Ator, M. A., and Ortiz de Montellano, P. R. (1987) *J. Biol. Chem.* **262,** 1542-1551
28. Pogni, R., Baratto, M. C., Giansanti, S., Teutloff, C., Verdin, J., Valderrama, B., Lendzian, F., Lubitz, W., Vazquez-Duhalt, R., and Basosi, R. (2005) *Biochemistry* **44,** 4267-4264
29. Nienhaus, K., Deng, P. C., Belyea, J., Franzen, S., and Nienhaus, G. U. (2006) *J. Phys. Chem. B* **110,** 13264-13276
30. Royer, W. E., Hendrickson, W. A., and Chiancone, E. (1990) *Science* **249,** 518-521
31. Royer, W. E., Pardanani, A., Gibson, Q. H., Peterson, E. S., and Friendman, J. M. (1996) *Proc. Natl. Acad. Sci. U. S. A.* **93,** 14526-14531

32. Royer, W. E., Zhu, H., Gorr, T., A., Flores, J. F., and Knapp, J. E. (2005) *J. Biol.. Chem.* **280,** 27477-27480

33. Knapp, J. E., Pahl, R., Šrajer, V., and Royer. W. E. (2006) *Proc. Natl. Acad. Sci. U. S. A.* **103,** 7640-7654

34. Doyle, W. A., Blodig, W., Veitch, N. C., Piontek, K., and Smith, A. T. (1998) *Biochemistry* **37,** 15097-15105

35. Tünde, M., Ambert-Balay, K., Ciofi-Baffoni, S., Banci, L., Jones, A. D., and Tien, M. (2001) *J. Biol. Chem.* **276,** 22985-22990

36. Pérez-Boada, M., Ruiz-Dueñas, F. J., Pogni, R., Basosi, R., Choinowski, T., Martínez, M. J., Piontek, K., Martínez, A. T. (2005) *J. Mol. Biol.* **354,** 385-402

37. Ruiz-Dueñas, F. J., Pogni, R., Morales, M., Giansanti, S., Mate, M. J., Romero, A., Martínez, M. J., Basosi, R., and Martínez, A. T. (2009) *J. Biol. Chem.* **284,** 7986-7994

38. Hammel, K. E., and Tardone, P. J. (1988) *Biochemistry.* **27,** 6563-6568

39. Sivaraja, M., Goodin, D. B., Smith, M., and Hoffman, B. M. (1989) *Science* **245,** 738-740

40. Feducia, J., Dumarieh, R., Gilvey, L., B., G., Smirnova, T., Franzen, S., and Ghiladi, R. A. (2009) *Biochemistry* **48,** 995-1005

Figures

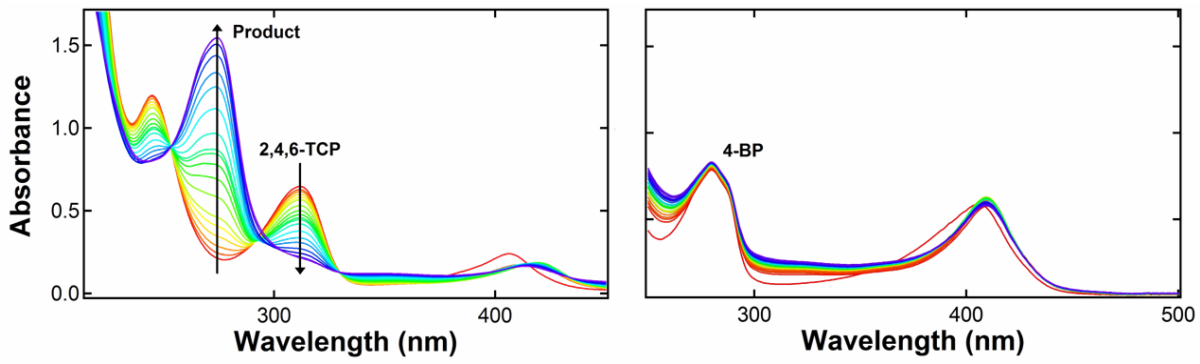

Figure 1. UV-Vis enzymatic assay illustrating 2,4,6-TCP and 4-BP activity. The differences in activity between 2,4,6-TCP (left) and 4-BP (right) are shown. The figures represent a 600s assay going from red (0s) to blue (600s). The 2,4,6-TCP molecule is completely converted to product 2,6-dichloro-1,4-benzoquinone (left) while the 4-BP molecule does not experience turnover (right).

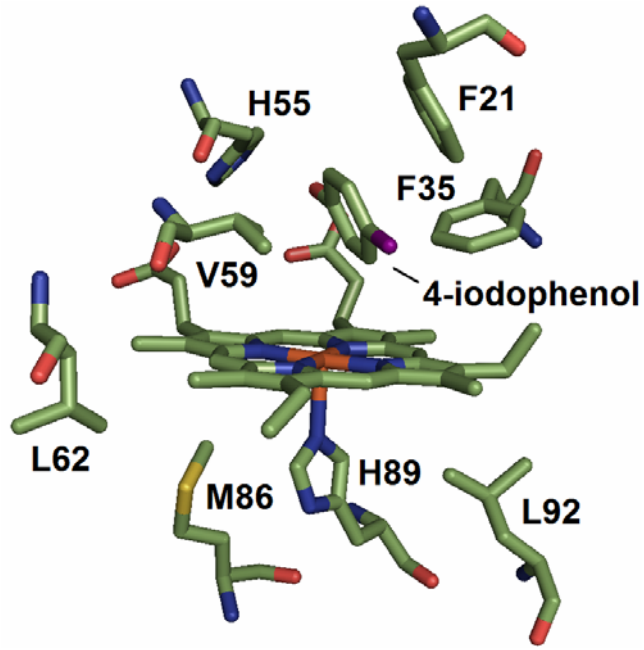

Figure 2. X-ray structure of the distal binding pocket of DHP. The X-ray structure (7) illustrates binding of monohalogenated 4-IP in the distal pocket. The closest residues to bound 4-IP are F35, V59, and F21.

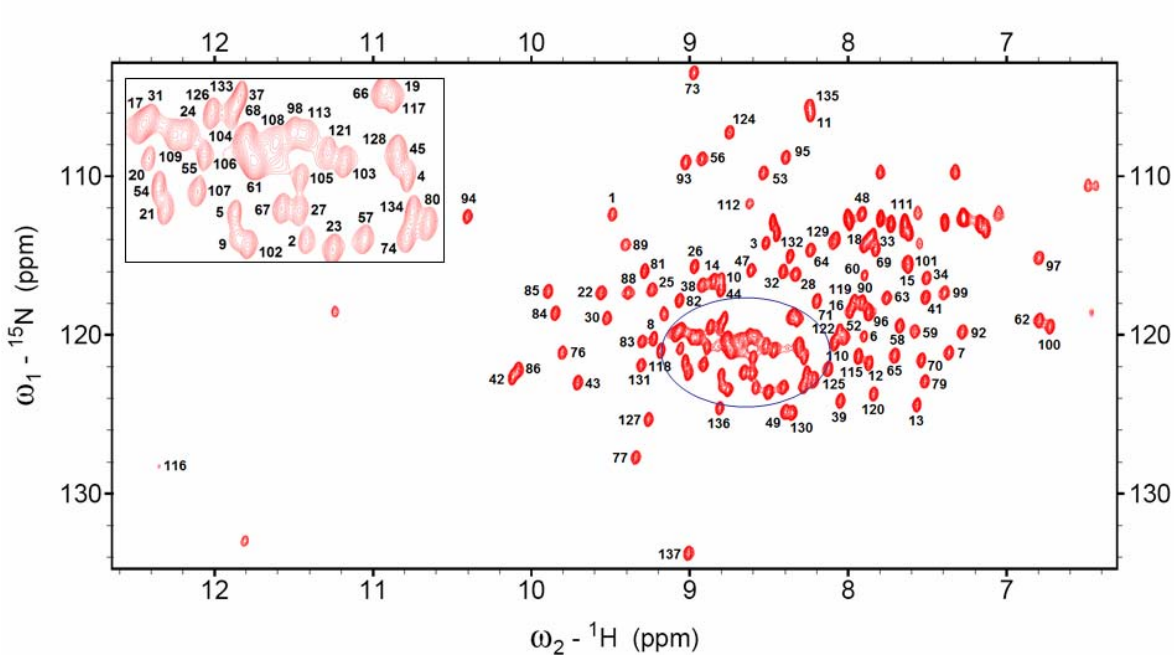

Figure 3. ^{15}N-^{1}H HSQC of DHPCN collected at 298K. The ^{15}N-^{1}H HSQC shows minimal overlap and the crowded area of the spectrum (blue circled region) is shown in the inset. Backbone amide ^{1}H resonances are labeled.

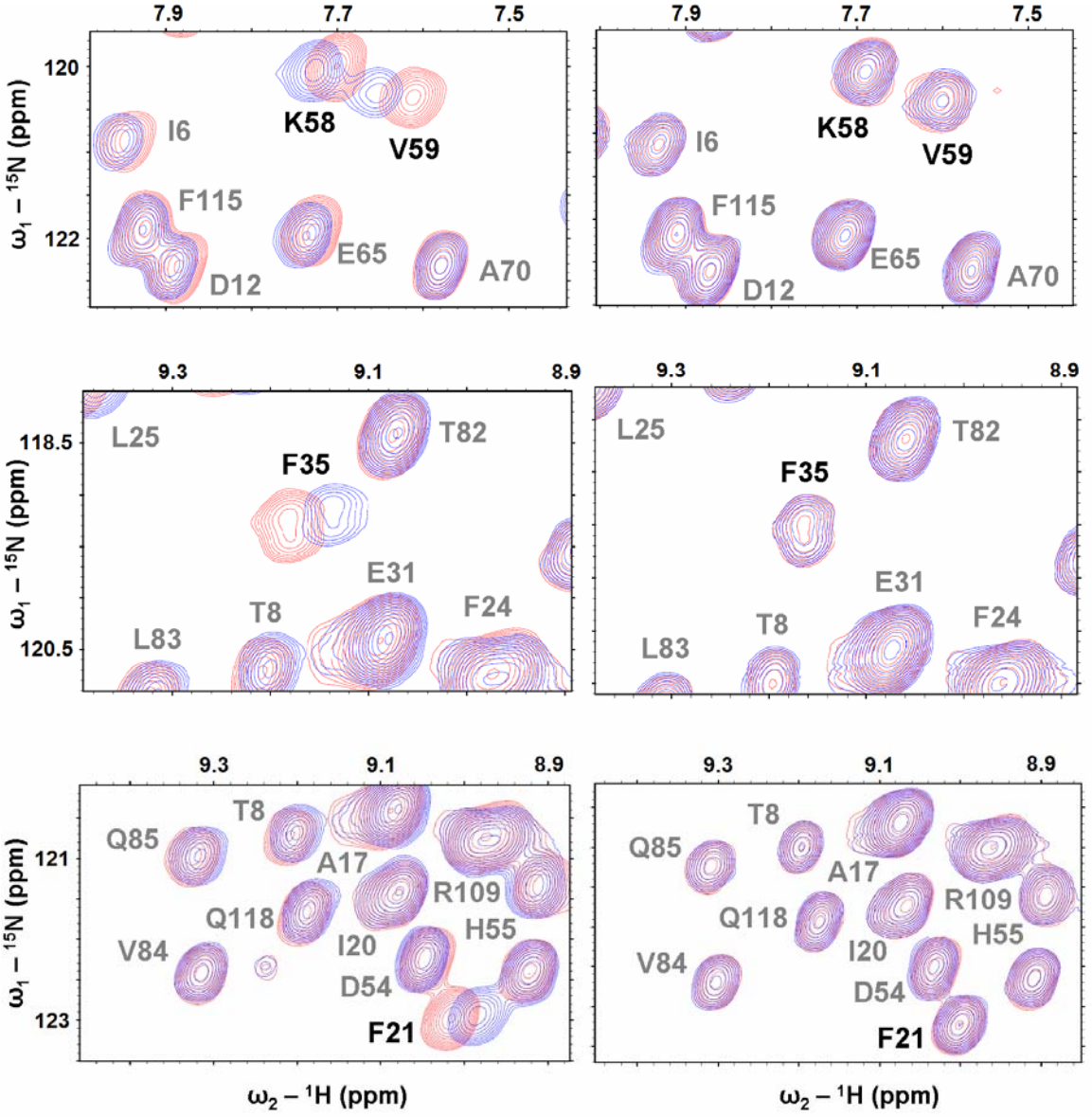

Figure 4. ^{15}N-^{1}H HSQC spectrum of DHPCN titrated with 4-BP (left column) and 2,4,6-TCP (right column). The amide ^{1}H resonances which exhibit the greatest change in chemical shift upon addition of 4-BP (left) are shown. Upon addition of 2,4,6-TCP (right) these same resonances show no observable deviations.

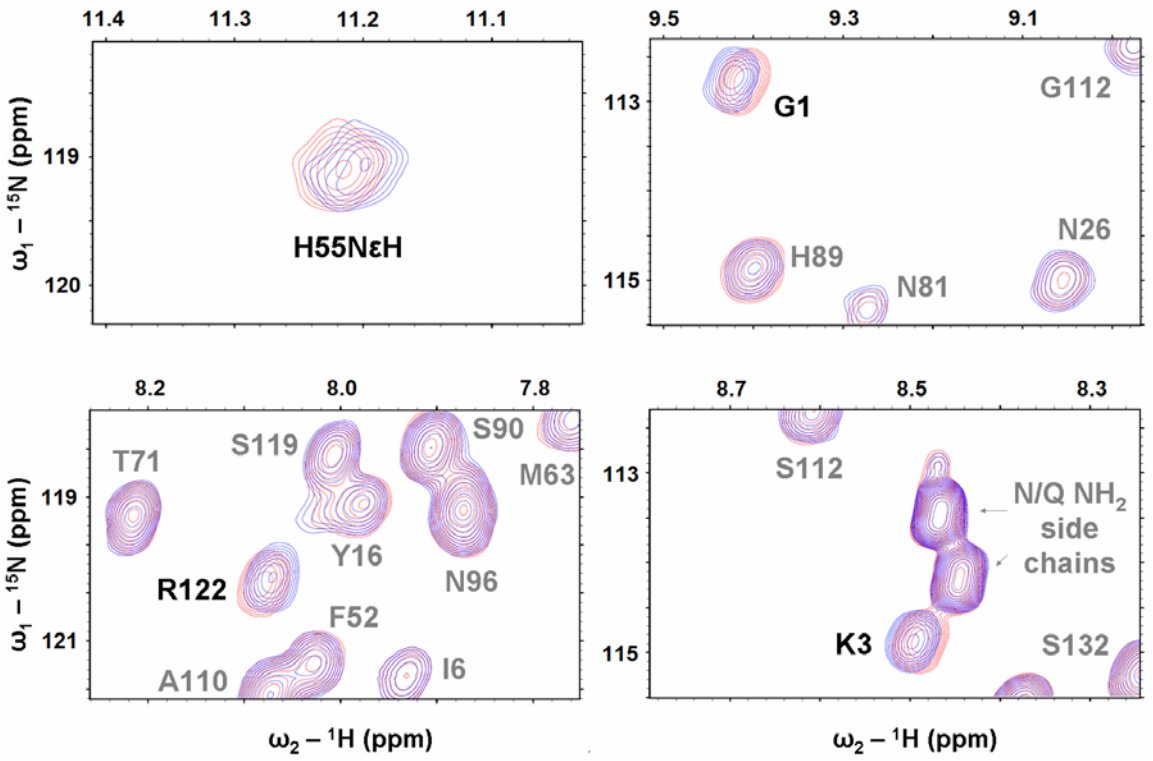

Figure 5. ^{15}N-^{1}H HSQC spectrum of DHPCN titrated with 2,4,6-TCP. The ^{1}H resonances exhibiting the largest deviations in chemical shift are shown. These include the exchangeable distal histidine H55 NεH, and amide protons of G1, R122, and K3.

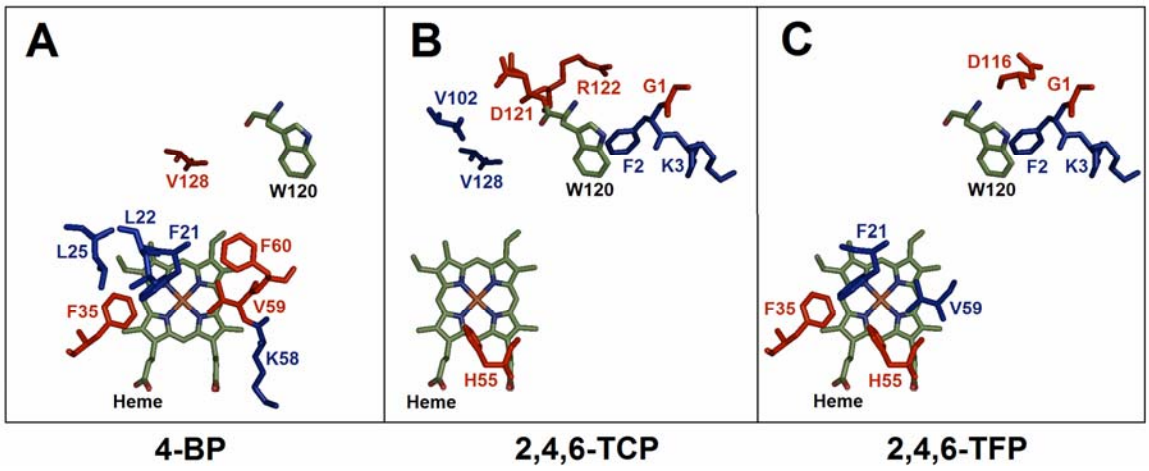

Figure 6. The residues experiencing the largest chemical shift deviations have been mapped onto an existing X-ray structure (6). The side chains in red represent the 4 largest chemical shift changes and the residues in blue represent the next 4 largest deviations. The heme and W120 residue are provided as focal points. Panels A, B, and C show the largest deviations caused by addition of 4-BP, 2,4,6-TCP, and 2,4,6-TFP, respectively.

APPENDICES

APPENDIX 1

Supporting Information for Chapter 3

Supporting Information

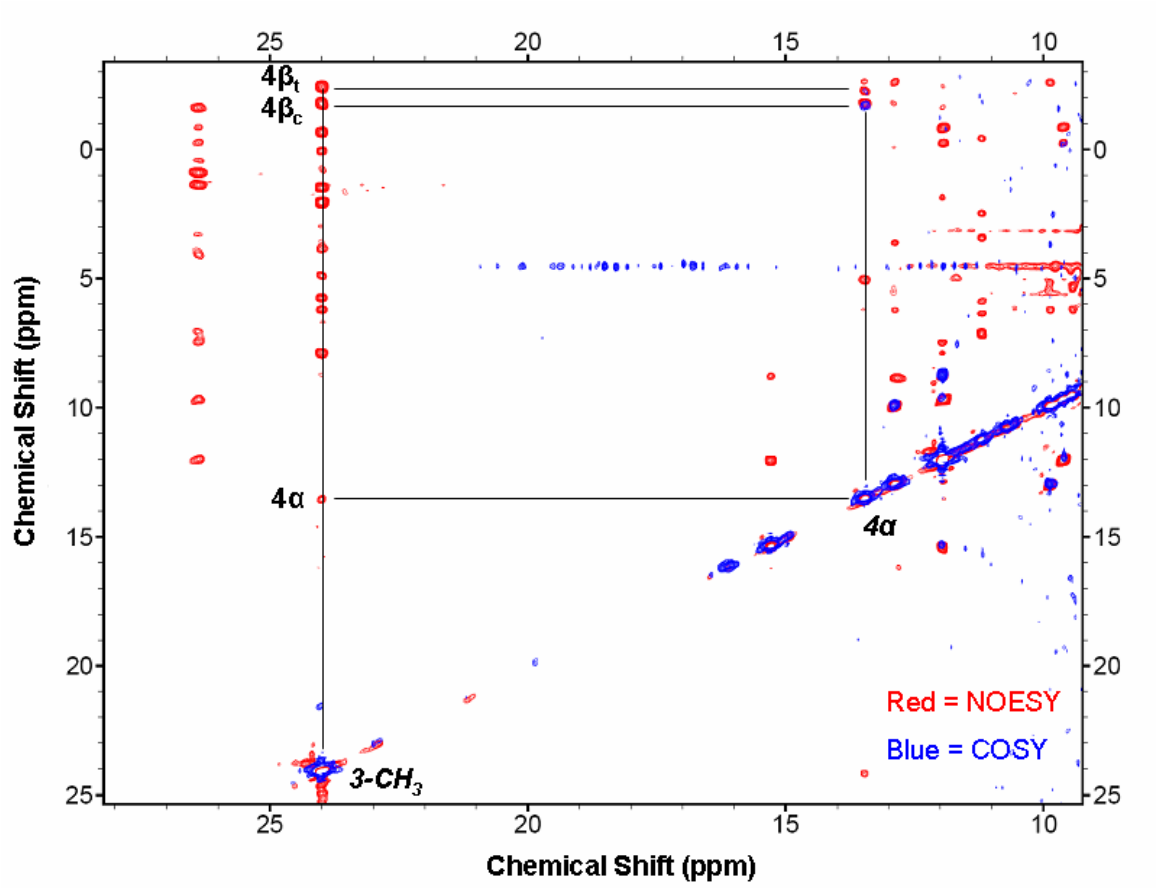

Figure S1. NOESY and COSY overlay map of DHPCN. NOESY crosspeaks (red) and COSY scalar coupling (blue) between the 3 proton spin system of the heme 4-vinyl group. Scalar coupling is observed between the 4α, $4\beta_c$, and $4\beta_t$ vinyl protons. NOESY cross peaks are observed from all three of these resonances to the heme 3-CH_3 methyl group.

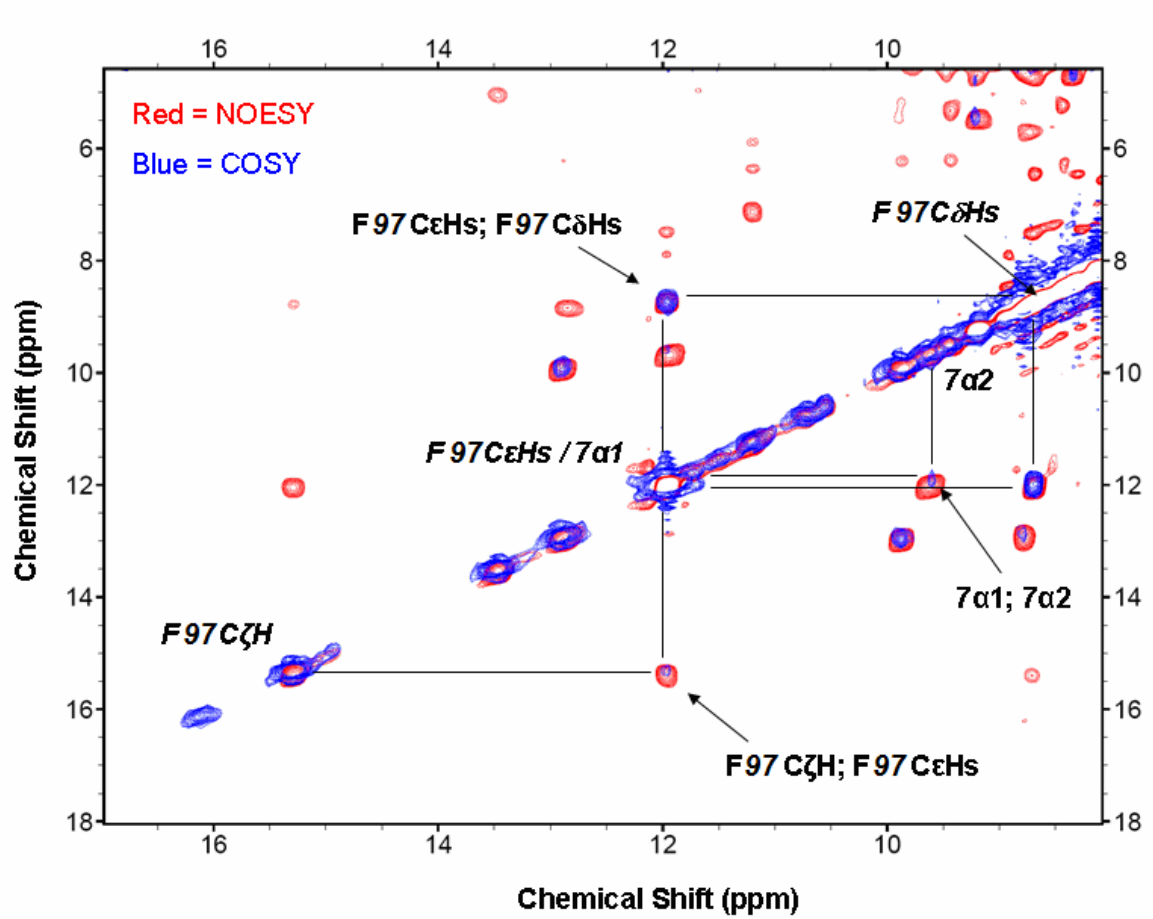

Figure S2. NOESY and COSY overlay map showing the dipolar and scalar connectivity between the F97 ring protons. Connectivity for the overlapping 7α propionate resonances can also be seen.

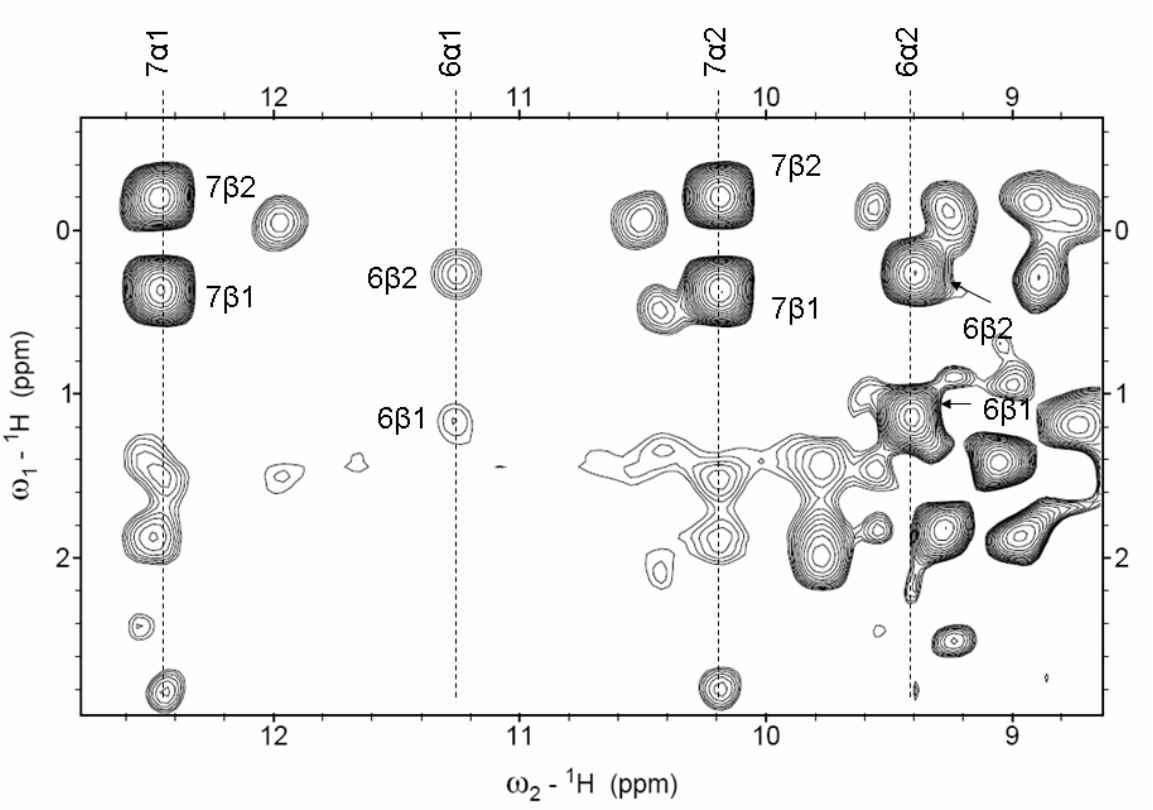

Figure S3. WEFT-NOESY map showing dipolar connectivity exhibited in the 6- and 7-propionate chains.

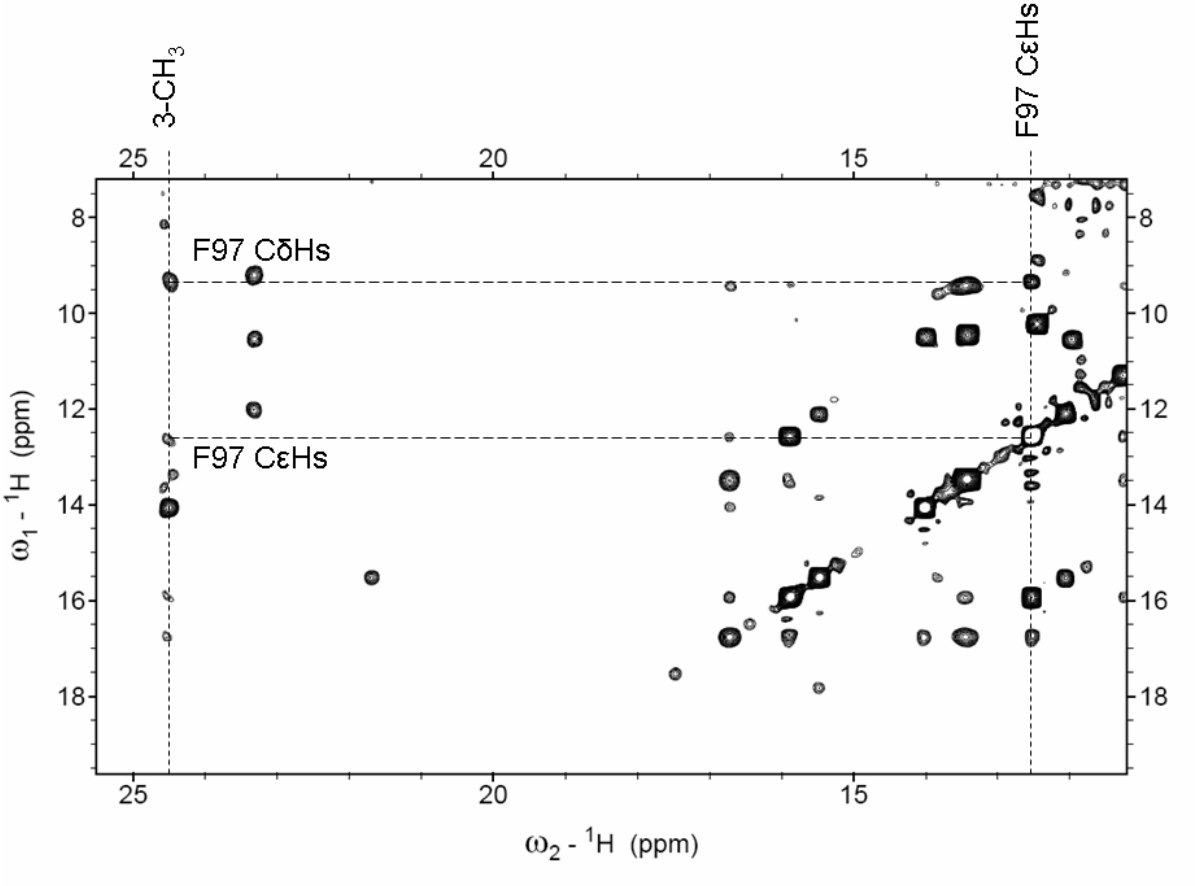

Figure S4. WEFT-NOESY map showing dipolar connectivity exhibited in the 3-CH_3 heme methyl and F97 ring resonances.

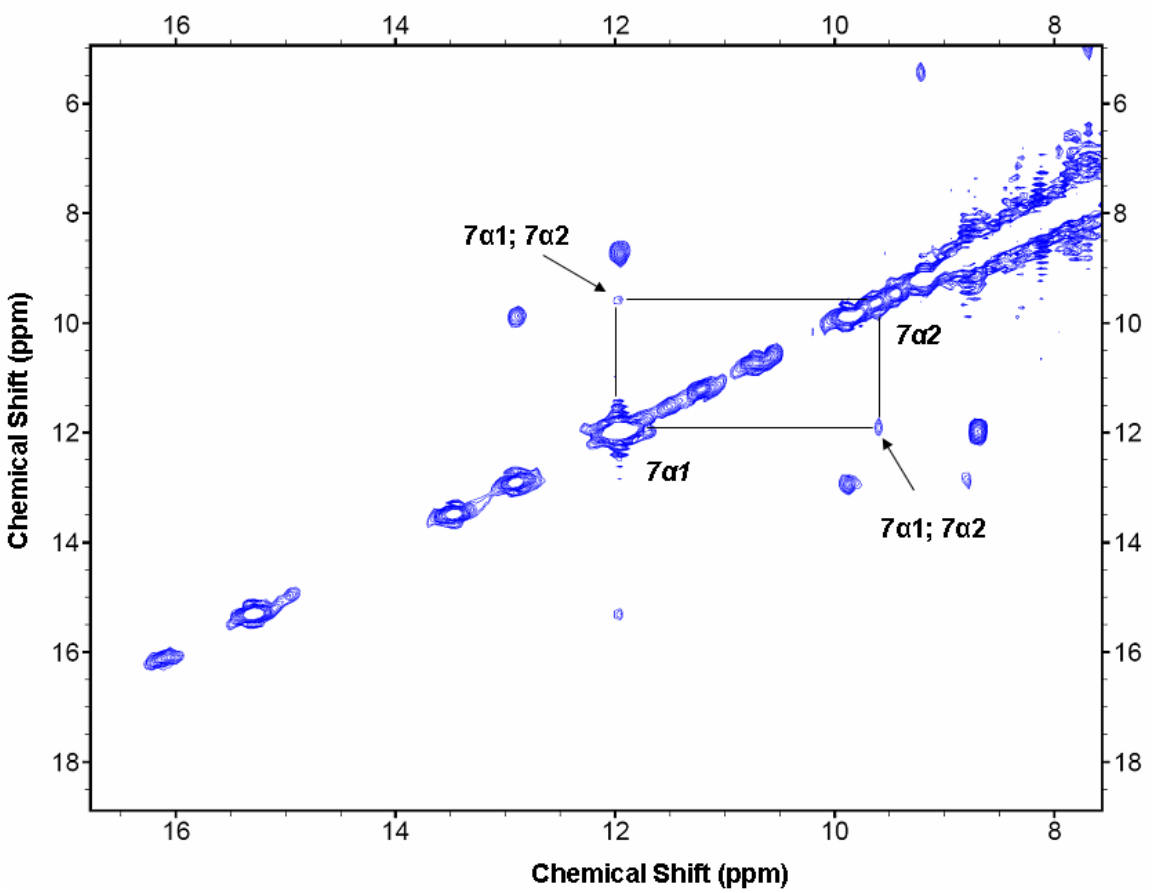

Figure S5. COSY map of DHPCN. COSY crosspeaks between the 7α1 and 7α2 propionate protons.

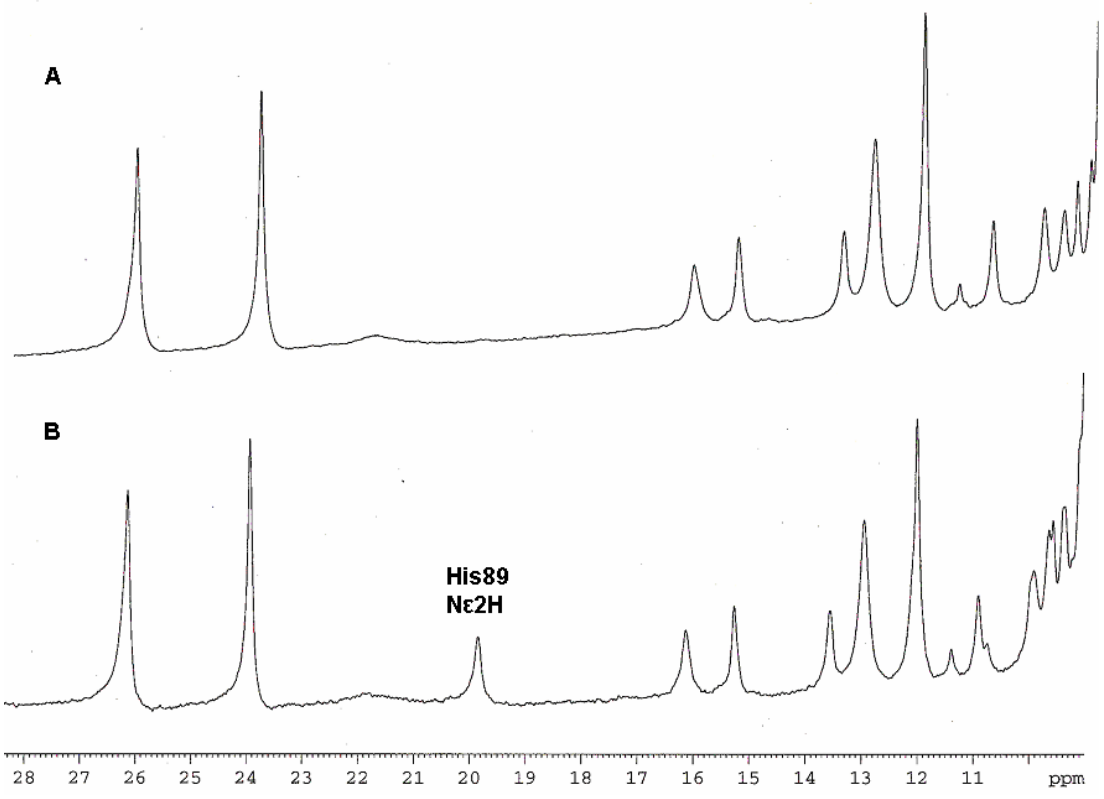

Figure S6. DHPCN spectrum at 25 °C. A) DHPCN sample in 99.9% D_2O, 100mM KP, pH 7.0. B) DHPCN sample in 90% H_2O / 10% D_2O, 100mM KP, pH 7.0. The spectrum shown in B shows the appearance of an exchangeable proton at 19.9 ppm in an H_2O sample. This peak is assigned as His89 Nε2H. The exchangeable His89 Nε2 proton is the only labile proton in DHP close enough to the heme iron to exhibit hyperfine-shifting while transferring NOEs to a scalar coupled spin system (ie. His89 Cβ1H and His89 Cβ2H). In addition, mutation of the distal histadine to valine (H55V) does not effect this labile proton, therefore ruling out H55 as the possible source of this resonance.

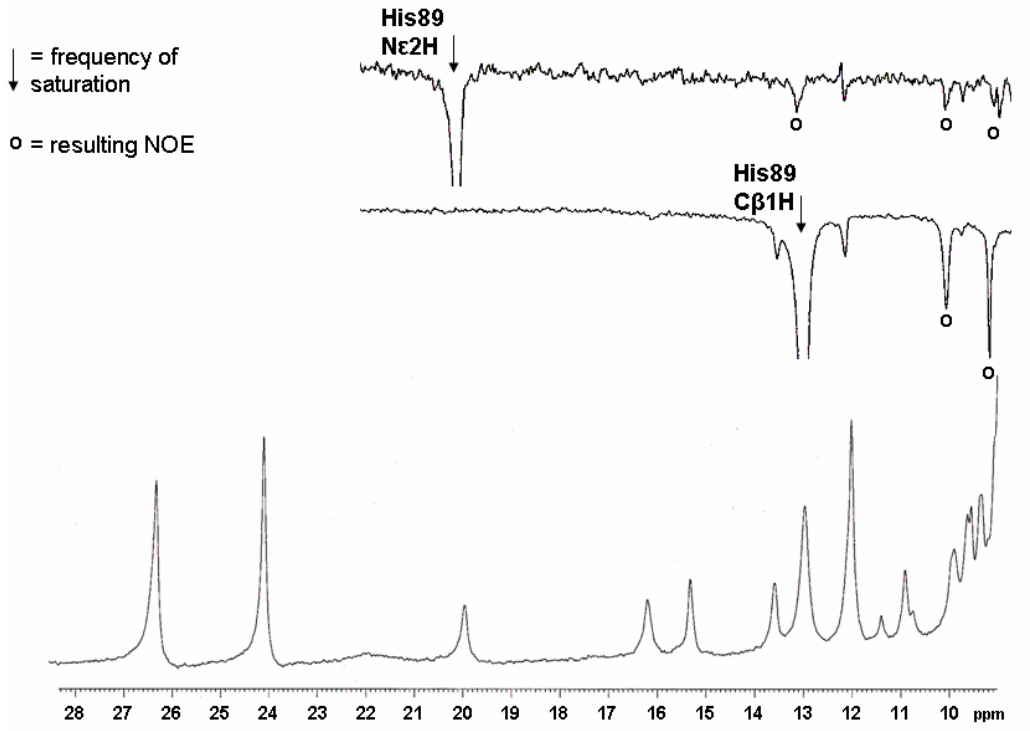

Figure S7. 1D NOE difference spectra of DHPCN in 90% H_2O / 10% D_2O, 100mM potassium phosphate, pH 7.0 at 25 °C. Irradiation of the exchangeable proton at 19.9 ppm gives rise to NOEs at 12.9 and 9.8 ppm. Irradiation at 13.4 gives rise to NOEs at 10.4 and 8.8 ppm (note: This difference spectra was taken in 99.9% D_2O and is presented for clarity. The difference spectra taken in 90% H_2O / 10% D_2O showed a small reciprocal NOE to 19.9 ppm and is not shown because of large signal-to-noise). The bottom spectrum is DHPCN in 90% H_2O / 10% D_2O, 100mM potassium phosphate prior to irradiation.

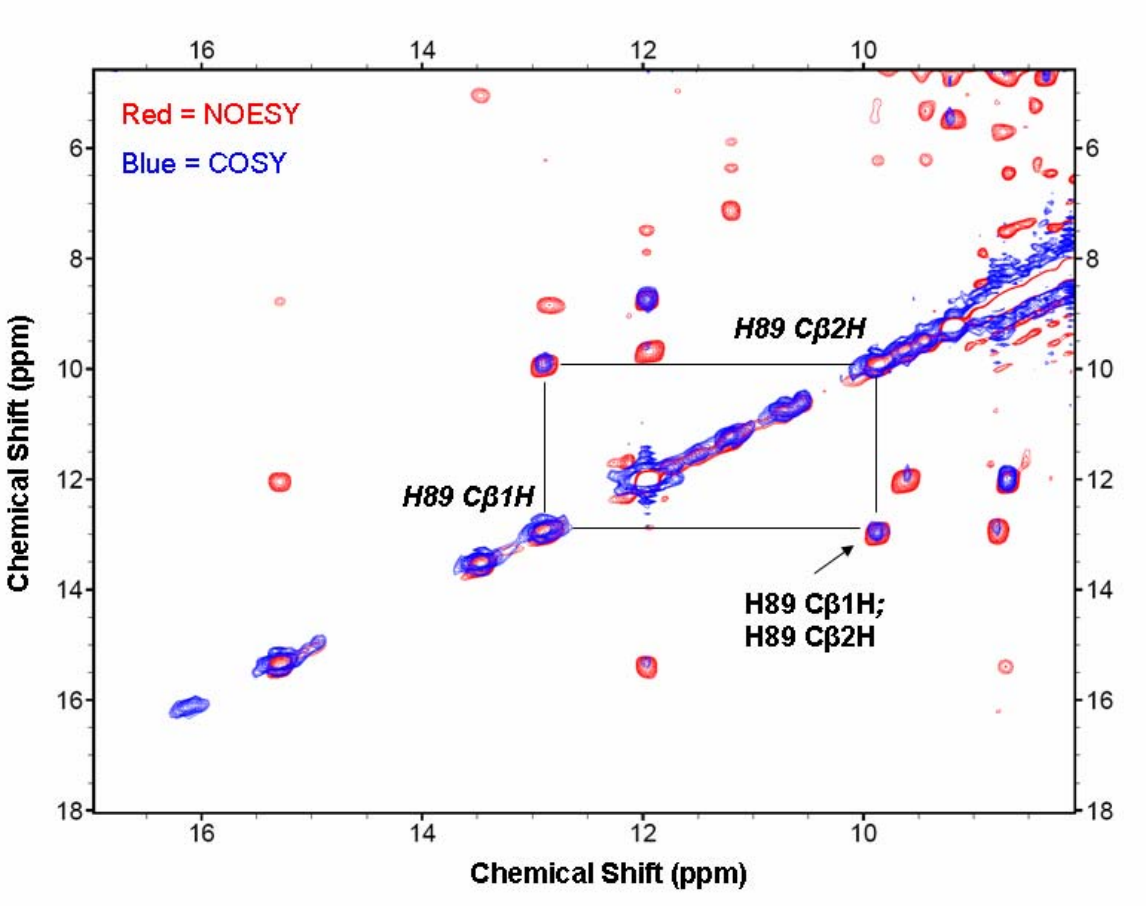

Figure S8. NOESY and COSY overlay showing the connectivity between the two protons which exhibit NOEs to the exchangeable H89 Nε2H resonances. The connectivity and hyperfine-shifting of these resonances confirms their identity as the two Cβ protons on H89.

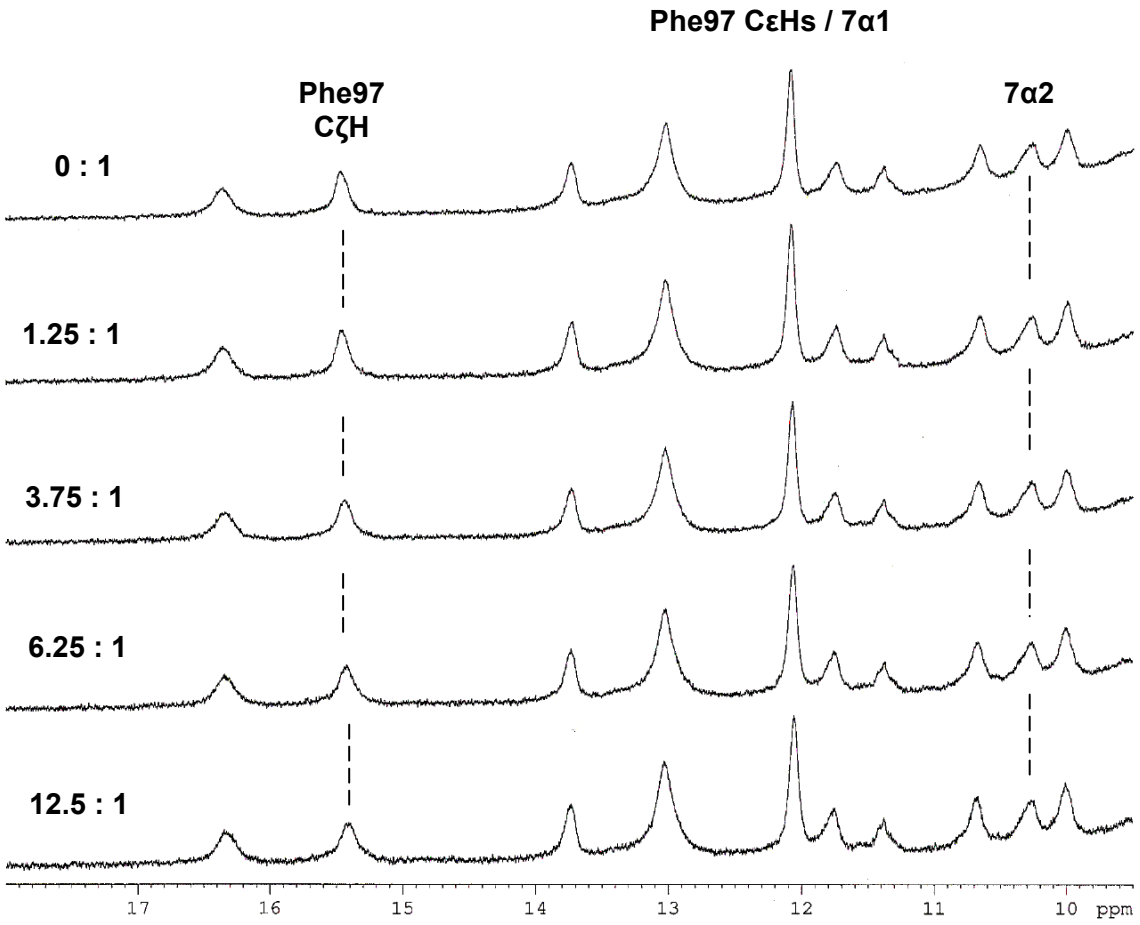

Figure S9. Titration of 2,4,6-TFP to DHPCN, pH 6.0, 25 °C. Upon titration of 2,4,6-TFP at pH 6.0 (below the pKa of 2,4,6-TFP) no changes were observed in the hyperfine-shifted resonances of the active site.

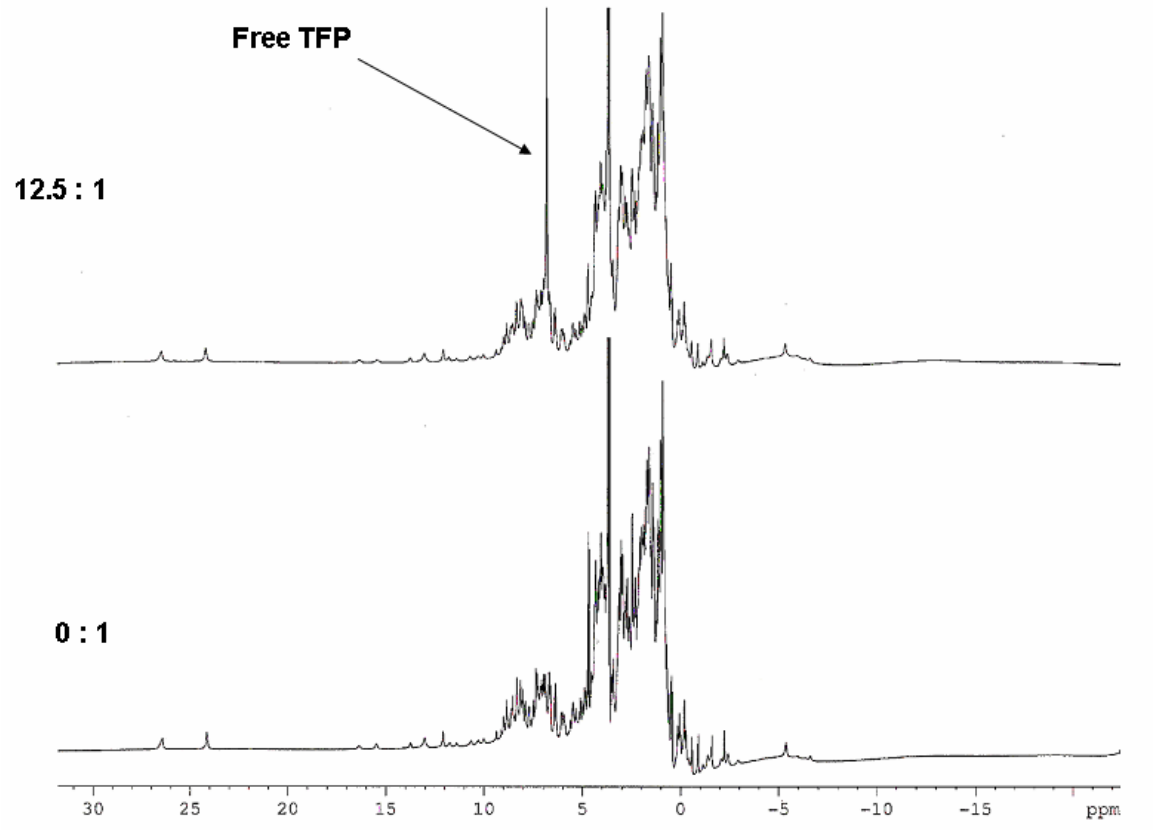

Figure S10. Titration of 2,4,6-TFP to DHPCN (full spectra shown), pH 6.0, 25 °C. The top spectrum shows that 2,4,6-TFP is indeed present in appreciable amounts in the solution. The single resonance of the two chemically equivalent protons of 2,4,6-TFP is shown at ~7 ppm. This shows that 2,4,6-TFP is in solution in appreciable amounts and does not result in any perturbations of substrate binding site resonances (see Figure S9).

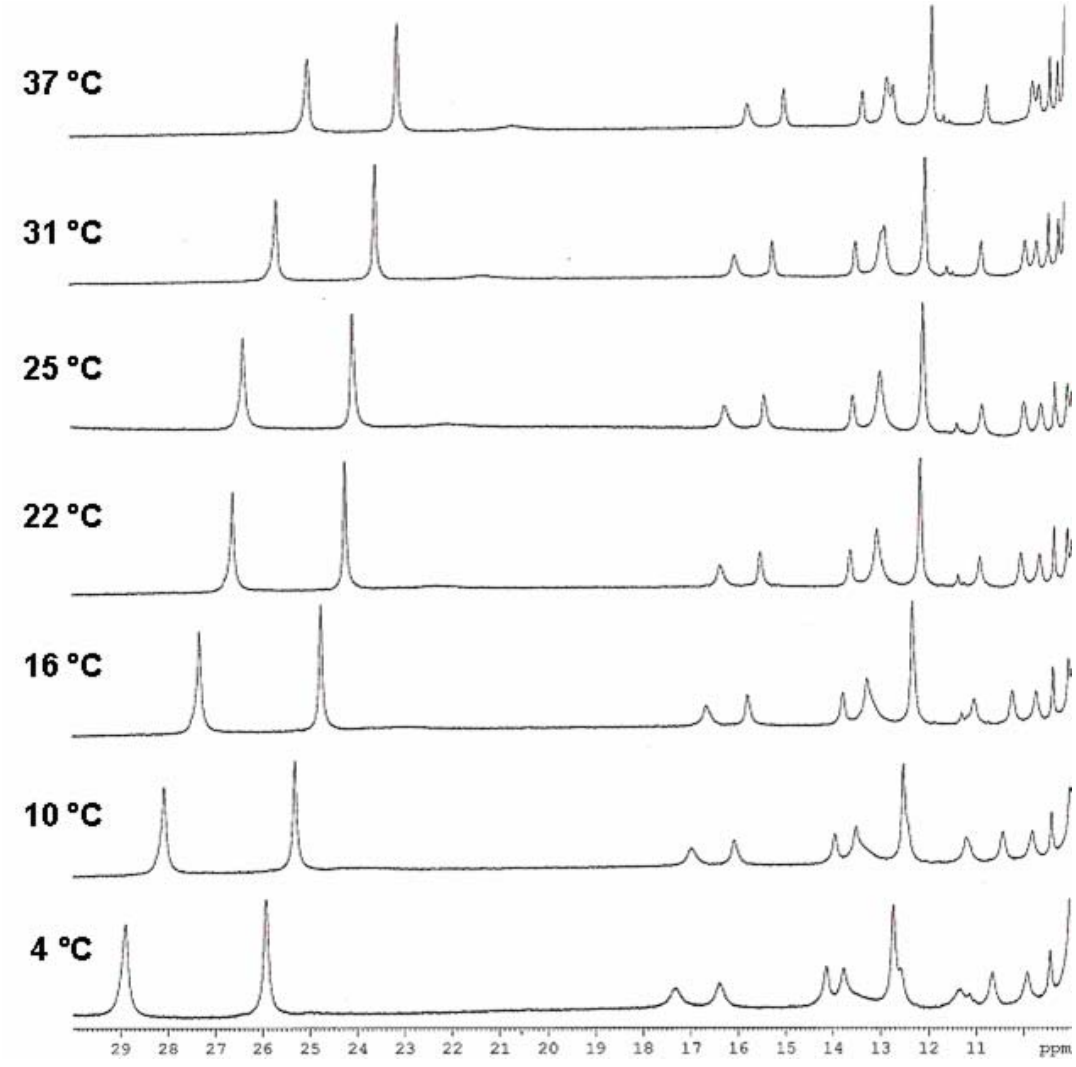

Figure S11. Variable temperature ^{1}H NMR spectra of the hyperfine-shifted region of DHPCN. The temperature range is from 37 °C to 4 °C. The 7α1H signal appears from underneath the Phe97 CεHs signal at 4 °C (12.5 ppm).

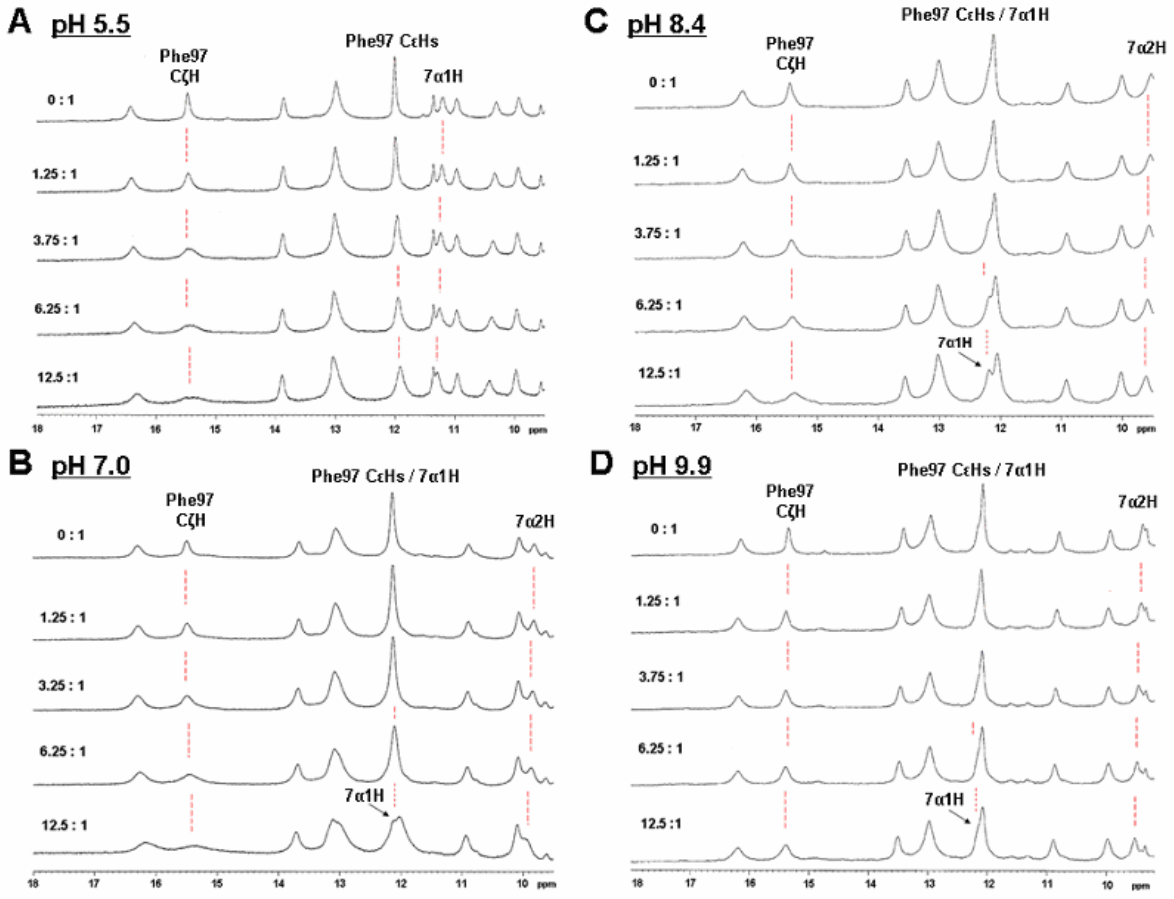

Figure S12. Titration of substrate 2,4-DCP to fully formed DHPCN, 100mM potassium phosphate, 25 °C. A) Titration at pH 5.5. B) Titration at pH 7.0. C) Titration at pH 8.4. D) Titration at pH 9.9. The internal Phe97 ring protons exhibit substantial loss of intensity and line broadening at acidic and neutral pH. The effect becomes less pronounced, although still present, at pH 8.4 and 9.9 when the substrate is in the phenolate form. The changes in chemical shifts of the 7α1 and 7α2 propionate resonances can be seen at all pH values studied, but are substantially less at alkaline pH 9.9.

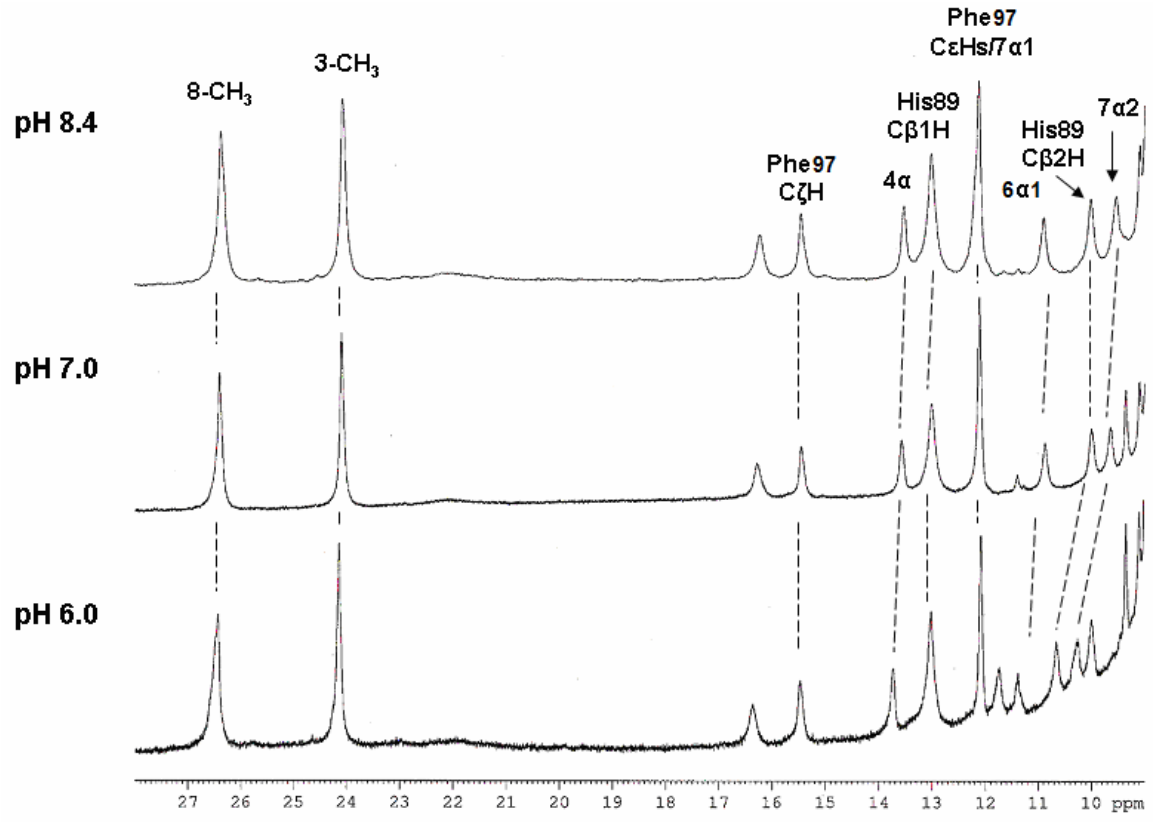

Figure S13. ^{1}H NMR spectra of the hyperfine shifted region of DHPCN, pH 8.4, 7.0, and 6.0, at 25 °C. Significant changes in the chemical shifts of H89 Cβ2H and 7α2H can be seen throughout the pH range.

Interpretation of Relaxation Data

The NMR linewidth is related to the transverse relaxation time (T_2) according to

$$\nu_{1/2} = \frac{1}{\pi T_2} \qquad \text{(S1)}$$

The discussion of ^{19}F linewidths in the text relies on this relation. Changes in T_1 and T_2 are related to the rotational correlation time (τ_c) of the molecule. The rotational correlation time is related to the Stoke's radius, r, according to

$$\tau_c = \frac{4/3\pi r^3 \eta}{k_B T} \qquad \text{(S2)}$$

where η is the viscosity. Equation S2 is the Stokes-Einstein equation which provides an estimate of τ_c = 34 ns for DHPCN assuming that the radius is r = 20 Å at a viscosity of η = 1 centipoise. This value is referred to in the text. The relationship between the T_1 and T_2 relaxation times and the correlation time is given by

$$\frac{1}{T_1} = \frac{3}{20}\left(\frac{g_N^4 \beta_N^4}{\hbar^2 r^6}\right)\left\{\frac{2\tau_c}{1+\omega_o^2\tau_c^2} + \frac{8\tau_c}{1+4\omega_o^2\tau_c^2}\right\} \qquad \text{(S3)}$$

and

$$\frac{1}{T_2} = \frac{3}{40}\left(\frac{g_N^4 \beta_N^4}{\hbar^2 r^6}\right)\left\{3\tau_c + \frac{5\tau_c}{1+\omega_o^2\tau_c^2} + \frac{2\tau_c}{1+4\omega_o^2\tau_c^2}\right\} \qquad \text{(S4)}$$

where r is the distance between the proton and the vicinal F (1.4 Å) and ω_o is the Larmor frequency (500 MHz). These standard equations, which are adapted from the article by Bloembergen, Purcell and Pound entitled "Relaxation Effects in Nuclear Magnetic Resonance Absorption" *Physical Review* (1948), 73, 679-746. Using the values g_N = 5.595, $\beta_N = 5.050 \times 10^{-27}$ J/T, the prefactor can be expressed as

$$\frac{g_N^4 \beta_N^4}{\hbar^2 r^6} = \frac{8.649 \times 10^{10}}{R_A^{\,6}} s^{-2} \qquad \text{(S5)}$$

where R_A is the effective distance of the dipole causing relaxation in units of Å. Since there is an excess of free 2,4,6-TFP we need to account for the fact that the observed T_1 and T_2 times are a combination of free and bound species. Since the decays are single exponential we can assume that the free and bound phenols are in fast exchange. Thus, the observed times will be given by:

$$\frac{1}{T_{obs}} = \frac{f_a}{T_a} + \frac{f_b}{T_b}$$

or (S6)

$$T_{obs} = \frac{T_a T_b}{f_a T_b + f_b T_a}$$

where $T_{a,b}$ corresponds to the T_1 or T_2 time of a (free) or b (bound), respectively. Since the ratio of 2,4,6-TFP to DHP is 15:1 the maximum $f_b = 0.067$. Given the experimental values and the T_{1a} and T_{2a} values of 8.1 s and 6.4 s, for free 2,4,6-TFP, and T_{1obs} and T_{2obs} values of 5.8 s and 1.5 s, we obtain T_{1b} and T_{2b} values of 1.2 s and 0.13 s, respectively. The results of this calculation are shown in Figure S14 along with a plot of the T_1 and T_2 curves according to Eqns. S3 and S4, respectively. In the calculation the distance $R_A = 2.47$ Å was assumed in the prefactor given in Eqn. S5.

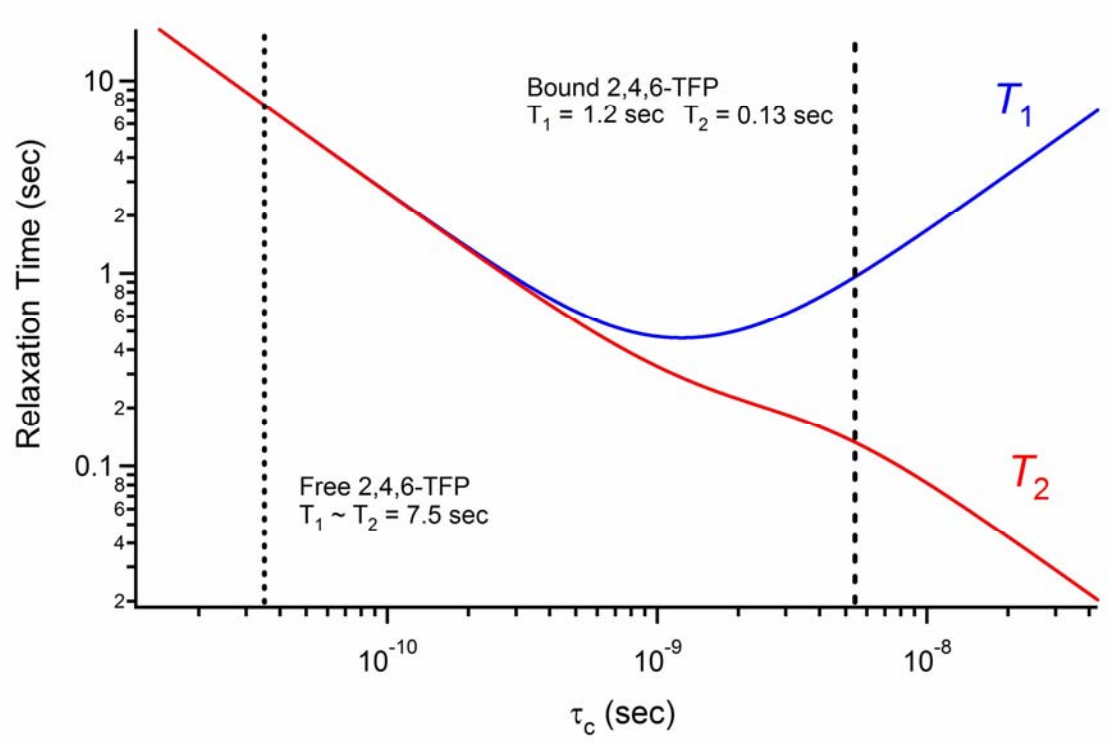

Figure S14. Analysis of the relaxation data for ^{1}H NMR inversion recovery and spin echo experiments within the assumption of fast exchange. The curves were plotted assuming that the dipolar relaxation is caused by a ^{19}F nucleus at a distance of 2.47 Å.

The analysis using these equations provides a justification for the statement that 2,4,6-TFP interacts with DHPCN to provide a significant increase in τ_c from ~35 ps to ~50 ns. These values correspond approximately to the expected values for free and bound 2,4,6-TFP according to Eqn. S2.

Enzyme kinetic study of molecules used in the ^{1}H NMR study

Studies of the oxidation of the substrates 4-BP, 2,4-DCP and 2,4,6-TFP by DHP were carried out under standard assay conditions, and are shown in Figures S15, S16 and S17,

respectively. The major point of these kinetic studies is to demonstrate the significant difference between the molecules 4-BP and 2,4,-DCP, which bind in the internal site and 2,4,6-TFP, which binds in an external site. The conditions used in these studies are benchtop mixing detecting using a HP8454A photodiode array spectrophotometer. The concentrations of reagents are [DHP] = 5 μM, [phenol] = 120 μM and [H2O2] = 360 μM. The times ranging from 0 s to 60 s shown in each of the Figures are the same.

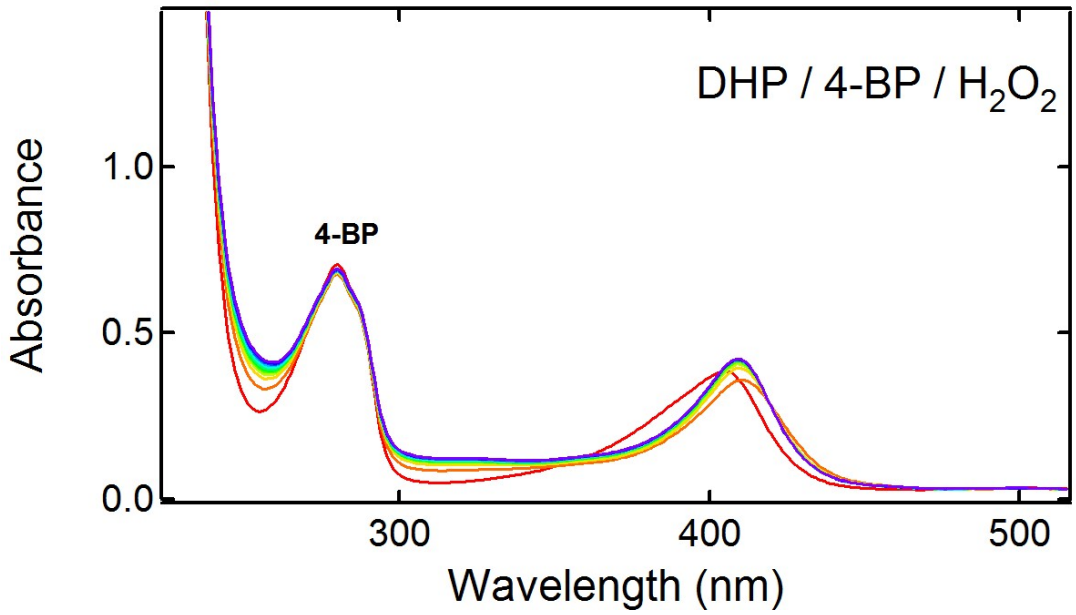

Figure S15. Spectra of 4-BP and DHP ranging form 0 s (red) to 60 s (blue) following addition of H_2O_2 in 100 mM potassium phosphate, pH 7.0.

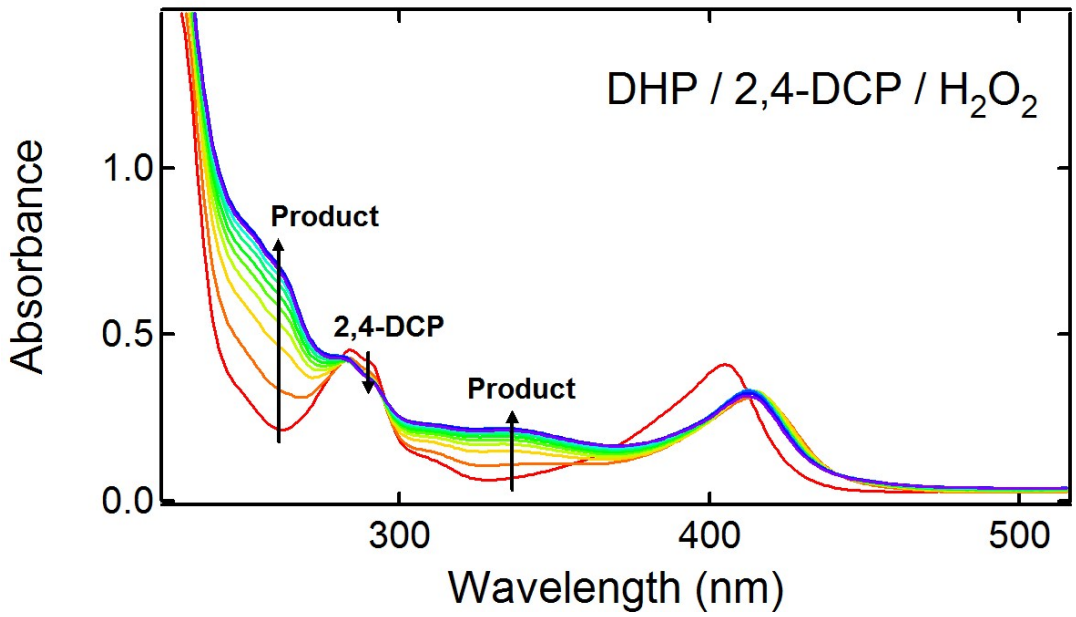

Figure S16. Spectra of 2,4-DCP and DHP ranging form 0 s (red) to 60 s (blue) following addition of H_2O_2 in 100 mM potassium phosphate, pH 7.0.

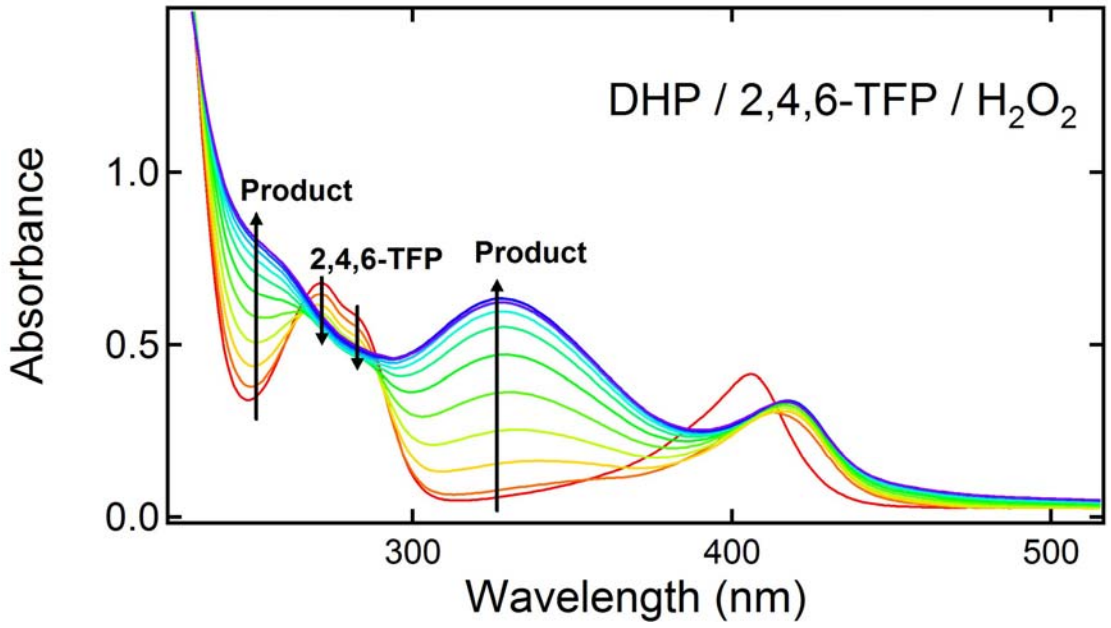

Figure S17. Spectra of 2,4,6-TFP and DHP ranging form 0 s (red) to 60 s (blue) following addition of H_2O_2 in 100 mM potassium phosphate, pH 7.0.

APPENDIX 2

Supporting Information for Chapter 4

Supporting Information

Figure S1. NOESY and COSY overlay map of DHPCN V59W. NOESY crosspeaks (red) and COSY scalar coupling (blue) between the hyperfine-shifted high frequency protons. The boxes represent scalar coupling observed at high contour levels. Scalar coupling is observed between the three proton spin system of the H89 proximal histidine α and β protons. The characteristic scalar coupling of the F97 ring protons is also observed, although the crosspeak for F97 Cζ and CεHs is very close to the diagonal. The four proton spin system indicative of the 7-propionate chain is readily observed. Mutual scalar coupling between all four resonances is observed at higher contour levels. The 4α and one of the 4β vinyl resonances are observed. The -1 ppm crosspeak for 4α is believed to be the other 4β proton even though scalar coupling between the two resonances is not observed.

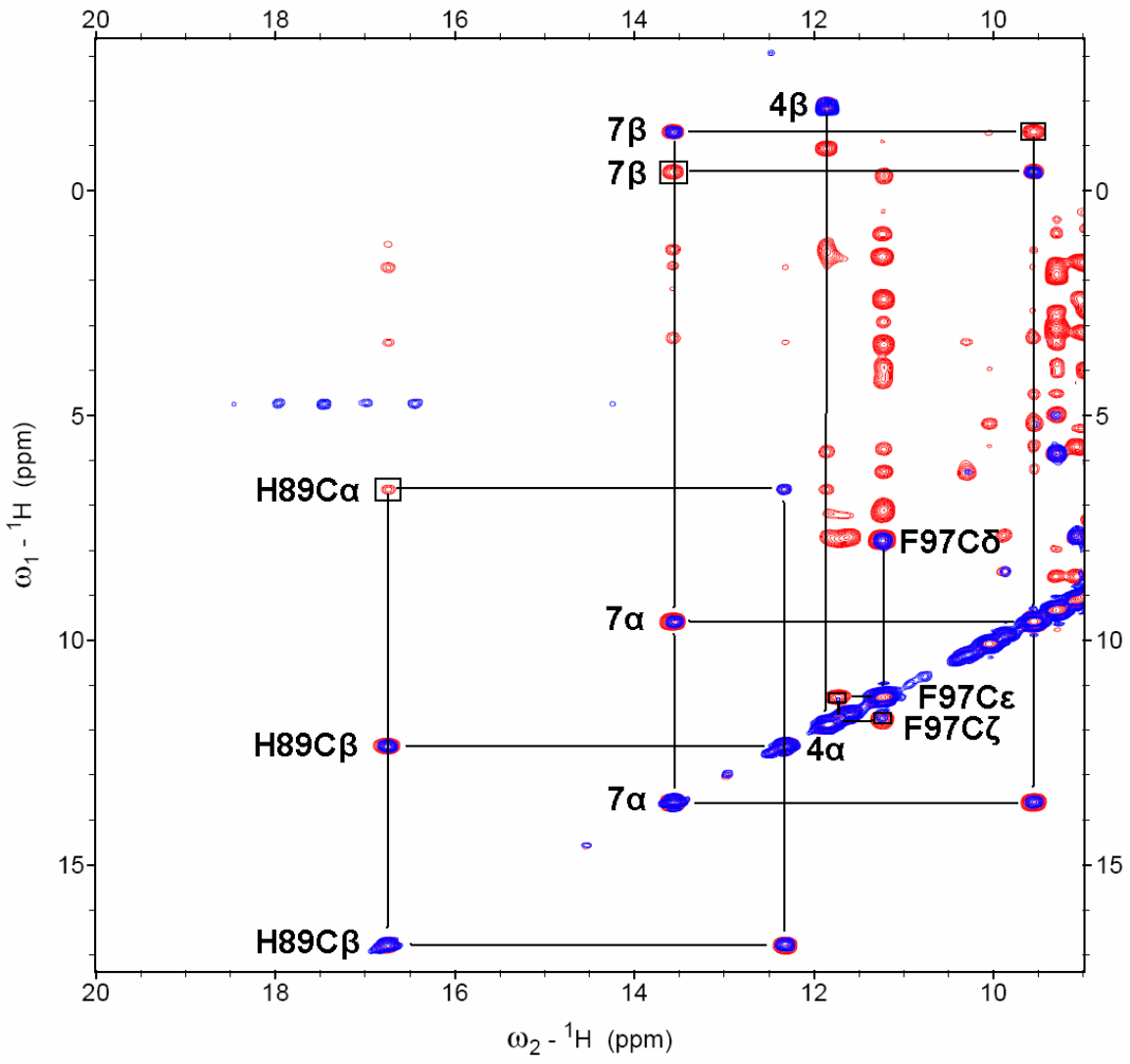
4β
7β
7β
H89Cα
F97Cδ
7α
F97Cε
F97Cζ
H89Cβ
4α
7α
H89Cβ
20
18
16
14
12
10
0
5
10
15
ω1 - 1H (ppm)
ω2 - 1H (ppm)

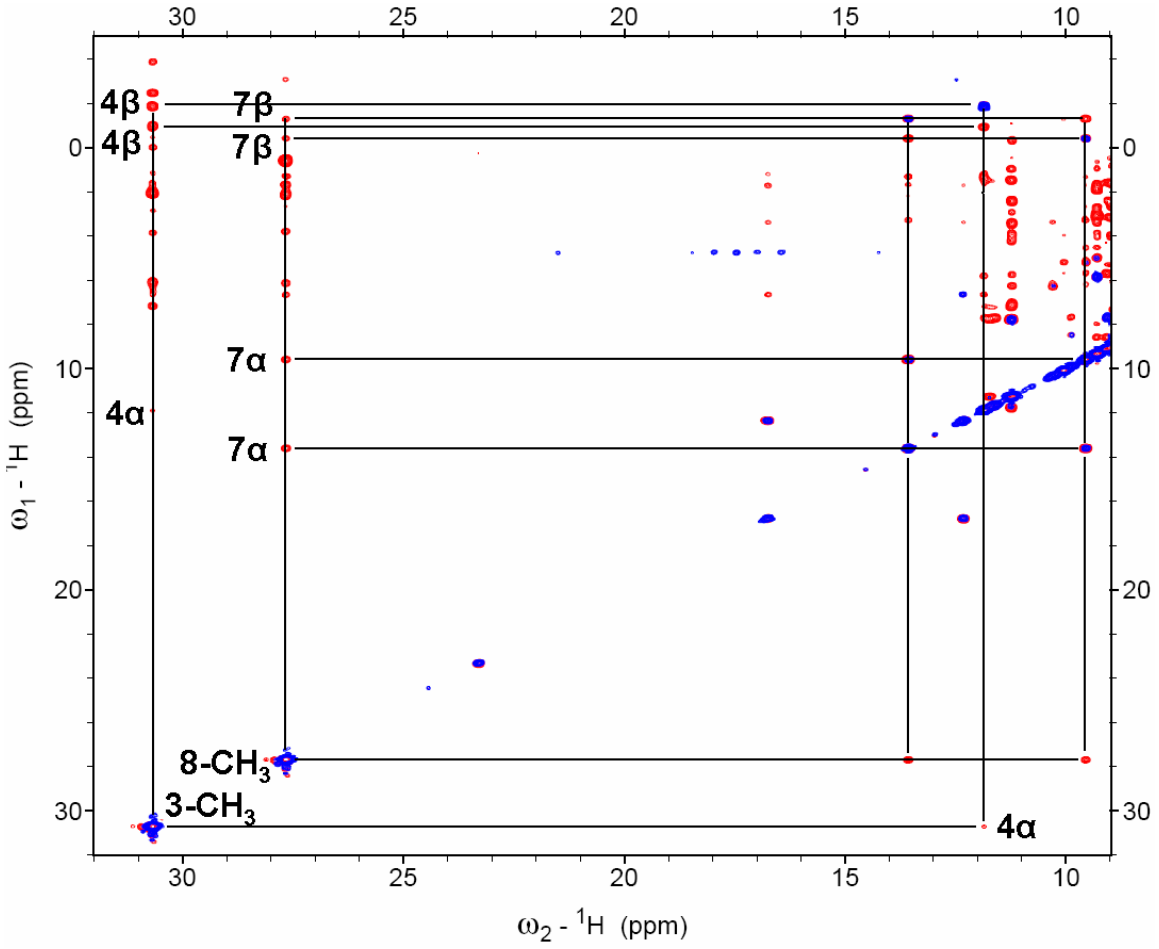

Figure S2. NOESY and COSY overlay map of DHPCN V59W showing dipolar connectivity between the heme methyls and the adjacent propionate or vinyl substituent. NOESY crosspeaks (red) and COSY scalar coupling (blue) are shown. NOESY crosspeaks are observed between the 8-CH_3 and four protons of the 7-propionate chain. NOESY crosspeaks are also observed between the 3-CH_3 heme methyl and the 4-vinyl heme substituent.

APPENDIX 3

Supporting Information for Chapter 6

Supporting Information

Table S1. Backbone $^{13}C\alpha$, $^{13}C\beta$, carbonyl ^{13}C, amide ^{1}H and amide ^{15}N resonances for metcyano DHP, pH 7, 25 °C.

DHPCN 25 C 13CO (i-1)	CB (i-1)	CA (i-1)	15N (i)	15N-1H (i)	CA (i)	CB (i)	13CO (i)	Notes
176.418	31.993	57.671	112.414	9.489	46.725			GLY 1
173.903		46.712	123.341	8.585	61.81	40.895	176.745*	PHE 2
176.735	40.874	61.795	114.221	8.52	58.988	32.316	180.619	LYS 3
180.622	32.28	58.969	121.42	8.279		28.097		GLN 4
178.401	28.003	58.966	122.484	8.799	57.743	41.415		ASP 5
178.281	41.44	57.712	120.087	7.9	65.786	39.349	178.3*	ILE 6
177.826	39.286	65.758	121.115	7.365	55.591	18.037	181.713	ALA 7
181.71	18.01	55.576	120.229	9.228	66.652	68.739	177.397	THR 8
177.41	68.813	66.631	123.28	8.787	65.083	37.073	179.252	ILE 9
	37.034	65.065	116.457	8.798	60.715	31.05		ARG 10
178.847	31.094	60.705	106.031	8.238	46.546			GLY 11
174.166		46.525	121.792	7.869	53.584	40.289	178.892*	ASP 12
176.005	40.294	53.559	124.41	7.566	60.321	43.334	178.715	LEU 13
178.717	43.374	60.306	116.592	8.851	60.761	30.735		ARG 14
178.901	30.705	60.753	115.715	7.612	66.477	68.196	178.55	THR 15
176.823	68.222	66.457	118.445	7.984	63.376	39		TYR 16
179.493	39.004	63.362	119.957	9.084	54.862	19.852		ALA 17
179.616	19.778	54.854	113.993	7.869	60.309	31.057	178.341	GLN 18
178.756		60.327	118.641	8.339	58.15	40.756		ASP 19
180.75	40.761	58.131	120.847	9.059	66.048	36.844	177.794	ILE 20
177.792	36.82	66.04	122.414	9.01	64.54	41.828	180.178	PHE 21
180.169		63.532	117.372	9.56	59.202	41.946		LEU 22
179.814	41.965	59.19	123.597	8.504	56.219	17.748	181.579*	ALA 23
181.565	17.754	56.205	120.153	8.95	60.812	39.415	176.028	PHE 24
176.026	39.427	60.787	117.133	9.239	57.579	42.023	179.688	LEU 25
179.69	41.999	57.573	115.685	8.969	55.978	40.332	177.164	ASN 26
177.174	40.286	55.954	122.411	8.606	59.301	34.059	179.391	LYS 27
176.924	34.026	59.276	116.178	8.333	55.364	39.022	173.615	TYR 28
181.021	32.38	65.459	118.918	9.523	57.416	40.538	179.491	ASP 30
177.152*	40.509	57.402	119.815	9.074	58.169	30.649	179.584	GLU 31
178.736		58.143	116.014	8.412	60.02	31.637	178.194	ARG 32
178.181		59.999	114.289	7.894	58.458	29.698		ARG 33

177.155	29.681	58.436	116.41	7.507	60.232	38.215	174.832	TYR 34
177.057*		60.207*	118.687	9.162				PHE 35
	32.598	59.931	119.094	8.789	55.253	37.95		ASN 37
176.283		55.267	116.85	8.921	54.947	38.802	178.227	TYR 38
178.222	38.795	54.883	124.143	8.049	65.662	32.872	177.716	VAL 39
		65.676	116.272	9.849	46.431			GLY 40
174.535		46.424	117.627	7.512	54.358	35.085		LYS 41
177.618	35.07	54.34	122.657	10.117	57.845	65.925	174.663	SER 42
174.678	65.909	57.821	123.009	9.707	58.431	40.363	178.503	ASP 43
179.22	40.355	58.42	117.162	8.803	59.576	28.783	178.618	GLN 44
179.585		59.558	120.918	8.305	59.817	30.785	180.576	GLU 45
179.368	39.519	58.936	115.906	8.614	60.354	32.944	178.586	LYS 47
178.585	32.917	60.331	112.375	7.912	59.376	64.663	173.922	SER 48
173.915	64.666	59.354	124.846	8.396	55.757	35.216	177.29	MET 49
179.458	33.713	59.714	120.12	8.026	61.63	40.696		PHE 52
179.329	40.662	61.614	109.808	8.535	47.923			GLY 53
175.869		47.905	121.678	9.029	58.072	41.303		ASP 54
178.658	41.302	58.057	120.754	8.891	60.357	33.103	177.955	HIS 55
177.958	33.088	60.338	108.896	8.922	67.209	68.877	175.874	THR 56
177.72	68.921	67.19	123.285	8.408	60.719	30.376		GLU 57
177.866	30.369	60.702	119.407	7.675	60.053	32.848	179.796	LYS 58
179.779	32.804	60.029	119.779	7.579	63.577	30.557	176.23	VAL 59
176.226	30.525	63.571	116.24	7.897	61.993	38.416	177.548	PHE 60
177.54		61.987	121.019	8.727	57.07	38.829		ASN 61
177.796	38.751	57.06	119.073	6.795	57.3	40.287		LEU 62
177.903	40.218	57.329	117.638	7.757	59.497	33.266		MET 63
177.65		59.487	114.637	8.239	56.475	33.481	178.55	MET 64
178.553	33.56	56.466	121.305	7.707	60.393	29.72		GLU 65
178.349	29.727	60.33	118.814	8.349	65.963	31.957	180.761	VAL 66
179.563	32.004	65.955	122.368	8.658	55.436	18.038	176.943*	ALA 67
179.418	18.025	55.425	119.287	8.798	56.82	41.912	178.029	ASP 68
178.008	41.876	56.806	114.605	7.828	57.814	33.202	178.818	ARG 69
176.368	33.146	57.8	121.602	7.537	52.24	18.582	177.244	ALA 70
	18.557	52.219	118.65	8.212	62.985	69.992		THR 71
175.079		56.615	103.497	8.974	61.069		173.649	CYS 73
173.665		61.049	123.227	8.281	60.731		175.18	VAL 74
								PRO 75
175.457	32.913	62.323	121.109	9.805	55.189	43.371	179.655	LEU 76
179.654	43.299	55.17	127.716	9.342	55.704	18.504	180.996	ALA 77
178.051		61.533	122.92	7.518	58.146	42.399	178.745	ASP 79
178.755	42.375	58.124	122.824	8.218	56.437		179.629	ALA 80

179.629	19.098	56.413	115.981	9.286	58.118	39.366	178.486	ASN 81
178.49	39.36	58.1	117.845	9.066	68.276	70.048		THR 82
178.546	70.046	68.253	120.411	9.302	61.949	45.694	182.6	LEU 83
182.592	45.697	61.927	118.619	9.85	67.18	33.978	179.239	VAL 84
179.242	33.953	67.163	117.241	9.893	58.087	29.894	178.526	GLN 85
178.527	29.87	58.068	122.192	10.085	59.224	38.776	180.559	MET 86
179.233	32.066	60.05	117.357	9.39	57.534	25.39	174.196	GLN 88
174.207	25.318	57.517	114.321	9.405	54.256	28.027	177.28	HIS 89
177.287	28.059	54.232	117.916	7.913	62.243	63.915	175.79	SER 90
173.952	63.404	58.698	119.797	7.279	54.121	43.303	175.87	LEU 92
175.87	43.312	54.105	109.13	9.026	60.088	73.092	177.117	THR 93
177.126	73.088	60.072	112.531	10.404	66.841	68.832	177.916	THR 94
177.921	68.785	66.819	108.798	8.394	47.309			GLY 95
176.56		47.291	118.588	7.873	58.485	42.02	177.52*	ASN 96
175.67	41.997	58.46	115.147	6.796	61.074	39.468	176.968	PHE 97
176.969	39.458	61.055	120.054	8.621	60.079	30.527	178.949	GLU 98
178.946	30.538	60.055	117.329	7.392	60.249	33.592	177.588	LYS 99
177.584	33.599	60.274	119.504	6.727	58.516	40.143	177.6*	LEU 100
178.074	40.049	58.504	115	7.625	63.934	38.747		PHE 101
178.654	38.738	63.925	123.439	8.76	67.804	31.811	179.504	VAL 102
179.508	31.774	67.789	120.978	8.47	55.728	18.541		ALA 103
174.838		55.717	120.375	8.765	56.646	41.204	176.319	LEU 104
176.325	41.238	56.629	121.433	8.602	59.996	32.578	175.444	VAL 105
179.488		60.12	120.671	8.757	60.567			GLU 106
179.913	29.932	60.575	121.848	8.911	61.858	37.96	178.9	TYR 107
178.894	37.953	61.836	120.38	8.676	61.085	32.657	180.152	MET 108
181.167*	32.6	61.075	120.128	8.979	60.154	31.027	178.262	ARG 109
178.263	31.011	60.132	120.473	8.084	53.238	19.459	178.98	ALA 110
178.973	19.52	53.218	113.827	7.853	60.653	64.311	176.117	SER 111
176.125	64.221	60.646	111.742	8.623	46.447			GLY 112
175.013		46.428	120.119	8.594	54.933	29.786		GLN 113
174.523	62.763	58.515	121.339	7.936	58.029	43.457	177.491	PHE 115
177.508		58.013	128.264	12.348	52.311		178.007	ASP 116
178.002	38.86	52.289	119.126	8.321	63.318			SER 117
176.348		63.317	120.982	9.184	59.606	28.866	179.827	GLN 118
179.857	28.853	59.581	117.951	7.966	62.258		175.929	SER 119
175.75		63.086	123.706	7.841	62.105	29.18	178.035	TRP 120
178.032	29.204	62.088	120.696	8.52	57.43	42.371	178.65	ASP 121
	57.416	42.37	119.321	8.081	60.052	30.946		ARG 122
	30.919	60.013	119.045	8.876	60.292	40.073		PHE 123
176.743	40.077	60.349	107.244	8.75	46.333			GLY 124
176.131		46.326	122.098	8.126	59.964	32.692		LYS 125
180.258		60.013	119.49	8.87	55.276	38	179.077	ASN 126
179.062	37.924	55.227	125.314	9.262	58.242	40.151	177.718	LEU 127

	40.168	58.233	120.483	8.323	68.466			VAL 128
178	31.467	68.465	113.995	8.081	62.035	63.047	177.386	SER 129
177.395	63.092	62.016	124.914	8.356	55.241	18.816	181.239	ALA 130
181.238	18.851	55.217	121.878	9.306	58.734	40.579	179.612	LEU 131
179.613	40.573	58.718	115.026	8.367	61.405	63.13	180.509	SER 132
180.513		61.383	118.97	8.785	62.363	63.261	175.653	SER 133
175.656	63.288	62.339	122.443	8.263	52.97	19.522	177.334	ALA 134
177.337	19.62	52.95	105.714	8.243	45.712			GLY 135
175.034		45.694	124.607	8.811	57.611	35.82		MET 136
176.063	35.8	57.597	133.734	9.009	58.487	33.177	180.27	LYS 137

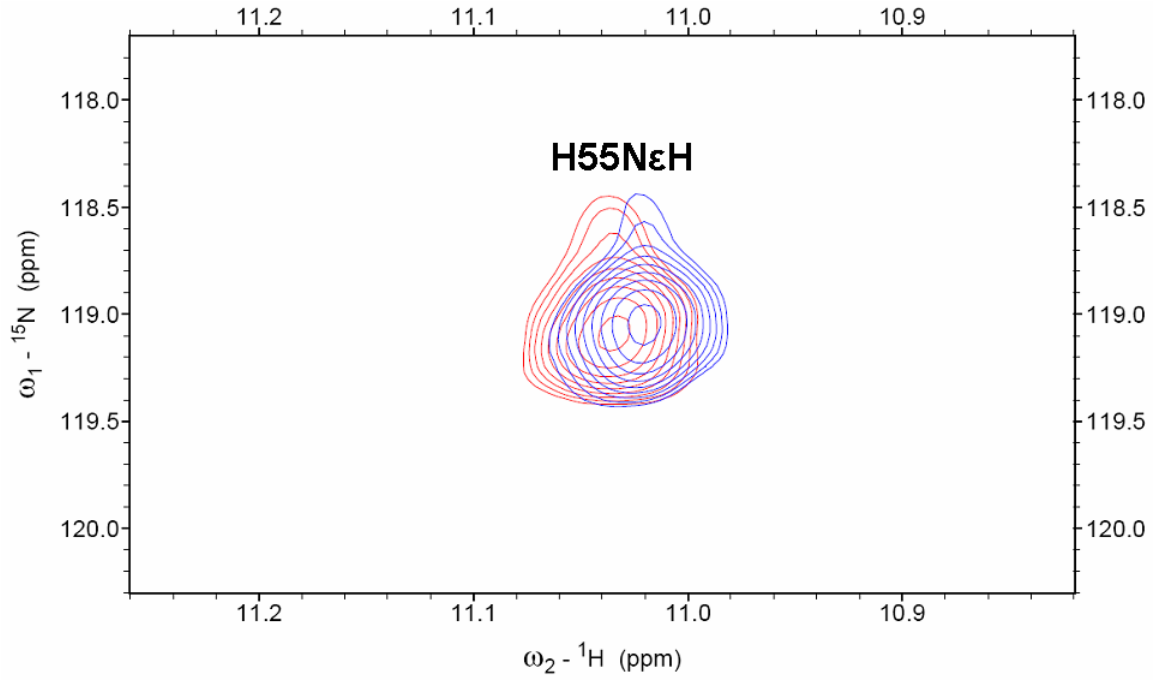

Figure S1. Chemical shift deviations induced by addition of the substrate 2,4,6-TFP. The largest overall deviation in ^{1}H chemical shift (H55 NεH) is shown.

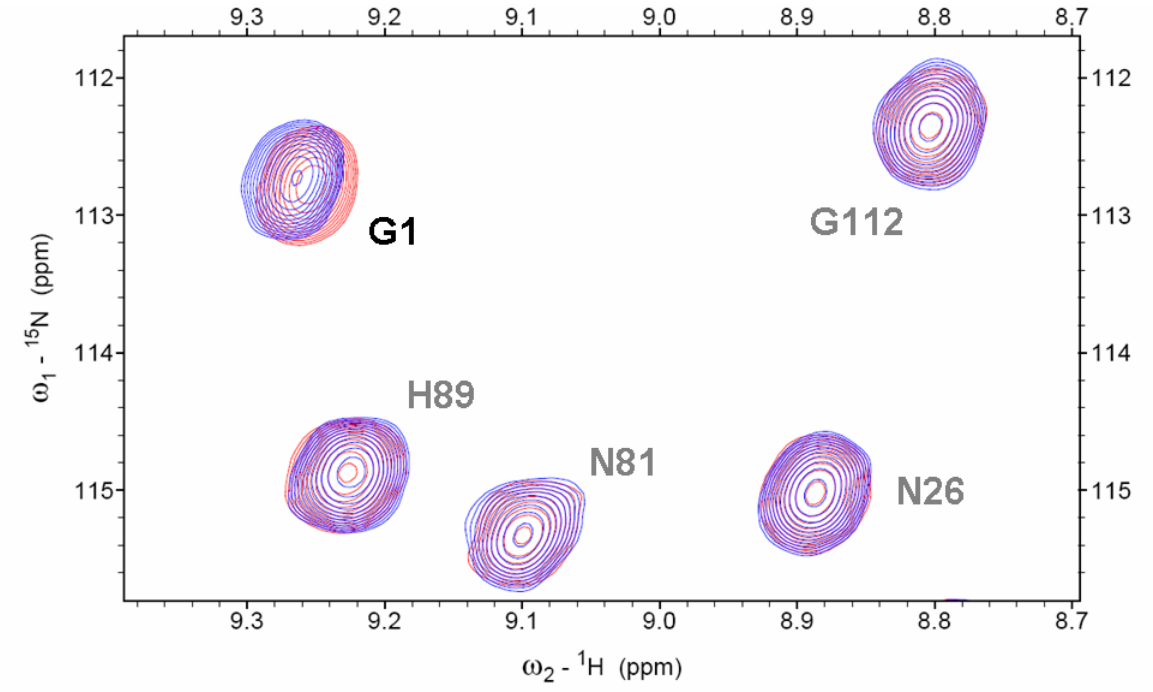

Figure S2. Chemical shift deviations induced by addition of the substrate 2,4,6-TFP. The 2nd largest deviation in amide ^{1}H chemical shift (G1) is shown.

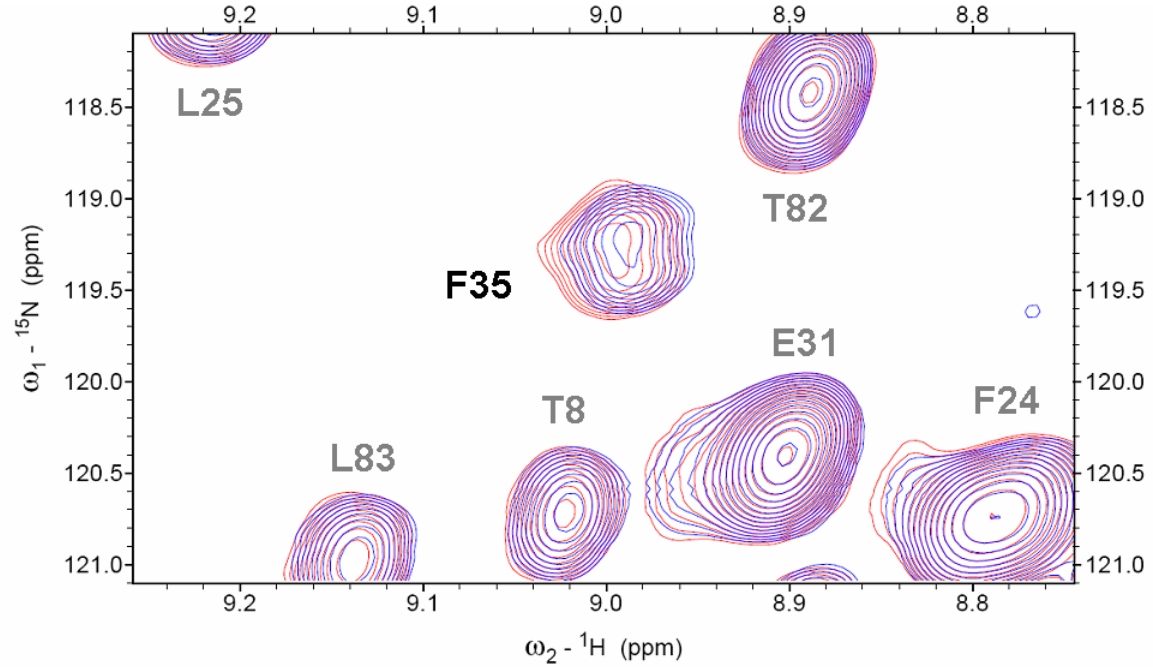

Figure S3. Chemical shift deviations induced by addition of the substrate 2,4,6-TFP. The 3rd largest deviation in amide ^{1}H chemical shift (F35) is shown.

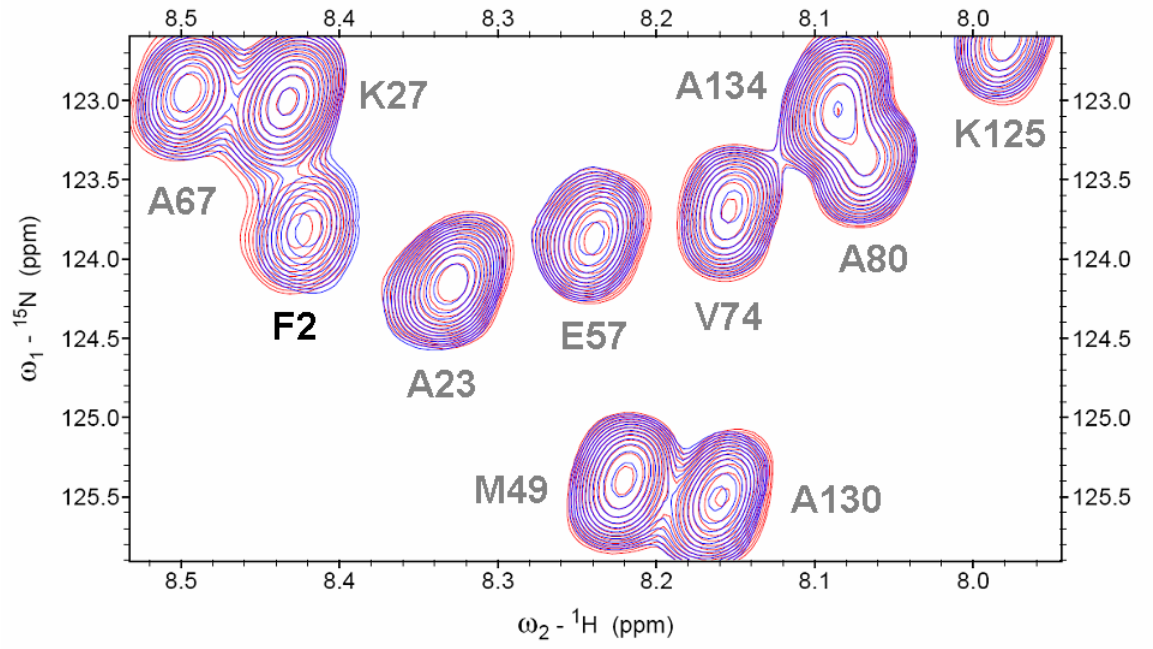

Figure S4. Chemical shift deviations induced by addition of the substrate 2,4,6-TFP. The deviation in amide ^{1}H chemical shift (F2) is shown.

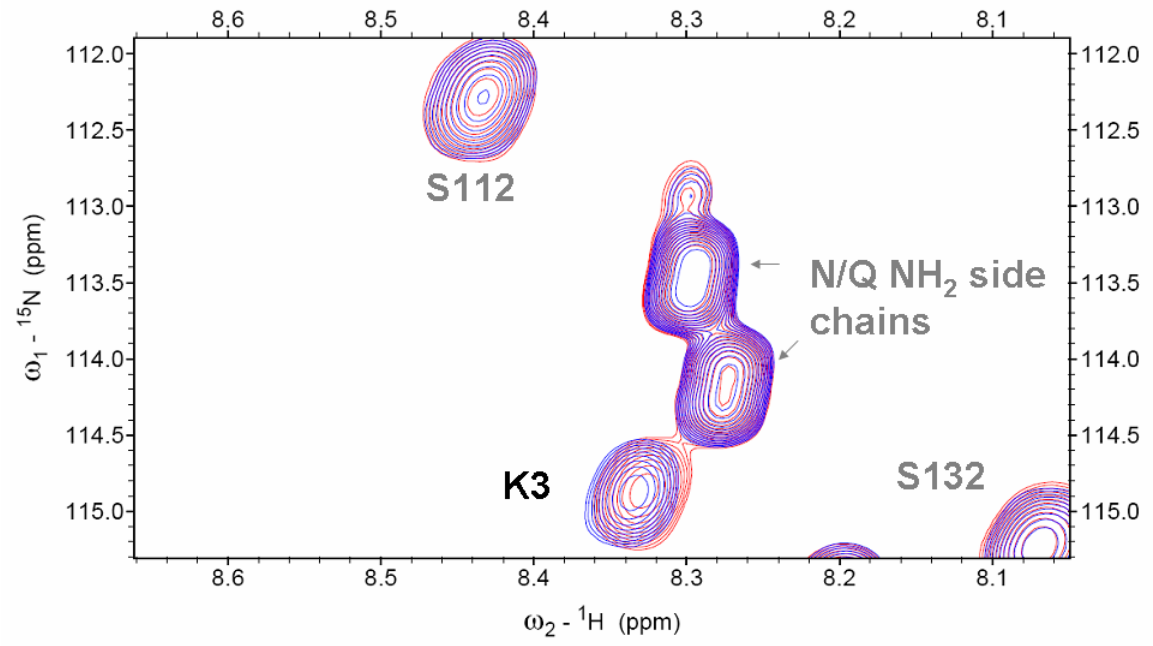

Figure S5. Chemical shift deviations induced by addition of the substrate 2,4,6-TFP. The deviation in amide ^{1}H chemical shift (K3) is shown.

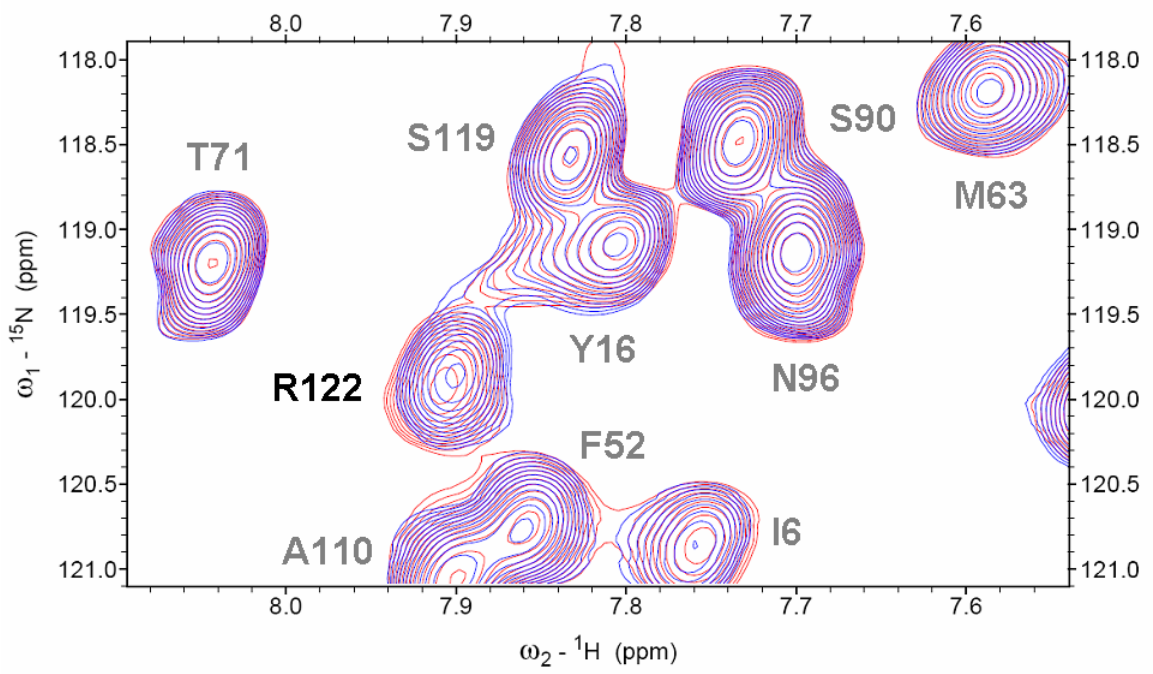

Figure S6. Chemical shift deviations induced by addition of the substrate 2,4,6-TFP. The deviation in amide ^{1}H chemical shift (R122) is shown.